Doctoral thesis in theoretical physics

Cosmic expansion in homogeneous and inhomogeneous universes

Supernovae type Ia as cosmic probes

Marina Seikel

Theoretical High Energy Physics Group
Fakultät für Physik
Universität Bielefeld

Cover Picture:
SN 1994D in the galaxy NGC 4526
Source: Hubble Space Telescope (NASA/ESA)

Cosmic expansion in homogeneous and inhomogeneous universes

Supernovae type Ia as cosmic probes

Marina Seikel

September 13, 2010

Supervisor:	Prof. Dr. Dominik J. Schwarz
Referees:	Prof. Dr. Nicolas Borghini
	Prof. Dr. Dietrich Bödeker
	Prof. Dr. Bärbel Fromme

Abstract. Since it has been discovered in the late 1990s that the universe is likely to be expanding accelerated, a large variety of cosmological models have been developed that allow for cosmic acceleration. Some of the models include a dark energy term that causes the acceleration, while others modify gravity or drop the assumption of homogeneity and isotropy.

As an example of such a model, we analyze a braneworld model with one timelike extra-dimension. There are strong constraints to the parameter values of such a model resulting from the claim that there must be a physical solution to the Friedmann equation at least between now and the time of recombination. We fit the model to supernova type Ia data and check the consistency of the result with other observations. For parameter values that are consistent with observations, the braneworld model is indistinguishable from a ΛCDM universe as far as the considered cosmological tests are concerned.

Although all cosmological models that assume homogeneity and isotropy of the universe and have been tested so far conclude that the universe expands accelerated, this does not prove acceleration beyond doubt. Therefore, we constructed a test of acceleration, which is model-independent in the sense that no assumptions about the content of the universe or about the parameterization of the deceleration parameter are made and that it does not assume any dynamical equations of motion. Yet, the test assumes the universe and the distribution of supernovae to be statistically homogeneous and isotropic. Since the first version of the test is troubled by systematic effects, we modify the analysis to be independent of the calibration of the supernova absolute magnitude. As a result, all systematics are reduced. While most supernova data sets provide evidence for acceleration, when the test is applied, the SDSS data set lacks this evidence.

Due to structure in the universe, the assumption of homogeneity and isotropy might not be justified — especially on small scales. As the Einstein equations are non-linear, spatial averaging and temporal evolution do not commute. Consequently, a universe with structure evolves differently than a perfectly homogeneous universe. The size of this backreaction effect is, however, discussed very controversially. In this work, we test the influence of backreaction on the measurement of the present Hubble rate using supernova data. We find, however, no evidence for backreaction in the presently available supernova data sets.

Contents

List of Figures

List of Tables

Preface

This is a very interesting time to work in the field of cosmology. With the recent great improvement in observational techniques, cosmology has finally gained the status of real science. The observations yielded, however, some puzzling results. The universe seems to be expanding accelerated and it seems like we only know about 5% of the contents of the universe, namely baryonic matter. The rest belongs to the so-called dark sector — dark matter and dark energy. Knowing so little about the universe, a large amount of cosmological models has been suggested in order to describe the observations. While many theories assume that dark energy is the cause for cosmic acceleration, other models modify gravity or drop the usual assumption of homogeneity and isotropy.

With the amount of theories becoming more and more unmanageable, we try a different approach in this work and address more fundamental questions: Can we actually prove cosmic acceleration? Which assumptions do we need in order to find such an evidence? Is the common assumption of a homogeneous and isotropic universe justified even for observations at small scales? How large are the effects of local structure on the expansion rate?

This approach does not directly lead to a viable cosmological model. Its advantage is rather that one can test some requirements a cosmological theory needs to fulfil. If one for example could not find evidence for acceleration in a model-independent way, one should broaden the variety of theories by including models that do not allow for acceleration.

This thesis is structured as follows. The first chapter gives an overview over some important equations that are needed to describe the dynamics of an expanding universe. Furthermore, we describe how supernovae Ia can be used as standard candles for cosmological tests. As an example, we apply such tests to a braneworld model with timelike extra-dimension in chapter 2. In the following chapter, we present a model-independent test of cosmic acceleration. We test the influences of local inhomogeneities on the expansion rate in chapter 4 and finally conclude.

CHAPTER 1

Cosmic expansion and supernovae type Ia

1. Cosmic expansion

1.1. Dynamics of the expanding universe. The fundamental equation for analyzing the dynamics of the expanding universe is the Einstein equation, which connects the curvature of space-time — described by the Einstein tensor $G_{\mu\nu} = R_{\mu\nu} - \frac{1}{2}Rg_{\mu\nu}$ — to the stress-energy tensor $T_{\mu\nu}$, where $g_{\mu\nu}$ denotes the metric. $R_{\mu\nu}$ and R are the Ricci tensor and scalar, respectively. While in the simplest form of the Einstein equation, the Einstein tensor is proportional to the stress-energy tensor, the most general form also includes a cosmological constant Λ:

$$G_{\mu\nu} + \Lambda g_{\mu\nu} = 8\pi G T_{\mu\nu} \ , \tag{1.1}$$

where G is the gravitational constant and the speed of light is set $c = 1$.

One can yield the Einstein equation by varying the Einstein-Hilbert action

$$S = \frac{1}{8\pi G}\int (R - 2\Lambda)\sqrt{-\det g_{\mu\nu}}\, dx^4 + \int L(g_{\mu\nu}, \phi)\sqrt{-\det g_{\mu\nu}}\, dx^4 \ . \tag{1.2}$$

$L(g_{\mu\nu}, \phi)$ is the Lagrange density of the matter fields ϕ.

A common assumption in cosmology is that the universe is homogeneous and isotropic. Any space-time that fulfils these assumptions can be described by the Friedmann-Robertson-Walker metric:

$$ds^2 = -dt^2 + a^2(t)\left(\frac{dr^2}{1 - kr^2} + r^2\left(d\theta^2 + \sin^2\theta\, d\phi^2\right)\right) \ , \tag{1.3}$$

where k denotes the spatial curvature, which equals zero for a flat universe. $k = 1$ corresponds to a closed and $k = -1$ to an open universe. $a(t)$ is the scale factor. We define its present value to be $a_0 = 1$.

The contents of the universe can be considered as a perfect fluid with energy density ρ and pressure p. Its stress-energy tensor is given by

$$T_{\mu\nu} = (\rho + p)u_\mu u_\nu + p g_{\mu\nu} \ , \tag{1.4}$$

where u_μ is the 4-velocity.

Inserting the metric and the stress-energy tensor into the Einstein equation leads to the Friedmann equations:

$$H^2 = \left(\frac{\dot{a}}{a}\right)^2 = \frac{8\pi G}{3}\rho - \frac{k}{a^2} + \frac{\Lambda}{3} \ , \tag{1.5}$$

$$\frac{\ddot{a}}{a} = -\frac{4\pi G}{3}(\rho + 3p) + \frac{\Lambda}{3} \ , \tag{1.6}$$

where $H = \dot{a}/a$ is the Hubble rate, which describes the expansion of the universe.

Combining these two equations, one obtains a continuity equation:

$$\frac{d}{dt}(a^3\rho) + p\frac{d}{dt}a^3 = 0 \ . \tag{1.7}$$

Introducing the volume expansion rate $\theta = \dot{V}/V = 3\dot{a}/a$, the continuity equation can be rewritten as

$$\dot{\rho} + \theta(\rho + p) = 0 \ . \tag{1.8}$$

Usually, the Friedmann equation (1.5) is given in terms of the present Hubble rate H_0 and dimensionless density parameters. These density parameters are defined using the critical density, which is the present energy density obtained from (1.5), when $k = 0$ and $\Lambda = 0$:

$$\rho_c = \frac{3H_0^2}{8\pi G} \ . \tag{1.9}$$

Then the dimensionless density parameter for the different contents of the universe are defined as (the index 0 always denotes the present day value):

non-relativistic matter:	$\Omega_m = \rho_{m0}/\rho_c$
radiation:	$\Omega_r = \rho_{r0}/\rho_c$
cosmological constant:	$\Omega_\Lambda = \Lambda/(8\pi G\rho_c)$
spatial curvature:	$\Omega_k = -3k/(8\pi G\rho_c)$

The non-relativistic matter consists of baryonic and cold dark matter. Radiation refers to photons as well as to relativistic particles. Note that we have listed here only the densities of the standard constituents of the universe. The energy density in (1.5) could, however, include also other terms than only matter and radiation. These possible terms are considered in a variety of different cosmological models.

The dimensionless density parameters as defined above are constants that reflect the present values. The actual matter density is, however, proportional to the volume and thus changes as a^{-3} as the universe expands. While also the photon number density is proportional to a^{-3}, this is not true for the energy density of the photons. Due to the expansion of the universe the photons are redshifted and the energy of a single photon decreases as a^{-1}. Thus the radiation energy density scales as a^{-4}. With the redshift z given by $1 + z = 1/a$, the Friedmann equation can be rewritten as:

$$\frac{H^2(z)}{H_0^2} = \Omega_m(1+z)^3 + \Omega_r(1+z)^4 + \Omega_\Lambda + \Omega_k(1+z)^2 \ . \tag{1.10}$$

While the radiation density is negligible in the late universe, it becomes important at high redshifts.

A more general form of the Friedmann equation is

$$\frac{H^2(z)}{H_0^2} = \sum_i \Omega_i(1+z)^{3(1+w_i)} \ , \tag{1.11}$$

where the sum is over all density parameters included in the considered cosmological model. $w_i = p_i/\rho_i$ is the equation of state. For non-relativistic matter, the pressure is negligible compared to the energy density. Therefore, one can assume $w_m = 0$. Radiation has an equation of state of $w_r = 1/3$. Spatial curvature and the cosmological constant have negative values, namely $w_k = -1/3$ and $w_\Lambda = -1$. Although w is a constant for the standard constituents of the universe, it can in general be a function of z.

Setting $z = 0$ in (1.11) leads to a constraint equation for the density parameters:

$$1 = \sum_i \Omega_i \ . \tag{1.12}$$

As we are not only interested in the expansion rate at a certain time, but also in its change, it is useful to introduce the deceleration parameter:

$$q = -\frac{\ddot{a}}{aH^2} = \frac{H'(z)}{H(z)}(1+z) - 1 \ . \tag{1.13}$$

A negative value of q would correspond to an accelerated expansion. When there is only one constituent with equation of state w, then the deceleration parameter can be calculated to be $q = \frac{1}{2}(1+3w)$. The universe expands accelerated if q is negative, i.e. if $w < -1/3$. Therefore, the cosmological constant with $w = -1$ can cause an acceleration.

1.2. Distance measures. In cosmology, distance is not uniquely defined. This is due to the expansion of the universe and the finite speed of light. Different ways of measuring distances, which would be equivalent in a non-expanding Euclidian space, lead to differing results in an expanding universe. In the following, we will summarize three important distance measures, which will be used in this thesis.

1.2.1. *Comoving distance.* The comoving distance is the distance two objects would have at the present time. This distance can obviously not be measured directly. As the speed of light is finite, we can only observe a past image of an object, the light of the object being emitted at a scale factor a_e. Although the distance to the object at the present scale factor a_0 can therefore not be directly observed, it can be inferred from other distance measurements. For a given cosmological model, the relation between the comoving distance r and the redshift z is given by:

$$r(z) = \frac{1}{H_0\sqrt{|\Omega_k|}}\, \mathcal{S}\left(\sqrt{|\Omega_k|}\int_0^z \frac{H_0}{H(\tilde{z})}\, d\tilde{z}\right) \ , \tag{1.14}$$

where $\mathcal{S}(x) = x$ for a flat, $\mathcal{S}(x) = \sin(x)$ for a closed and $\mathcal{S}(x) = \sinh(x)$ for an open universe.

1.2.2. *Luminosity distance.* A method to actually determine the distance to an object is to measure its flux F, provided its luminosity L is known. Then the luminosity distance d_L is defined by

$$F = \frac{L}{4\pi d_L^2} \ . \tag{1.15}$$

In Euclidian space, d_L would thus correspond to the physical distance. In an expanding universe, the photon number decreases as a^{-3} and the energy of each photon decreases due to redshift. Both effects decrease the measured flux and thus lead to an inferred luminosity distance, which is larger than the comoving distance:

$$d_L(z) = (1+z)\, r(z) = \frac{1+z}{H_0\sqrt{|\Omega_k|}}\, \mathcal{S}\left(\sqrt{|\Omega_k|}\int_0^z \frac{H_0}{H(\tilde{z})}\, d\tilde{z}\right) \ . \tag{1.16}$$

1.2.3. *Angular diameter distance.* When knowing the diameter D of an object, e.g. a galaxy, one can observe its angular size Θ and define the angular diameter distance d_A as:

$$\Theta = \frac{D}{d_A} \ . \tag{1.17}$$

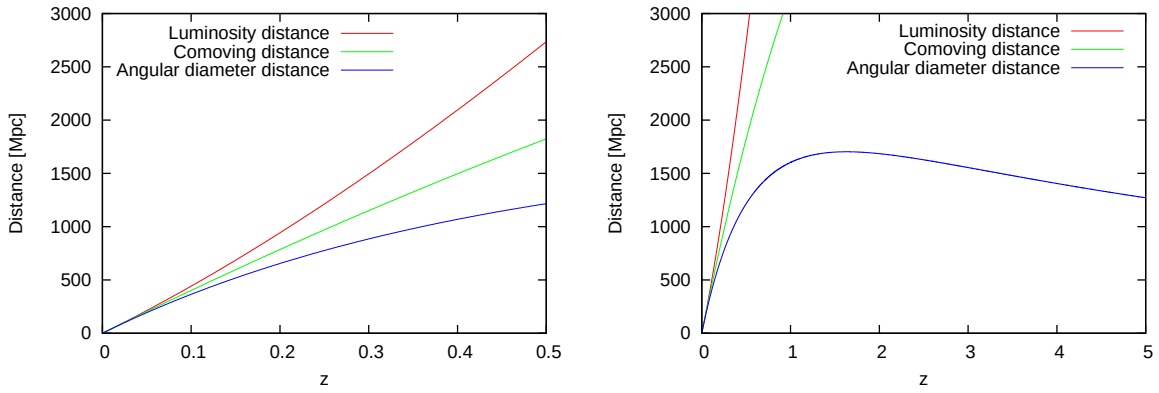

Figure 1.1: Different distance measures in a flat ΛCDM universe.

D can also be the distance between two objects, which is perpendicular to the line of sight of the observer. Here, one needs to take the distance at the time, when the light was emitted from the objects. Θ is then the angular separation of these objects.

The theoretical values of the angular diameter distance is smaller than that of the two above mentioned distance measures, namely:

$$d_A(z) = \frac{r(z)}{1+z} = \frac{1}{(1+z)H_0\sqrt{|\Omega_k|}}\,\mathcal{S}\left(\sqrt{|\Omega_k|}\int_0^z \frac{H_0}{H(\tilde{z})}\,d\tilde{z}\right)\,. \tag{1.18}$$

While the comoving and the luminosity distance to an object increase with increasing redshift of that object, this is not necessarily the case for the angular diameter distance. In a ΛCDM universe, $d_A(z)$ reaches its maximum at $z \simeq 1.6$. A comparison of the three distance measures is plotted in figure 1.1.

1.3. Models of dark energy.

1.3.1. *ΛCDM.* The cosmological constant was introduced by Einstein in order to allow for a static universe [**Ein17**]. When Hubble discovered the expansion of the universe in 1929 [**Hub29**], the general belief was that the cosmological constant is not needed anymore. This belief changed, when it was discovered in 1998 that the luminosity distances of supernovae Ia are more consistent with a cosmological model that includes Λ [**R$^+$98, P$^+$99**]. This result has been confirmed by recent supernova observations as well as by measurements of the cosmic microwave background (CMB) [**K$^+$09b**] and of baryon acoustic oscillations (BAO) [**T$^+$04, S$^+$05**].

The simplest model that is consistent with these observations is ΛCDM. This model contains, besides baryonic matter and radiation, a cosmological constant and cold dark matter (CDM). The baryonic matter makes up only about 5% of the energy density of the universe. The largest contribution comes from the cosmological constant with $\Omega_\Lambda = 0.73$. The remaining energy results from CDM. The universe seems to be very close to flat, which is in agreement with the scenario of cosmological inflation [**Gut81, Lin82, Lin83**].

The constraints from SNe, CMB and BAO on Ω_m and Ω_Λ assuming a ΛCDM model are shown in figure 1.2, where one can clearly see that a flat universe is preferred, when the results

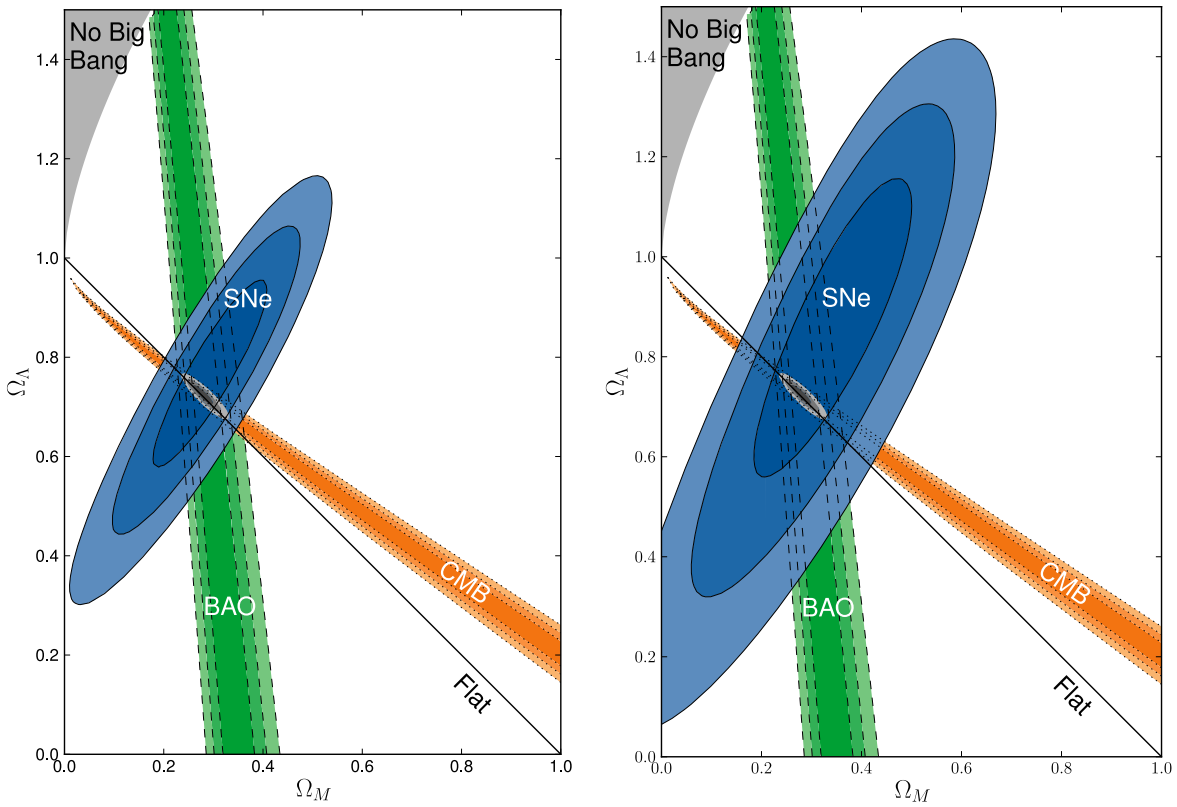

(a) without systematic errors (b) with systematic errors

Figure 1.2: 68.3%, 95.4% and 99.7% confidence regions in the $(\Omega_m, \Omega_\Lambda)$ plane assuming a ΛCDM model. Figure taken from [**A**$^+$**10**].

from all observations are combined. When allowing for an arbitrary equation of state for the dark energy component, the constraint on Ω_m and w are plotted in figure 1.3. Obviously, a cosmological constant, i.e. $w = -1$, is perfectly consistent with these observations.

Despite the great successes of ΛCDM, which describes the vast majority of observations very well, there are some observations, which do not seem to fit this model: The low multipoles of the CMB angular power spectrum are aligned, which seems quite unlikely when isotropy is assumed. Another problem with the CMB is that the two-point correlation function almost vanishes on large scales, which is in contradiction to ΛCDM [**CHSS10**]. A couple of other tensions between observations and ΛCDM are summarized in [**Per08**]: observed velocity flows, whose scale and amplitude are larger than predicted; the voids in the universe seem to be too empty; observed galaxy and cluster halo profiles are different from the predicted ones.

Besides these issues, there are some theoretical problems with the cosmological constant: the fine tuning problem and the coincidence problem.

- Fine tuning problem
  The cosmological constant is indistinguishable from vacuum energy and thus one might assume that this energy is the origin of Λ. But while the observed energy

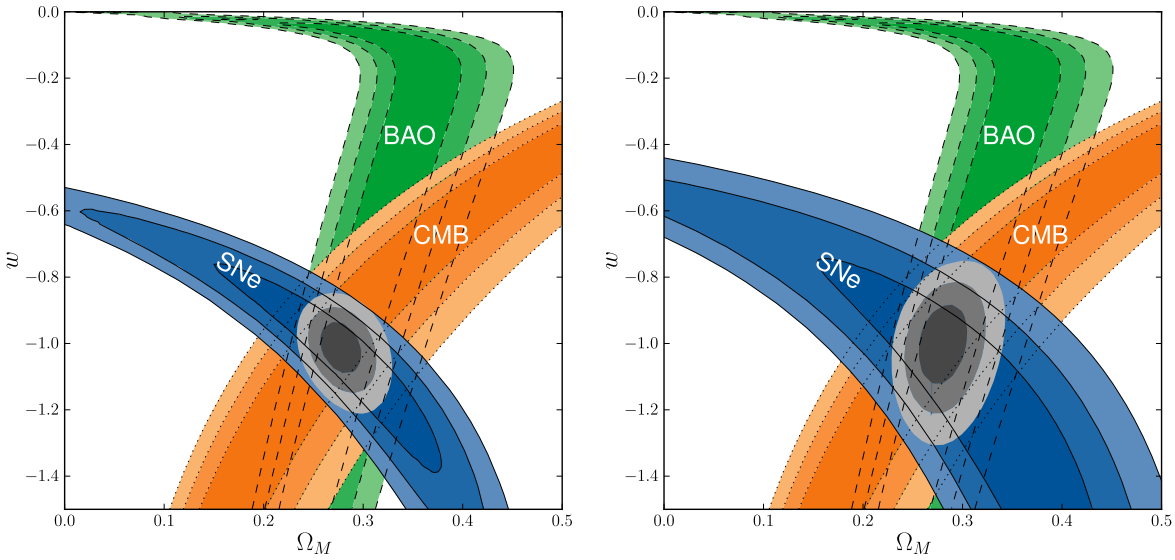

(a) without systematic errors (b) with systematic errors

Figure 1.3: 68.3%, 95.4% and 99.7% confidence regions in the (Ω_m, w) plane. Figure taken from [**A**$^+$**10**].

density of Λ is $\rho_\Lambda \simeq 10^{-47}\,\mathrm{GeV}^4$, the theoretical vacuum energy density ρ_{vac} is many orders of magnitude larger. The zero-point energy of a quantum field with mass m is given by:

$$\rho_{\mathrm{vac}} = \frac{1}{4\pi^2}\int_0^{k_{\mathrm{max}}} dk\, k^2 \sqrt{k^2+m^2}\ .$$

The result depends on the cut-off scale k_{max}, up to which one assumes quantum field theory to be valid. When assuming the Planck mass as cut-off scale ($k_{\mathrm{max}} = M_{\mathrm{P}}$), the vacuum energy density is $\rho_{\mathrm{vac}} \simeq 10^{74}\,\mathrm{GeV}^4$, which is about 10^{121} larger than ρ_Λ. Even if we use the electro-weak scale instead of the Planck scale, the value of the vacuum energy density $\rho_{\mathrm{vac}} \simeq 10^{-3}\,\mathrm{GeV}^4$ is still much too large.
Thus, from the current understanding we cannot identify the cosmological constant with vacuum energy. Moreover, cosmological constant plus vacuum energy need to sum up to the observed value ρ_Λ, which is many orders of magnitude smaller than ρ_{vac}. Thus, a lot of fine tuning is needed, which does not seem very natural.

- Coincidence problem
  While the energy density of the cosmological constant does not change with time, the matter density scales as a^{-3}. Nevertheless, today both densities have the same order of magnitude $\Omega_m \simeq \Omega_\Lambda$, which seems to be quite a coincidence. Since this argument sounds rather anthropic, one might reformulate it in the following way: The cosmological constant starts to dominate, when structure formation on the matter-radiation equality scale starts to evolve non-linear. This might either be a strange coincidence or it could imply that accelerated expansion is triggered by structure

formation. Such a mechanism for triggering acceleration is, however, not present in ΛCDM.

1.3.2. *Alternative theories.* Although, ΛCDM is often referred to as the standard model of cosmology, it is — due to its various problems — not as established as the standard model of particle physics. Consequently, a plethora of alternative cosmological models has been suggested over the past couple of years (for a review see [**CST06**]). While these theories try to avoid some of the problems present in the ΛCDM model, each model is troubled by its own problems.

Some of the models replace the cosmological constant by some other dark energy term, which causes acceleration. Such a term can be included in the stress-energy tensor in the Einstein equation and needs to have an equation of state with $w < -1/3$. There are, however, alternatives to dark energy. In the following, we will mention only a few cosmological models. A complete list would be far beyond the scope of this work.

- Quintessence
  Various scalar fields have been suggested as candidates for dark energy. An important example are quintessence fields ϕ, which are minimally coupled to gravity. The quintessence equation of state is given by
  $$w_\phi = \frac{\dot{\phi}^2 - 2V(\phi)}{\dot{\phi}^2 + 2V(\phi)} ,$$
  where $V(\phi)$ is the potential of the field. For $V(\phi) \gg \dot{\phi}^2$, w_ϕ is close to -1 and thus a cosmological constant is mimicked.
- f(R) gravities
  In these theories, R is replaced by a function $f(R)$ in the Einstein-Hilbert action (1.2). As this ansatz is rather general, one can find functions $f(R)$ that are consistent with cosmological observations. Gravity is, however, changed on all scales. Consequently, there are constraints on these models by tests of general relativity in the solar system [**KPRS07, HS07**].
- Braneworld models
  These models assume that there exist one or more extra-dimension(s) in addition to the usual four-dimensional space-time. The extra-dimension(s) affect the Einstein equation, which can lead to accelerated expansion. See chapter 2 for more details on this class of models.
- Lemaître-Tolman-Bondi models
  When giving up the assumption of global homogeneity, one can construct spherically symmetric models — Lemaître-Tolman-Bondi models — which are consistent with observations without introducing a dark energy term [**Cel00, AA07, EM07, IRWG08, GBH08**]. The problem with these models is that we need to be very close to the center of the universe, which is highly unlikely.
- Backreaction
  The influence of local inhomogeneities on the expansion of the universe is neglected in most cosmological models. According to the backreaction theory, these structures could, however, have a significant effect on the evolution of the universe. This might explain why the beginning of accelerated expansion coincides with non-linear structure formation. For more details on backreaction, see chapter 4.

2. Supernovae type Ia

2.1. Types of supernovae. Supernovae (SNe) are very luminous stellar explosions, which can be as bright as their host galaxy. There are different ways how SNe can occur. For SNe type Ib, Ic and II, their progenitors are thought to be massive stars with mass $M \gtrsim 8M_\odot$, where $M_\odot$ is the mass of the sun [**UB05**]. Over time these stars develop a layer structure, with heavy elements in the inner layers and hydrogen in the outer layer. This development takes place in subsequent stages with different nuclear fusion processes: When the supply of hydrogen in the core of the star is exhausted, helium fusion sets in while there is still hydrogen fusion in the outer layer. This stage is followed by carbon fusion in the core and subsequently by fusion of heavier elements. Finally, a core of iron develops and fusion stops in that core. Without the pressure that is caused by the fusion process, the electron degeneracy pressure can only support a certain amount of mass, the so-called Chandrasekhar limit, which is approximately $1.38M_\odot$. When the core of the star exceeds this limit, a gravitational collapse takes place and the core becomes a neutron star. The collapse causes a shock wave in the neutron star. Now there are two possibilities:

- The shock wave comes to a halt very fast. Then the neutron star keeps accreting matter from the outer layers. When it exceeds a mass of about $1.8M_\odot$, it collapses to become a black hole.
- The shock wave causes an expulsion of the outer layer — a supernova of type II or Ib/c occurs. The difference between type II and type Ib/c is that SNe Ib/c have already lost their outer hydrogen layer at an earlier time, while this layer is still present at the time of explosion for SNe II.

The mechanism for SN Ia is quite different. The progenitors of this type of SNe are thought to be carbon-oxygen white dwarfs in close binary star systems. The white dwarf accretes matter from its companion red giant. Shortly before the Chandrasekhar limit is reached, the temperature and density in the core of the white dwarf becomes large enough for carbon fusion to set in. This fusion process takes place within a very short time period, thus leading to an explosion of the white dwarf. In contrast to other types of SNe, the progenitors of SNe Ia therefore have approximately the same chemical composition and mass at the time of explosion. Consequently, all SNe Ia have more or less the same brightness, making them relatively good standard candles.

SNe are classified according to the absorption lines in their spectrum. The basic distinction is that (in contrast to type II SNe) type I SNe have no hydrogen lines in their spectrum. While type I SNe are further classified according to helium and silicon lines in their spectra, SN IIP and SN IIL are distinguished by the shape of their light-curves, i.e. the change in brightness over time (see table 1.1). The brightness of SNe IIL measured in magnitudes decreases linearly with time, while the light-curve of a SN IIP first reaches a plateau, where the brightness stays approximately constant for some time before it further decreases. SNe IIb show features of SN II, namely the hydrogen lines, in the early spectrum, but become helium dominated at later times, thus resembling SNe Ib. The spectra of some SNe Ia at different redshifts are shown in figure 1.4.

2.2. SNe Ia as standard candles. Standard candles are a class of objects that all have the same intrinsic brightness. In astronomy, the brightness of an object is usually measured logarithmically in magnitudes. Given two objects, their magnitudes, m_1 and m_2, and fluxes,

SN I	early spectrum does not contain hydrogen line	
	SN Ia	contains silicon line
	SN Ib	no silicon, helium rich
	SN Ic	no silicon, helium poor
SN II	early spectrum contains hydrogen line	
	SN IIP	hydrogen dominant, light-curve has a plateau before it further decreases
	SN IIL	hydrogen dominant, light-curve decreases linear in magnitude
	SN IIb	helium dominant

Table 1.1: Supernova classification according to the absorption lines in the spectrum and the shape of the light-curve.

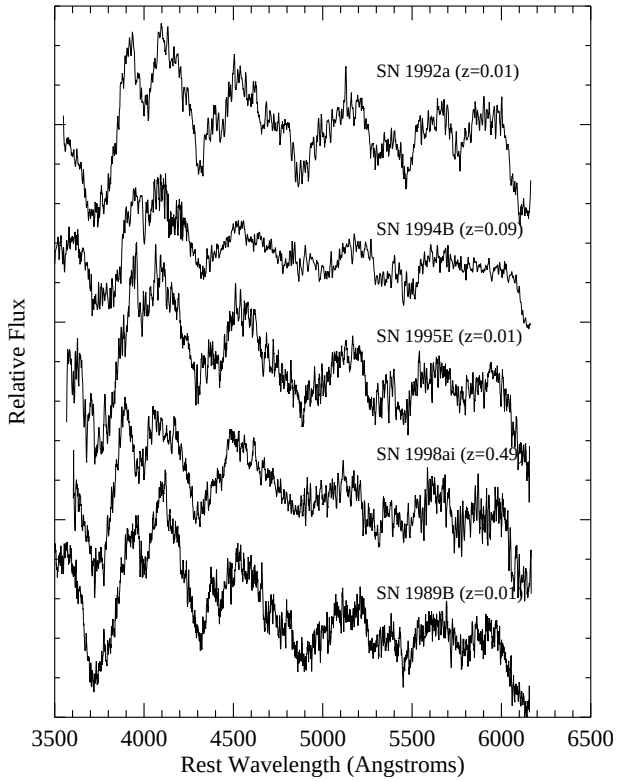

Figure 1.4: Spectra of SNe Ia at different redshifts. Figure taken from [**R**$^+$**98**].

F_1 and F_2, are related by:

$$m_1 - m_2 = 2.5 \log \frac{F_2}{F_1} \,, \tag{1.19}$$

where log denotes the logarithm with base 10. Thus, the brighter object has a smaller value of m. Vega is used as a reference star with $m = 0$. While the apparent magnitude m is

the magnitude actually measured by the observer, the absolute magnitude M refers to the magnitude measured at a distance of 10pc from the object.

Given the apparent and absolute magnitude of an object, one can define the distance modulus as

$$\mu = m - M \ , \tag{1.20}$$

which can be used as a measure of distance. The further the object is away, the larger is μ. The distance modulus is related to the luminosity distance via:

$$\mu(z) = 5 \log d_L(z) + 25 \ , \tag{1.21}$$

where $d_L(z)$ is given in units of Mpc.

For a set of standard candles with given absolute magnitude M, one can then measure their apparent magnitudes m_i to obtain observational values μ_i. Using equations (1.21) and (1.16), one can calculate the theoretical $\mu(z)$ for any cosmological model with a given Hubble rate $H(z)$. The model parameters can then be constrained by fitting $\mu(z)$ to the observed μ_i. In this way, standard candles are used for cosmological tests. Figure 1.5 shows the redshifts and distance moduli of the SNe published by Riess et al. [**R**$^+$**98**] that led to the discovery of accelerated expansion in a so-called Hubble diagram. The data have been obtained by using the MLCS light-curve fitter [**RPK96**] (see section 2.3 for more details on light-curve fitters). The observed data are compared to three different cosmological models, showing that introducing a cosmological constant leads to a better fit.

Observations show that the spectra, light-curve shapes and absolute magnitudes of the vast majority of SNe Ia are strikingly similar [**BT92**]. This is supported by the theory of these stellar explosions. SNe Ia are the explosions of white dwarfs that all have approximately the same mass at the time of the explosion. The light-curve of these SNe is then dominated by two decay processes, with the decay of ^{56}Ni being predominant in the first weeks and ^{56}Co becoming important at later times [**Bea10**]. Although one might assume that this mechanism implies that SNe Ia are very good standard candles, there is some variation in their peak brightness. There is, however, a strong correlation between the peak brightness and the width of the light-curve, which is given by the Phillips relation [**Phi93**]: The light-curves of the brighter SNe decreases more slowly than that of the fainter ones. Thus, it is possible to correct for this effect. Therefore, SNe Ia are standardizable candles, rather than standard candles.

The effect of applying the Phillips relation to the SN light-curves in order to standardize them can be seen in figure 1.6, which has been taken from Frieman et al. [**FTH08**]. The top panel shows measurements of the B-band magnitudes at different times with light-curves fitted to the data points. B-band means that a filter for blue light has been used for the observations. Day 0 is defined as the time, when the B-band magnitude reaches its maximum. In the plot, one can clearly see the correlation between peak brightness and the width of the light-curve. The 1-σ spread in the peak brightness is roughly 0.3 mag. This spread is significantly reduced, when the correction according to the Philips relation is applied, which can be seen in the bottom panel of the figure.

2.3. Observation of supernovae. In order to perform cosmological tests with SN data, one needs to know at least the redshift and the apparent magnitude of the SNe. For some tests, also the absolute magnitude is needed. While the redshift can be easily measured, the determination of the magnitudes is more complicated and is subject to systematic errors. In

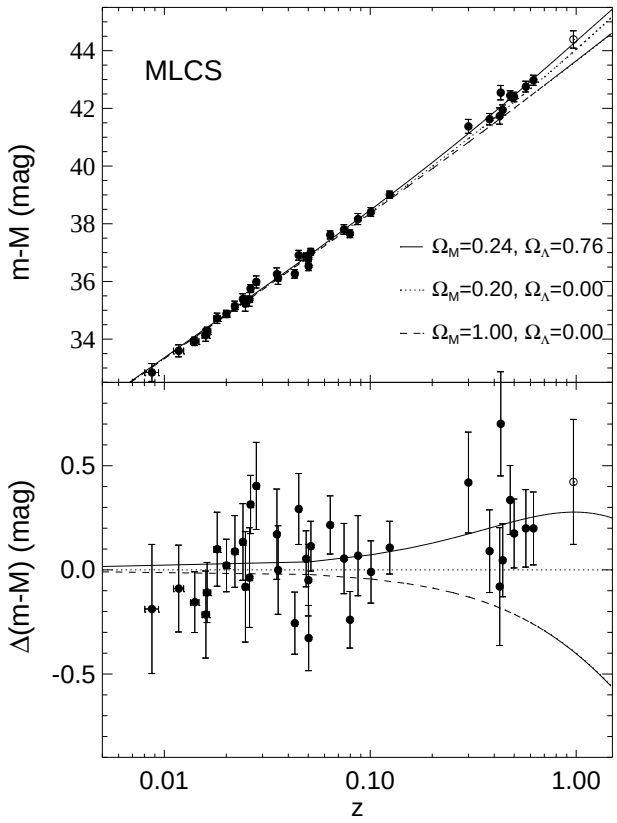

Figure 1.5: Hubble diagram for the SNe published by Riess et al. (1998). Also shown are three cosmological models. In the bottom panel, the distance modulus from the model with $\Omega_m = 0.20$ and $\Omega_\Lambda = 0.00$ is subtracted from the data. Figure taken from [$\mathbf{R}^+\mathbf{98}$].

this section, we will summarize some important aspects that need to be considered, when inferring the magnitudes from the raw observational data.

From the observational point of few, one needs to make sure that the SNe are observed at different times (preferably before and after the peak brightness is reached) and at different frequencies. Measurements of the apparent magnitude at different times are obviously needed in order to determine the light-curve of the SN and thus obtain the peak apparent magnitude. The shape of the light-curve is also needed to standardize the absolute magnitude of the SNe using the Phillips relation.

Observations at different frequencies are necessary because part of the light, that is emitted by the SN, is absorbed by dust (mainly host galaxy dust) before it reaches the observer. Thus, SNe appear fainter. Without correcting for extinction, one would infer a luminosity distance that is too large. Such a correction is, however, in principle possible as the amount of absorption depends on the frequency of the light. When knowing the intrinsic color of the SN (i.e. its magnitude in different frequency pass bands) and the absorption properties of the dust, one can thus reconstruct the total amount of extinction by measuring the magnitude in different frequency bands. These frequency bands are usually denoted by letters referring to the color: B stands for blue, V for visible and U for ultra-violet light and so on.

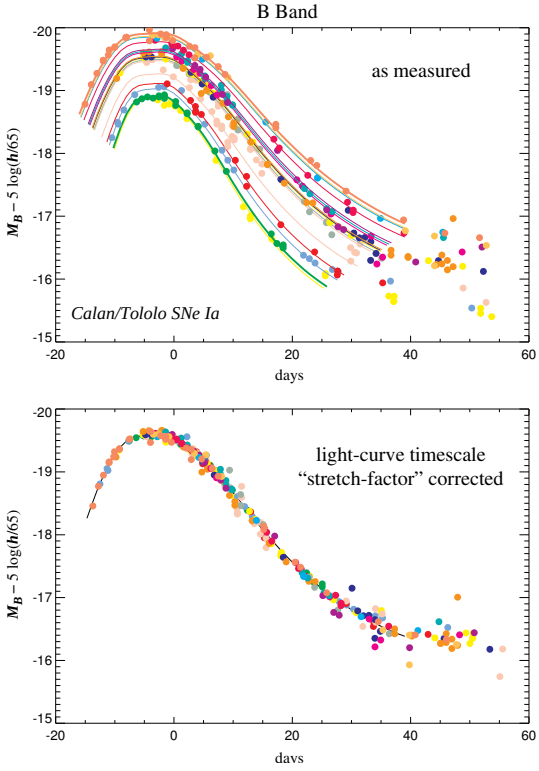

Figure 1.6: Top panel: Light-curves of low redshift SNe from the Calan-Tololo survey [**HPS$^+$96**], showing an intrinsic dispersion of 0.3 mag in peak absolute magnitude. Bottom panel: Light-curves after correction according to the Phillips relation. (Figure taken from Frieman et al. [**FTH08**])

Note that these are fixed frequencies as measured by the observer. Thus, in a survey the magnitudes of all SNe are measured e.g. in the B-band. As the light of the different SNe is, however, redshifted by a different amount, this observed frequency corresponds to differing frequencies emitted by the SNe. Therefore, the observed magnitudes cannot be directly compared. It is rather necessary to correct for the redshift. This process is called K-correction.

Part of the light emitted by a SN is absorbed or scattered by dust in the host galaxy. This effect changes the color of the SN as blue light is stronger absorbed than red light. The change in the observed color can be described by a single parameter — the reddening parameter R_V, which is defined as

$$R_V = \frac{A_V}{E_{B-V}} \,, \tag{1.22}$$

where A_V is the total extinction in the V-band and $E_{B-V} = A_B - A_V$ is the color excess, which denotes the difference in the extinction in the B-band compared to that in the V-band. In the Milky Way, the reddening parameter has been measured to be $R_V = 3.1$ [**FM07**].

In order to obtain the apparent magnitude from the observed magnitudes measured at different times and frequencies, one needs a light-curve fitter that corrects the observed values

for the above mentioned effects, namely the reddening of SN color and the correlation between the peak magnitude and the width of the light-curve. Here, we will consider two light-curve fitters MLCS2k2 [**JRK07**] and SALT [**GAN$^+$05**] and some modifications thereof. The two fitters use a different set of parameters to infer the apparent magnitude. Both models include, however, one parameter to describe the light-curve shape and one for the color. The main difference between the two fitters is that in MLCS2k2 it is assumed that all variations in the observed SN color are due to dust. In the original version of this fitter, the dust is assumed to have the same absorption properties as the dust in the Milky Way, i.e. $R_V = 3.1$. In contrast, SALT allows for arbitrary reasons for the variation in color. SALT rather fits the color parameter such that the scatter in the Hubble diagram is minimized. When assuming that the only reason for color variations is dust extinction, it interestingly turns out that the dust in the SN host galaxies must be quite different from the dust in the Milky Way [**C$^+$07**].

The absolute magnitude M of SNe can be determined if one knows the apparent magnitude m and the distance of a SN. The distance can be obtained by observing other standard candles in the same host galaxy as nearby SNe. Cepheids are such standard candles. They are pulsating variable stars with a certain period-luminosity relation. This relation is, however, different for cepheids in the Milky Way and cepheids in the Large Magellanic Cloud [**TSR03, STR04, T$^+$05**] and thus seems to depend on the metallicity[1] of the host galaxy. The actual dependence of the period-luminosity relation on the metallicity is discussed quite controversially. As this affects the determination of the cepheid distances, also the calibration of the absolute magnitude M of the SNe is subject to these systematics. In this work we will consider two very discrepant calibrations, namely that by Riess et al. [**R$^+$05**] and that by Sandage et al. [**S$^+$06**].

[1]Note that astronomers refer to all elements except hydrogen and helium as metals.

CHAPTER 2

Braneworlds with a timelike extra-dimension

1. The idea of extra-dimensions

1.1. Compact extra-dimensions. The idea that there could be one or more extra-dimensions in addition to the well-known four spacetime dimensions is quite old. In 1914 Nordström [**Nor14**] and a couple of years later Kaluza [**Kal21**] and Klein [**Kle26**] suggested an additional space dimension in order to unify gravity and the electromagnetic force. While those theories assume a five-dimensional spacetime, the later upcoming string theory (see e.g. [**GSW87a, GSW87b, Pol98a, Pol98b**]) needs at least 10 dimensions. However, our everyday life experience tells us that there are only three space and one time dimension. Therefore, one needs a mechanism to hide the extra-dimension(s). Until the late 90's, the way to do that was to assume that the extra-dimensions are compactified on a very small scale, with the compactification radius R_c being of the order of the Planck length $\ell_P \simeq 10^{-33}$cm.

Gravity has, however, only been tested on distances down to about 0.1mm [**K$^+$07**], i.e. 31 orders of magnitude larger than the Planck length. This provides the possibility of modifying gravity on a sub-millimeter scale by introducing extra-dimensions. Such a theory was proposed by Arkani-Hamed, Dimopoulos and Dvali in 1998 in order to solve the hierarchy problem [**AHDD98**]. They argue that the Planck mass might not be a fundamental quantity as it is so much larger than the electroweak scale, namely $M_{\rm P}/M_{\rm ew} \sim 10^{17}$. Instead a higher-dimensional Planck mass, which is of the same order as $M_{\rm ew}$, could be the fundamental quantity.

How the usual four-dimensional Planck mass and its higher-dimensional equivalent are connected, can be understood in the following way: We consider a model with n extra-dimensions. Then two particles with distance $r \ll R_c$ have the potential energy [**AHDD98**]

$$V(r) \sim \frac{m_1 m_2}{M_{\rm P(4+n)}^{2+n}} \frac{1}{r^{n+1}} \,, \tag{2.1}$$

where $M_{\rm P(4+n)}$ is the $(4+n)$-dimensional Planck mass. If the distance of the particles is, however, much larger than the compactification radius (i.e. $r \gg R_c$), then the potential energy is given by

$$V(r) \sim \frac{m_1 m_2}{M_{\rm P(4+n)}^{2+n} R_c^n} \frac{1}{r} \,. \tag{2.2}$$

By comparing this formula to classical Newtonian gravity one obtains

$$M_{\rm P}^2 \sim M_{\rm P(4+n)}^{2+n} R_c^n \,. \tag{2.3}$$

With two extra-dimensions and compactification radius of order 1mm[1], the six-dimensional Planck scale and the electroweak scale have the same order of magnitude [**AHDD98**].

1.2. Randall-Sundrum model. Only one year later, Randall and Sundrum proposed a model with a non-compact fifth dimension that can be infinitely large [**RS99a, RS99b**]. Again, the reason to introduce an additional dimension was to solve the hierarchy problem. According to this Randall-Sundrum (RS) model, five-dimensional spacetime, the so-called bulk, is bounded by two branes, where a brane is a four-dimensional spacetime. Then we would be living on one of these branes.

Following the argumentation of the previous section, an additional dimension is only compatible with observations if it is compactified on a radius $R_c \ll 0.1\text{mm}$. Thus, a non-compact extra-dimension does not seem to be possible. This problem can, however, be avoided if one uses a metric that is not factorisable. Randall and Sundrum suggest to multiply the four-dimensional metric by a so-called warp factor, which is a function of the fifth dimension. Then the five-dimensional metric is given by:

$$ds^2 = e^{-2k|y|}\eta_{ab}dx^a dx^b + dy^2 \,, \tag{2.4}$$

where k is a scale of the order of the Planck scale, x^a are the four-dimensional coordinates. $0 \leq y \leq R_c$ denotes the coordinate of the extra-dimension, where R_c is essentially the "compactification radius" which can be infinitely large. The locations of the branes are at $y = 0$ and $y = R_c$, respectively. Then, $R_c \to \infty$ can be considered as the case when there is only one existing brane.

In contrast to the case of compact extra-dimensions, where the four-dimensional Planck mass is proportional to R_c^n (with n being the number of extra-dimensions), in the Randall-Sundrum scenario it depends on R_c in the following way:

$$m^2 = \frac{M^3}{k}\left[1 - e^{-2kR_c\pi}\right] \,. \tag{2.5}$$

Here, m and M denote the four- and five-dimensional Planck masses, respectively. One can clearly see that m stays finite even if $R_c \to \infty$, which shows that an infinitely large extra-dimension is possible.

An important property of the RS model is that ordinary matter fields are confined to the brane, whereas gravity is influenced by the additional dimension(s). This is also true for other braneworld theories that have been proposed subsequent to the work of Randall and Sundrum. One of those models that has received a lot of attention is that suggested by Dvali, Gabadadze and Porrati, the so-called DGP model [**DGP00, DG01**]. As in all braneworld models gravity deviates from predictions of four-dimensional general relativity, there has been a lot of research on the question to what extent astrophysical and cosmological observations are affected by extra-dimensions. For reviews on these issues see [**Maa04, Koy08**].

2. A braneworld model

In this work, we consider a rather general braneworld model with one extra-dimension that has been suggested by Shtanov and Sahni [**SS03b, Sht02**]. According to their theory,

[1]Note that at that time gravity has only been tested on a centimeter scale. Thus, assuming a compactification radius of 1mm was justified.

the brane is the boundary of the five-dimensional bulk. The model is described by the action:

$$\begin{aligned} S &= M^3 \left[\int_{\text{bulk}} (\mathcal{R} - 2\Lambda_5) \sqrt{-\epsilon g}\, d^5x - 2\epsilon \int_{\text{brane}} K \sqrt{-h}\, d^4x \right] \\ &\quad + \int_{\text{brane}} (m^2 R - 2\sigma) \sqrt{-h}\, d^4x + \int_{\text{brane}} L(h_{ab}, \phi) \sqrt{-h}\, d^4x \,, \end{aligned} \tag{2.6}$$

where M and m are the five- and four-dimensional Planck masses, respectively. The two masses are related by an important length scale $\ell = 2m^2/M^3$. On short length scales ($r \ll \ell$) the usual four-dimensional general relativity is recovered, while on large length scales ($r \gg \ell$) five-dimensional effects play an important role [**SS03a, DGP00**]. $\mathcal{R}$ denotes the scalar curvature of the bulk metric g_{ab} and R the scalar curvature of the induced brane metric $h_{ab} = g_{ab} - \epsilon n_a n_b$, with n^a being the inner unit normal vector field to the brane. K is the trace of the extrinsic curvature of the brane $K_{ab} = h^c{}_a \nabla_c n_b$. Λ_5 denotes the bulk cosmological constant and σ the brane tension, which is connected to the brane cosmological constant Λ_4 via $\sigma = m^2 \Lambda_4$. As ordinary matter fields are confined to the brane, the Lagrangian density L does not depend on the bulk metric g_{ab}, but on the induced metric h_{ab}. Here, we neglect the theoretical possibility of five-dimensional matter fields in the bulk. In this rather general model, we allow the extra-dimension to be spacelike ($\epsilon = 1$) or timelike ($\epsilon = -1$).

The second line of equation (2.6) is just the action describing a four-dimensional ΛCDM universe. So, by setting the five-dimensional Planck mass M equal to zero, one regains classical general relativity. Also the RS and DGP braneworld models are included in the considered theory when assuming a spacelike extra-dimension. The results of the RS model are obtained by setting m to zero, e.g. in the generalized Einstein equations that are specified below. Analogously, one gets the DGP model by putting $\sigma = 0$ and $\Lambda_5 = 0$.

By variation of the action (2.6) one obtains Einstein equations in four and five dimensions [**SS03a, DGP00**]. In the bulk they read

$$\mathcal{G}_{ab} + \Lambda_5 g_{ab} = 0 \,. \tag{2.7}$$

They are equivalent to the usual four-dimensional Einstein equations with vanishing stress-energy tensor, but with the difference the tensors $\mathcal{G}_{ab}$ and g_{ab} are five-dimensional quantities. On the brane the equations differ from those of classical general relativity:

$$m^2 G_{ab} + \sigma h_{ab} = T_{ab} + \epsilon M^3 (K_{ab} - K h_{ab}) \,. \tag{2.8}$$

Here, we have an additional term including the extrinsic curvature. Note that the tensors in this equation are four-dimensional, i.e. their indices run from 0 to 3.

As we are interested in the expansion history of the universe, we need some form of Friedmann equation. In order to calculate this equation one has to consider that the intrinsic curvatures of the brane and the bulk as well as the extrinsic curvature are not independent quantities. They are, however, related by the Gauss-Codacci relation:

$$R_{abc}{}^d = h_a{}^f h_b{}^g h_c{}^k h^d{}_j \mathcal{R}_{fgk}{}^j + K_{ac} K_b{}^d - K_{bc} K_a{}^d \,. \tag{2.9}$$

Contracting this equation on the brane by multiplication with $h^{ac} h_d{}^b$ and considering the Einstein equations (2.7) and (2.8), one obtains:

$$\begin{aligned} &M^6 (R - 2\Lambda_5) - \frac{1}{3} \left(m^2 R - 4\sigma + T \right)^2 \\ &+ \left(m^2 G_{ab} + \sigma h_{ab} - T_{ab} \right) \left(m^2 G^{ab} + \sigma h^{ab} - T^{ab} \right) \;=\; 0 \,, \end{aligned} \tag{2.10}$$

where $T = h^{ab}T_{ab}$.

Until now, we have not made any assumptions about homogeneity or isotropy. Those assumptions are, however, necessary to proceed. Then, the above equation can be integrated under consideration of stress-energy conservation [**Sht02, Def01**]:

$$m^4\left(H^2+\frac{k}{a^2}-\frac{\rho+\sigma}{3m^2}\right)^2=\epsilon M^6\left(H^2+\frac{k}{a^2}-\frac{\Lambda_5}{6}-\frac{C}{a^4}\right)\,, \tag{2.11}$$

where a denotes the scale factor and $H=\dot{a}/a$ the Hubble rate. $k=0,\pm1$ corresponds to the spatial curvature. ρ is the matter density on the brane. C is an integration constant, the dark radiation term, which transmits bulk graviton influence onto the brane. Introducing the length scale $\ell=2m^2/M^3$ this equation can be written as an effective Friedmann equation on the brane:

$$H^2+\frac{k}{a^2} = \frac{\rho+\sigma}{3m^2}+\epsilon\frac{2}{\ell^2}\left[1\pm\sqrt{1+\epsilon\ell^2\left(\frac{\rho+\sigma}{3m^2}-\frac{\Lambda_5}{6}-\frac{C}{a^4}\right)}\right] \tag{2.12}$$

$$= \frac{\Lambda_5}{6}+\frac{C}{a^4}+\epsilon\frac{1}{\ell^2}\left[1\pm\sqrt{1+\epsilon\ell^2\left(\frac{\rho+\sigma}{3m^2}-\frac{\Lambda_5}{6}-\frac{C}{a^4}\right)}\right]^2\,. \tag{2.13}$$

The $\pm$-sign corresponds to the two different ways the brane can be embedded in the bulk. The model which is described by the equation with the lower sign will from now on be referred to as BRANE1 and the one with the upper sign as BRANE2.

Analogously to the usual dimensionless density parameters

$$\Omega_m=\frac{\rho_0}{3m^2H_0^2},\quad \Omega_k=-\frac{k}{a_0^2H_0^2},\quad \Omega_\sigma=\frac{\sigma}{3m^2H_0^2} \tag{2.14}$$

one can define

$$\Omega_\ell=\frac{1}{\ell^2H_0^2},\quad \Omega_{\Lambda_5}=-\frac{\Lambda_5}{6H_0^2},\quad \Omega_C=-\frac{C}{a_0^4H_0^2}\,. \tag{2.15}$$

Then the Friedmann equation can be rewritten as

$$\frac{H^2(z)}{H_0^2} = \Omega_m(1+z)^3+\Omega_k(1+z)^2+\Omega_\sigma + 2\epsilon\Omega_\ell\pm2\epsilon\sqrt{\Omega_\ell}\sqrt{\Omega_\ell+\epsilon\left[\Omega_m(1+z)^3+\Omega_\sigma+\Omega_{\Lambda_5}+\Omega_C(1+z)^4\right]} \tag{2.16}$$

$$= \Omega_k(1+z)^2-\Omega_{\Lambda_5}-\Omega_C(1+z)^4 + \epsilon\left[\sqrt{\Omega_\ell}\pm\sqrt{\Omega_\ell+\epsilon\left(\Omega_m(1+z)^3+\Omega_\sigma+\Omega_{\Lambda_5}+\Omega_C(1+z)^4\right)}\right]^2\,. \tag{2.17}$$

The first line of equation (2.16) is just the Friedmann equation in a ΛCDM model.

A constraint equation for the density parameters can be obtained by setting $z=0$ in equation (2.17):

$$1=\Omega_k-\Omega_{\Lambda_5}-\Omega_C+\epsilon\left[\sqrt{\Omega_\ell}\pm\sqrt{\Omega_\ell+\epsilon\left(\Omega_m+\Omega_\sigma+\Omega_{\Lambda_5}+\Omega_C\right)}\right]^2\,. \tag{2.18}$$

This is however not the only constraint that needs to be fulfilled. The terms under square roots in the Friedmann equation must not become negative within the considered redshift range. A detailed analysis for these constraints is given in section 3 for the braneworld model with timelike extra-dimension.

The described model is quite general. Depending on whether one considers a timelike or spacelike extra-dimension, the BRANE1 or the BRANE2 model and depending on the choice of parameter, the model can have very different properties. The model can mimic a ΛCDM model as well as a phantom-like or a quintessence-like model, both of which will approach a ΛCDM universe in the far future. The braneworld model can also be fine-tuned in a way that dark energy is just a transient phenomenon, i.e. dark energy is negligibly small in the past as well as in the future. The model can also give rise to some peculiar singularity, where the the scale factor and the Hubble parameter stay finite, while the deceleration parameter becomes singular. Those and other properties are in detail described in [**Sah05, SSV05, SS02**]. The special characteristics of a braneworld model with timelike extra-dimension are analyzed in the next section.

3. Timelike extra-dimension

3.1. General equations. In the following we will concentrate on a braneworld model with timelike extra-dimension. Some basic properties of this model have already been described in [**SS03b**]. We have done a more detailed analysis concerning parameter constraints and comparison with observations [**SC09**]. For reasons of clarity, we repeat the Friedmann equation for the braneworld model with timelike extra-dimension

$$\begin{aligned} \frac{H^2(z)}{H_0^2} &= \Omega_m(1+z)^3 + \Omega_k(1+z)^2 + \Omega_\sigma \\ &\quad - 2\Omega_\ell \mp 2\sqrt{\Omega_\ell}\sqrt{\Omega_\ell - [\Omega_m(1+z)^3 + \Omega_\sigma + \Omega_{\Lambda_5} + \Omega_C(1+z)^4]} \end{aligned} \tag{2.19}$$

and the according constraint equation

$$1 = \Omega_k - \Omega_{\Lambda_5} - \Omega_C - \left[\sqrt{\Omega_\ell} \pm \sqrt{\Omega_\ell - (\Omega_m + \Omega_\sigma + \Omega_{\Lambda_5} + \Omega_C)}\right]^2 . \tag{2.20}$$

While five of the density parameters can be chosen relatively freely, the sixth one is fixed by the constraint equation. We choose to determine Ω_σ by the other parameters. Using equation (2.20), we get:

$$\begin{aligned} \sqrt{\Omega_\ell} \pm \sqrt{\Omega_\ell - \Omega_m - \Omega_\sigma - \Omega_{\Lambda_5} - \Omega_C} &= \pm\sqrt{\Omega_k - \Omega_{\Lambda_5} - \Omega_C - 1} \\ \left[\sqrt{\Omega_\ell} \mp \sqrt{\Omega_k - \Omega_{\Lambda_5} - \Omega_C - 1}\right]^2 &= \left[\mp\sqrt{\Omega_\ell - \Omega_m - \Omega_\sigma - \Omega_{\Lambda_5} - \Omega_C}\right]^2 \\ \Omega_\sigma &= 1 - \Omega_m - \Omega_k \pm 2\sqrt{\Omega_\ell}\sqrt{\Omega_k - \Omega_{\Lambda_5} - \Omega_C - 1} \end{aligned} \tag{2.21}$$

So, Ω_σ is not uniquely determined. Note that the ±-sign in (2.21) does *not* correspond to the BRANE1 and BRANE2 models, respectively. In the following, we will refer to Ω_σ with the +-sign as positive brane tension and to the one with the −-sign as negative brane tension.

Additionally, the following inequalities have to be fulfilled:

$$\Omega_\ell \geq 0 \tag{2.22}$$

$$\Omega_\ell \geq \Omega_m + \Omega_\sigma + \Omega_{\Lambda_5} + \Omega_C \tag{2.23}$$

$$1 \leq \Omega_k - \Omega_{\Lambda_5} - \Omega_C \tag{2.24}$$

where the first inequality follows directly from the definition $\Omega_\ell = 1/(\ell H_0)^2$ and the other two follow from the claim that the terms under the square roots in (2.20) and (2.21) do not become negative.

If the above conditions are fulfilled, the Friedmann equation has a physical solution at present time. However, when going to higher redshifts, either the term under the square root in (2.19) or the complete right hand side can eventually become zero. From that point on it is impossible to go to higher redshifts. The two mentioned cases are quite different. If $H(z)^2$ becomes zero at a certain redshift (with the term under the square root staying strictly positive), a bounce takes place, i.e. at earlier times the universe was collapsing and then started expanding again at a certain point.

The case when the term under the square root becomes zero needs further analysis. Let us say that happens at redshift z^*. Then,

$$\frac{H^2(z^*)}{H_0^2} = \Omega_m(1+z^*)^3 + \Omega_k(1+z^*)^2 + \Omega_\sigma - 2\Omega_\ell \ . \tag{2.25}$$

So, the Hubble rate as well as the scale factor $a = 1/(1+z^*)$ stay finite at that point. This is, however, not true for the deceleration parameter q. Its general formula for the considered braneworld model is

$$\begin{aligned} q(z) &= \frac{H'(z)}{H(z)}(1+z) - 1 \\ &= \frac{H_0^2}{2H^2(z)}\Big[3\Omega_m(1+z)^3 + 2\Omega_k(1+z)^2 \\ &\qquad \pm \sqrt{\Omega_\ell}\frac{3\Omega_m(1+z)^3 + 4\Omega_C(1+z)^4}{\sqrt{\Omega_\ell - [\Omega_m(1+z)^3 + \Omega_\sigma + \Omega_{\Lambda_5} + \Omega_C(1+z)^4]}}\Big] - 1 \ . \end{aligned} \tag{2.26}$$

Here, the square root that becomes zero occurs in the denominator. Therefore,

$$\lim_{z\to z^*} q(z) \to \pm\infty \ .$$

This is a kind of singularity that is unknown to standard cosmology: While the sale factor and the Hubble rate are finite, the universe experiences an infinitely large acceleration or deceleration. In the case of acceleration (i.e. in the BRANE1 scenario), this can be considered as an alternative Big Bang without the problem of infinite energy density. The corresponding singularity for a braneworld model with spacelike extra-dimension has been described in [**SS02**].

3.2. Flat universe without dark radiation. We have seen that either a bounce or a singularity can occur within the framework of the considered braneworld model. However, these scenarios could have happened only at very high redshift, as otherwise there would be a contradiction to observations. Thus, we claim that none of these events took place between now and the time of recombination. That claim leads to strong constraints on the density parameters.

For simplicity, we restrict the analysis of these constraints to the case of a flat universe without dark radiation, i.e. $\Omega_k = 0$ and $\Omega_C = 0$. Then, the only density parameter that scales with redshift is the matter density. The constraints depend strongly on whether one considers a BRANE1 or BRANE2 model and on the choice of the brane tension. Therefore, we discuss these different cases separately. Keep in mind that in all cases the inequalities $\Omega_\ell \geq 0$ and $\Omega_{\Lambda_5} \leq -1$ must be fulfilled.

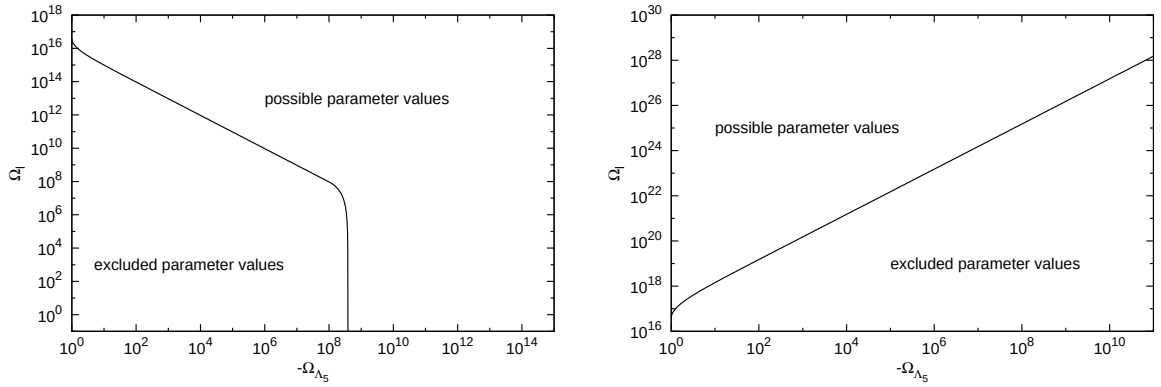

(a) negative brane tension (b) positive brane tension

Figure 2.1: Constraints on the density parameters Ω_ℓ and Ω_{Λ_5} of a BRANE1 model with matter density $\Omega_m = 0.3$.

3.2.1. *BRANE1.* In order to get a physical solution for the Friedmann equation, neither the right hand side of (2.19) nor the term under the square root must become negative for all redshifts at least up to the time of recombination ($z \simeq 1100$). Thus, inequalities

$$\Omega_m(1+z)^3 + \Omega_\sigma - 2\Omega_\ell + 2\sqrt{\Omega_\ell}\sqrt{\Omega_\ell - \Omega_m(1+z)^3 - \Omega_\sigma - \Omega_{\Lambda_5}} \geq 0 \tag{2.27}$$

and

$$\Omega_m(1+z)^3 \leq \Omega_\ell - \Omega_{\Lambda_5} - \Omega_\sigma \tag{2.28}$$

have to be fulfilled, where the brane tension is given by

$$\Omega_\sigma = 1 - \Omega_m \pm 2\sqrt{\Omega_\ell}\sqrt{-1-\Omega_{\Lambda_5}}\ . \tag{2.29}$$

We want to reformulate the above inequalities in a way that one can easily see how one of the density parameters is constrained by the others. Here, we only show the results of this reformulation. The detailed calculations can be found in appendix E.

In the case of a *negative* Ω_σ, either the inequality

$$\Omega_\ell \geq \left(\frac{\Omega_m(1+z_{\text{rec}})^3 + 1 - \Omega_m}{2\left(\sqrt{-\Omega_{\Lambda_5}} + \sqrt{-\Omega_{\Lambda_5}-1}\right)} \right)^2 \tag{2.30}$$

or the inequalities

$$\begin{aligned} \sqrt{\Omega_\ell} &\geq \sqrt{\Omega_m(1+z_{\text{rec}})^3 - \Omega_m} - \sqrt{-1-\Omega_{\Lambda_5}} \quad \text{and} \\ \Omega_\ell &\leq -\Omega_{\Lambda_5} \end{aligned} \tag{2.31}$$

have to be fulfilled, where $z_{\text{rec}} \simeq 1100$ is the redshift at recombination. Assuming that Ω_m is of the same order of magnitude as in a ΛCDM model, this means that at least one of the parameters Ω_ℓ and $|\Omega_{\Lambda_5}|$ needs to be very large as can be seen in figure 2.1a.

For the *positive* brane tension, the constraints are even stronger. Here,

$$\Omega_\ell \geq \left(\frac{\Omega_m (1+z)^3 + 1 - \Omega_m}{2\left(\sqrt{-\Omega_{\Lambda_5}} - \sqrt{-\Omega_{\Lambda_5} - 1}\right)} \right)^2 \tag{2.32}$$

must be fulfilled. In this case Ω_ℓ needs to be very large, which is shown in figure 2.1b.

3.2.2. *BRANE2.* We start with the two constraints

$$\Omega_m (1+z)^3 + \Omega_\sigma - 2\Omega_\ell - 2\sqrt{\Omega_\ell}\sqrt{\Omega_\ell - \Omega_m (1+z)^3 - \Omega_\sigma - \Omega_{\Lambda_5}} \geq 0 \tag{2.33}$$

and

$$\Omega_m (1+z)^3 \leq \Omega_\ell - \Omega_{\Lambda_5} - \Omega_\sigma \tag{2.34}$$

For the *positive* brane tension, they imply that

$$\Omega_\ell \leq \frac{1}{4\left(\sqrt{-\Omega_{\Lambda_5}} - \sqrt{-1 - \Omega_{\Lambda_5}}\right)^2} \tag{2.35}$$

as well as

$$\Omega_\ell \geq \left(\sqrt{\Omega_m (1+z)^3 - \Omega_m} + \sqrt{-1 - \Omega_{\Lambda_5}} \right)^2 \tag{2.36}$$

(see appendix E for the calculations). Both inequalities must be fulfilled simultaneously, which is only possible for small redshifts $z \lesssim 0.2$. As this is in contradiction to our claim that the constraints are fulfilled up to z_{rec}, we can rule out a BRANE2 model with positive brane tension in the case of vanishing spatial curvature and dark radiation.

For the *negative* brane tension, we get

$$\left(\sqrt{\Omega_m (1+z)^3 - \Omega_m} - \sqrt{-1 - \Omega_{\Lambda_5}} \right)^2 \leq \Omega_\ell \leq \frac{1}{4\left(\sqrt{-\Omega_{\Lambda_5}} + \sqrt{-1 - \Omega_{\Lambda_5}}\right)^2}\,, \tag{2.37}$$

which can only be fulfilled if

$$\Omega_m (1+z)^3 - \Omega_m \leq \frac{1}{4}\left(\sqrt{-\Omega_{\Lambda_5}} + \sqrt{-1 - \Omega_{\Lambda_5}} \right)^2\,. \tag{2.38}$$

Inserting this into (2.37) leads to

$$\Omega_\ell \leq \frac{1}{4\left(\sqrt{-\Omega_{\Lambda_5}} + \sqrt{-1 - \Omega_{\Lambda_5}}\right)^2} \tag{2.39}$$

$$\leq \frac{1}{16\left(\Omega_m (1+z)^3 - \Omega_m\right)} \tag{2.40}$$

Assuming $\Omega_m = 0.3$ and claiming that the above inequalities are at least valid up to z_{rec}, we find that $\Omega_{\Lambda_5} \gtrsim -2 \cdot 10^8$ and $\Omega_\ell \lesssim 1.6 \cdot 10^{-10}$ must be fulfilled for the BRANE2 model with negative brane tension.

In contrast to the BRANE1 model, where a very large value of Ω_ℓ was necessary, now this value needs to be very small. Remember that the definition of this density parameter is $\Omega_\ell = 1/(\ell^2 H_0^2)$, where $\ell = 2m^2/M^3$. As m is known precisely and H_0 has been determined at about 10% precision, the size of Ω_ℓ only depends on the size of the five-dimensional Planck mass M. The initial motivation to consider large extra-dimensions was to solve the hierarchy problem (see section 1). If we want our model not only to describe the expansion history of the universe, but also solve the hierarchy problem, then m/M should be roughly 10^{17}. Inserting this value, we get $\Omega_\ell \sim 6 \cdot 10^{17}$. Thus, we expect large values of Ω_ℓ, which is in

contradiction with the constraints of the BRANE2 model. However, fulfilling the constraint $\Omega_\ell \lesssim 1.6 \cdot 10^{-10}$ implies that $m/M \gtrsim 4 \cdot 10^{21}$, which would ameliorate the hierarchy problem, but would not solve it.

4. Test of the BRANE1 model

In this section, we want to test, whether the braneworld model with timelike extra-dimension is compatible with observations. Here, we allow for arbitrary spatial curvature and a non-vanishing dark radiation term. When constraining the parameter space by theoretical considerations, we restricted ourselves to the case of vanishing spatial curvature and dark radiation. Then the BRANE2 model with positive brane tension could be ruled out and the one with negative brane tension is not suitable to solve the hierarchy problem. For the BRANE1 model with negative brane tension the parameter space was less constrained than for the one with positive brane tension. Therefore, we only consider this model for the cosmological test, even though we give up the assumptions $\Omega_k = 0$ and $\Omega_C = 0$.

4.1. Fit to supernova type Ia data. Supernovae type Ia (SN Ia) are very often used for cosmological tests as they are the best standard candles known so far. When knowing the Hubble rate of a certain model, the analysis is in principle quite simple. One starts by calculating the luminosity distance

$$d_L(z) = \frac{1+z}{H_0\sqrt{|\Omega_k|}}\, \mathcal{S}\left(\sqrt{|\Omega_k|}\int_0^z \frac{H_0}{H(\tilde{z})}\, d\tilde{z}\right) , \tag{2.41}$$

where $\mathcal{S}(x) = x$ for a flat, $\mathcal{S}(x) = \sin(x)$ for a closed and $\mathcal{S}(x) = \sinh(x)$ for an open universe. Then, the distance modulus is given by

$$\mu(z) = m(z) - M = 5 \log d_L(z) + 25 , \tag{2.42}$$

where d_L is given in units of Mpc. $m(z)$ and M are the apparent and the absolute magnitude, respectively.

Given the redshift z_i and the distance modulus μ_i for each SN, we can fit the theoretical curve $\mu(z)$ (which depends on the density parameters and on H_0) to the data. As data set, we used the 2007 Gold sample, published by Riess et al. [**R**$^+$**07**]. In order to fit the data, one needs to chose a calibration, i.e. a certain value for the absolute magnitude M. We decided to take the calibration obtained by Riess et al. [**R**$^+$**05**]. In this calibration the V-band magnitude M_V at the time of the B-band maximum is $M_V(t_0) = -19.17 \pm 0.07$mag, while in the Gold sample $M_V(t_0)$ was considered to be -19.44mag. Therefore, we had to subtract 0.27mag from the distance moduli given in the data set. The value of the present Hubble rate corresponding to this calibration is $H_0 = 73 \pm 4(\text{statistical}) \pm 5(\text{systematic})$.

Although the concept of the test is quite simple, the actual χ^2-fit turns out to be somewhat problematic. There are multiple local minima for χ^2, many of which have the same value of χ^2. Part of the fit results could be dismissed at once, since their parameter values lead to the case where the Hubble rate becomes zero before z_{rec} is reached. Yet, we are left with a variety of different fit results, which makes it impossible to determine the actual parameter values in the considered model. Nevertheless, it turned out that Ω_k was always negative when we fitted all five parameters $(\Omega_m, \Omega_\ell, \Omega_{\Lambda_5}, \Omega_C, \Omega_k)$. Typically, the values for Ω_k were between -0.2 and -0.6. Thus, a closed universe is clearly favored in the considered braneworld model. The size of the spatial curvature is quite surprising. WMAP measurements suggest that Ω_k is close to zero [**K**$^+$**10**]. It is, however, not clear, if those results are also valid for braneworld models

	Ω_m	Ω_ℓ	Ω_{Λ_5}	Ω_C	Ω_k	$\chi^2_{\rm dof}$
5-parameter fit	0.38	$1.9 \cdot 10^{14}$	$-7.8 \cdot 10^{16}$	-1.15	-0.45	0.89
4-parameter fit	0.27	$1.7 \cdot 10^{15}$	$-6.0 \cdot 10^{13}$	-0.17	0	0.89
3-parameter fit	0.31	$2.0 \cdot 10^{14}$	$-1.5 \cdot 10^{16}$	0	0	0.91
ΛCDM	0.28		$\Omega_\Lambda = 0.72$			0.90

Table 2.1: Results of the χ^2-fits for 3-, 4- and 5-parameter fits of the BRANE1 model with negative brane tension and for ΛCDM.

as until now nobody has accomplished to predict the fluctuations in the CMB within the framework of extra-dimensions. Another result of the fit was that Ω_C needs to be negative. In the few fits when Ω_c came out positive, the result had to be rejected as the term under the square root in the Friedmann equation (2.19) became negative before $z = z_{\rm rec}$ was reached.

A typical example of best fit parameters is given in table 2.1 in the line "5-parameter fit". The χ^2 per degree of freedom is 0.89 and thus slightly better than that of ΛCDM with 0.90. Besides the mentioned problem with the size of the spatial curvature, there also seems to be a problem with Ω_C. The dark radiation term scales with $(1+z)^4$. Therefore, we would expect it to be very small at the present epoch, similar to the normal radiation density. If the value $\Omega_C = -1.15$ was true, then the dark radiation density must have been extremely large in the early universe.

In order to avoid the mentioned problems, we started by restricting the model to the flat case $\Omega_k = 0$. Thus, we fitted the four density parameters Ω_m, Ω_ℓ, Ω_{Λ_5} and Ω_C. Again, the χ^2 per degree of freedom is 0.89. An example of best fit parameters can be found in table 2.1. The absolute value of Ω_C has decreased compared to the previous fit, but still seems to be quite large. Therefore, we fixed $\Omega_C = 0$ in addition to $\Omega_k = 0$ and fitted the remaining three parameters Ω_m, Ω_ℓ and Ω_{Λ_5}. The χ^2 per degree of freedom has become slightly worse compared to the previous fits and to ΛCDM, namely $\chi^2_{\rm dof} = 0.91$. The density parameters given in table 2.1 have reasonable values. Figure 2.2 shows the tree braneworld fits and the ΛCDM fit compared to the SN data from the Gold sample. Here, $\Delta\mu$ is the distance modulus minus the distance modulus of an empty universe.

4.2. Angular separation. It is not surprising that the braneworld model can fit the SN data. In order to find out whether the model is actually a viable theory, we need to check its consistency with other observational data. One simple cosmological test is to take a look at the angular separation. The angle $\Theta(z)$ under which we see two objects in the universe depends on the cosmological model. As the universe expands, the distance $D(z)$ between those objects changes as

$$D(z) = \frac{D_0}{1+z}\,, \tag{2.43}$$

where $D_0 = D(z=0)$ is the separation in the present universe. The angular separation is described by

$$\Theta(z) = \frac{D(z)(1+z)^2}{d_L(z)} = \frac{D_0(1+z)}{d_L(z)}\,. \tag{2.44}$$

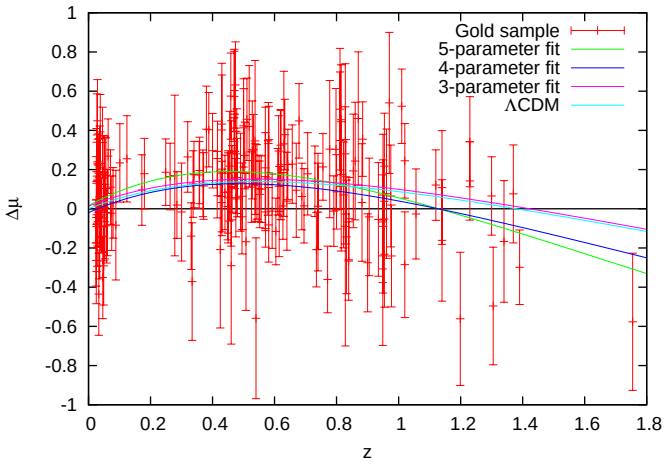

Figure 2.2: Distance modulus minus the distance modulus of an empty universe for the three braneworld model fits and ΛCDM.

The large-scale correlation function of luminous red galaxies has been obtained from Sloan Digital Sky Survey data showing a peak at 100 h^{-1} Mpc [**E$^+$05**]. The average redshift of those galaxies is $z = 0.35$. Assuming $h = 0.73$, we can determine the present separation to be $D_0 = 185$ Mpc. If one uses this typical distance of large objects in the present universe and calculates Θ for $z = z_{\text{rec}}$ with the above formula, the resulting angle should be a typical value for the structure observed in the CMB.

Figure 2.3 shows the angular separation as a function of redshift for the best fit parameters obtained from the three braneworld fits and the ΛCDM fit. In the ΛCDM universe, $\Theta(z_{\text{rec}}) = 47$ arcmin, which is approximately where the first peak of the CMB power spectrum is located. Thus, ΛCDM is perfectly consistent with the observations. On the other hand that means that the value $\Theta(z_{\text{rec}})$ of the braneworld models must be close to the value in the ΛCDM case. This is true for the best fit parameters of the 3-parameter fit. The values of $\Theta(z_{\text{rec}})$ for the 4- and 5-parameter fits are, however, much too large. This problem does not only occur in the case of the given examples. The absolute value Ω_C always turns out to be unexpectedly large, if it is not fixed by hand. That seems to cause the problem as it significantly increases the value of $H(z)$ at high redshifts, which leads to a larger angular separation $\Theta(z)$.

While the results of the 4- and 5-parameter fits can be clearly ruled out by the angular separation test, the result of the 3-parameter fit is almost indistinguishable from ΛCDM model as far as the distance modulus and the angular separation are concerned.

4.3. Other observations. Unfortunately, at the moment it is not possible to predict the anisotropies in the cosmic microwave background within the framework of a braneworld model, despite the fact that there has been some noticeable progress on that field during the past years. For a review on these issues see [**Maa04**]. Thus, we have to restrict ourselves to some simpler tests, namely: a) Determining the maximum possible redshift z_{max} in order to find out, if there is any contradiction to Big Bang nucleosynthesis (BBN) and b) calculating the age of the universe, which could be in conflict with the age of objects in the universe. Until now, we have neglected the normal radiation density Ω_r because it is very small compared

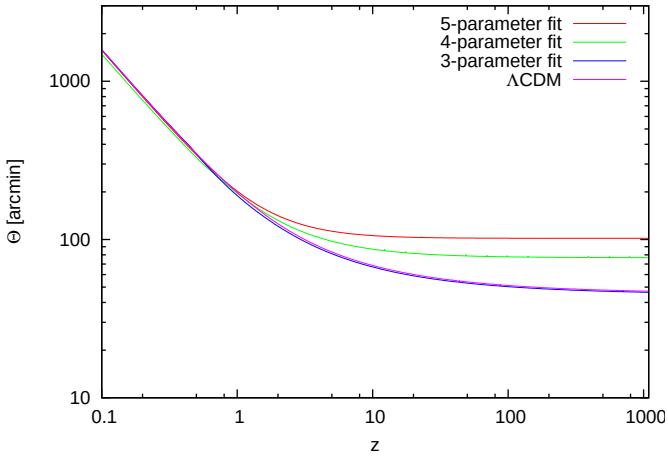

Figure 2.3: Angular separation for the three braneworld model fits and ΛCDM.

	$\Theta(z_{\mathrm{rec}})$[arcmin]	z_{max}	t_0 [Gyr]
5-parameter fit	104	∞	10.4
4-parameter fit	77	∞	12.9
3-parameter fit	46	120 000	15.0
ΛCDM	47	∞	13.2

Table 2.2: Angular separation Θ at recombination, maximum redshift z_{max} and age of the universe t_0 for the different fits.

to the other densities within the considered redshift range. For the calculation of the two mentioned quantities, we need to go back to very high redshifts, where the radiation density becomes important. Therefore, we have to add $\Omega_r(1+z)^4$ to $\Omega_m(1+z)^3$ every time it occurs in the Friedmann equation (2.19), where we assume $\Omega_r = 8.4 \cdot 10^{-5}$ [**K$^+$09b**].

The maximum possible redshift is the redshift beyond which there is no physical solution of the Friedmann equation. It turns out that the redshift is only limited for the result of the 3-parameter fit (see table 2.2). The age of the universe is calculated via

$$t_0 = \int_0^\infty \frac{dz}{(1+z)H(z)} \,. \tag{2.45}$$

The results are shown in table 2.2. Also given is the age for ΛCDM model. Note that this result, which is obtained by only considering the SN data from the Gold sample, is smaller than the age of the universe that is obtained by a combination of observation, with $t_0 = 13.78$ Gyr [**K$^+$10**].

For the interpretation of these results, we focus on the 3-parameter fits since the result from the other braneworld fits have already been excluded. In this model, the universe would be 15 billion years old and thus significantly older than in a ΛCDM model. The age of a ΛCDM universe is not in conflict with the oldest objects in the universe, e.g. with the oldest

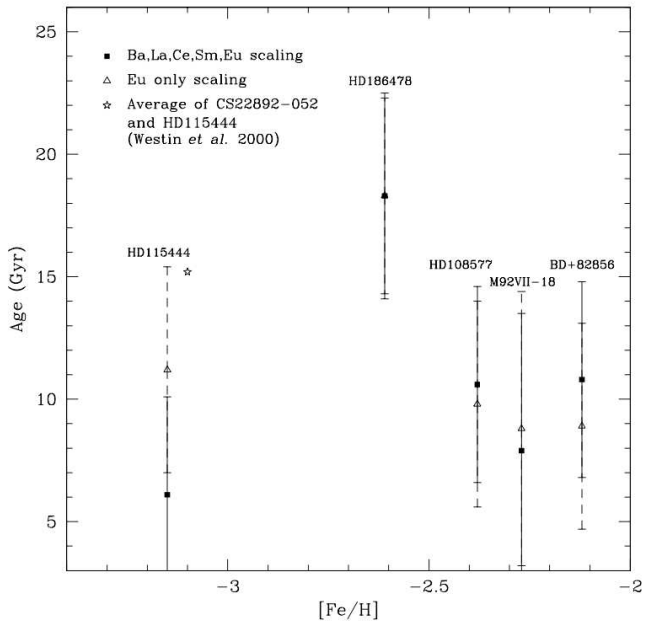

Figure 2.4: Ages of stars from Th abundances. Figure taken from [**JB01**].

known object in the Milky Way, the star HE 1523-0901 with an estimated age of 13.2±0.7 Gyr [**F**$^+$**07**]. Other age estimates of stars obtained from Th abundances are given in figure 2.4. Their average age is 11.4 Gyr. Thus, there is no problem concerning the age of the braneworld model.

BBN is, however, an issue. The maximum redshift of the 3-parameter fit is much smaller than the redshift of nucleosynthesis $z_{\mathrm{BBN}} \simeq 10^9$. We can solve this problem by reintroducing the dark radiation term Ω_C. However, its value must be small enough to ensure that the fit result and the cosmological tests up to the redshift of recombination are not affected. On the other hand, Ω_C needs to be larger than the radiation density Ω_r to prevent the term under the square root of the Friedmann equation from becoming negative. Thus, we choose Ω_C to be of order -10^{-4}. Then the model is radiation dominated at very high redshifts, just like the ΛCDM model. There is no limit to the redshift any more and the model is consistent with BBN observations as it does not differ from ΛCDM at these redshifts.

As a final test, we want to check, whether there is any conflict with tests of general relativity. As mentioned earlier, in the braneworld model the usual four-dimensional general relativity is regained on length scales that are much smaller than ℓ. Taking the fit result $\Omega_\ell = 2 \cdot 10^{14}$ and assuming $H_0 = 73$ km/(s Mpc), one obtains $\ell \simeq 300$ pc. Thus, especially the tests of general relativity within the solar system are not affected by any five-dimensional effects.

4.4. Conclusion. We have considered a braneworld model with a single timelike extra-dimension. After applying several cosmological tests, we have found parameter values that are consistent with observations. However, a lot of fine-tuning has been necessary to find

viable parameters, which does not make the model specifically attractive. Inserting the obtained parameter values into the equation for the deceleration parameter (2.26), we find an accelerated expansion at the present time with $q_0 = -0.7$.

In this work, we have only considered cosmological tests as our main goal is to examine the expansion history of the universe. Thus, we have analysed the impact of the additional time dimension on general relativity. For the various other aspects of a second time-dimension that have previously been studied, see [**BDA98, A$^+$00, Bar01, KW04, Bar06, BK07, Bar08**].

CHAPTER 3

Model-independent tests of accelerated expansion

1. Kinematical approach

In the previous chapter, we have shown an example of a cosmological model. The comparison to various observational data led to parameter values that indicate accelerated expansion. Such cosmological tests have been done for a plethora of different models. The expansion rate of the universe depends on the specific density parameters that characterize the model. This theoretical rate is then fitted to various observational data, constraining the parameter values. All homogeneous and isotropic models that have been tested until now led to the conclusion of cosmic acceleration in the late universe. The problem with this so-called dynamical approach is that it is impossible to test acceleration without any assumptions on the matter and energy content of the universe.

Some authors tried to avoid this problem by taking a kinematical approach, i.e. by only considering the scale factor a and its derivatives. Note that in all these tests a homogeneous and isotropic universe is assumed. The first kinematical analysis of SN data has been done by Turner and Riess [**TR02**] who considered averaged values q_1 for redshift $z < z_1$ and q_2 for $z > z_1$ concluding that a present acceleration and a past deceleration is favored by the data. While this test aimed at proving a change in the expansion from deceleration to acceleration without considering the nature of this change, subsequent analyses were designed to reconstruct the specific expansion history of the universe.

A first simple parameterization of the deceleration parameter $q(z)$ can be found in [**R$^+$04**]. The parameter is linearly expanded around its present value q_0 assuming a flat universe: $q(z) = q_0 + z\,(dq/dz)|_{z=0}$. The authors fitted this parameterization to the SNe of the Gold sample (that has been published in the same paper) and found a negative q_0 and a positive value for $(dq/dz)|_{z=0}$, thus confirming the present cosmic acceleration. In [**EM06**], this approach is broadened by considering various parameterizations $q(z) = \sum_i^N q_i z^i$ and $q(z) = \sum_i^N q_i (1+z)^{-3i}$ with $N = 0, 1, 2$ and by also allowing for spatial curvature.

The authors of [**WT05**] present a method to empirically determine $H(z)$ in uncorrelated redshift bins and thus to reconstruct the expansion history of the universe. Another published analysis is to determine the parameters of the scale factor a that has been expanded to fifth order polynomial [**Joh04**]. Instead of considering a special parameterization, a more general approach has been presented in [**ST06**], where the deceleration parameter q is expanded into principal components. In [**RAAB07**] the jerk parameter $j = \frac{1}{H_0^3}\frac{\dddot{a}}{a}$ is expanded into a series of orthonormal functions.

In general, one has to be careful when doing a series expansion in z. Any Taylor expansion will diverge for $z > 1$ as has been pointed out in [**CV07**]. The reason for this is that the smallest possible value for the redshift is -1, corresponding to an infinitly large scale factor. Thus, when for a Taylor expansion around $z = 0$ the radius of convergence can at most be 1. Similar problems can be expected for other series expansions. Thus, one should not use

expansions in z when considering SN data beyond redshift one. Instead, the authors suggest to reparameterize the redshift as $y = z/(1+z)$ and perform an expansion in y.

2. Model-independent test

2.1. Assumptions. In the present work, we are not interested in reconstructing the expansion history of the universe. Instead, we want to use SN data to quantify the evidence that there has been some phase of cosmic acceleration. This test is model-independent in the sense that we neither make any assumptions about the content of the universe, nor about the parameterization of $q(z)$ or any other kinematical quantity. Moreover, we do not need to assume the validity of Einstein's equations. The only assumptions needed for the analysis are homogeneity and isotropy of the universe and the assumption that SNe can be used as a fair representation of the universe. When giving up global homogeneity, it is possible to construct cosmological models (Lemaître-Tolman-Bondi models) that are consistent with observations without the need for an average acceleration [**Cel00, AA07, EM07, IRWG08, GBH08**]. As it is therefore impossible to find evidence for acceleration within the framework of an inhomogeneous universe, we restrict our test to the homogeneous case. In contrast to homogeneity, large scale isotropy is very well tested. The temperature fluctuations in the CMB are astonishingly small, namely $\Delta T/T \sim 10^{-5}$ [**S$^+$92**]. Thus, our assumption of isotropy is well justified.

Homogeneity and isotropy can, however, only be true statistically, but not in a strict sense. There exist large voids and superclusters on a scale of ∼100 Mpc. The largest known structure, the Sloan Great Wall [**G$^+$05**], even has an extension of ∼400 Mpc. The comoving distance of 400 Mpc corresponds approximately to a redshift of 0.1. Thus, the fact that SNe with smaller redshifts are used for cosmological tests could be problematic. Nevertheless, we follow the standard approach in this chapter and assume that the cosmic structure does not modify the observed SN magnitudes and redshifts apart from random peculiar motion. Possible other effects of local inhomogeneities and anisotropies on the measurement of the expansion rate will be considered in chapter 4.

2.2. Previous model-independent tests. The basic idea of a model-independent test has already been presented by Visser in 1997 [**Vis97**], where he published a method to test various energy conditions, especially the strong energy condition (SEC):

$$\rho + 3p \geq 0 \quad \text{and} \quad \rho + p \geq 0 \; . \tag{3.1}$$

As

$$-\frac{\ddot{a}}{a} = \frac{4\pi G}{3}(\rho + 3p) \; , \tag{3.2}$$

a violation of the SEC would correspond to a positive $\ddot{a}$, i.e. to an accelerated expansion. Assuming the validity of the SEC and considering bounds on the value of the Hubble rate H_0, the author determined limits on the look-back time, which is the time that has past between the emission of light from an object until now. If it were in some way possible to measure the age and the redshift of the oldest objects in the universe, these values could be compared to the obtained limits on the look-back time. Using some estimates for these values, the author finds a mild violation of the SEC, which indicates accelerated expansion.

Different groups have applied the tests of energy conditions to SN data [**SAPR07, GWWZ07**]. They did, however, not consider calibration effects due to different choices of the absolute magnitude of SNe, which led to the erroneous conclusion in [**SAPR07**] that

the equation of state w becomes smaller than -1 at the present epoch. While they only plotted the SN data compared to the calculated bounds on the distance modulus, they did not quantify the evidence for accelerated expansion.

In the following, we will present a test that can quantify this evidence and apply this test to different SN data sets, considering the calibration issue. Additionally, we analyze the influence of systematic effects on the test [**SS08**].

2.3. Method. The test is designed as an hypothesis test. We start with the null hypothesis that the universe has always been expanding decelerated, i.e. $q(z) \geq 0$ for all z. This corresponds to claiming that the strong energy condition has always been fulfilled. If we can reject this null hypothesis at a significant level, we have found evidence for acceleration.

We start by expressing the deceleration parameter $q(z)$ in terms of the Hubble rate:

$$q(z) = \frac{H'(z)}{H(z)}(1+z) - 1\,, \tag{3.3}$$

where the prime denotes the derivative with respect to z. Integrating this equation yields

$$\ln \frac{H(z)}{H_0} = \int_0^z \frac{1+q(\tilde{z})}{1+\tilde{z}}\, d\tilde{z}\,. \tag{3.4}$$

Considering the null hypothesis $q(z) \geq 0$, this equation turns into the inequality:

$$\ln \frac{H(z)}{H_0} \geq \int_0^z \frac{1}{1+\tilde{z}}\, d\tilde{z} = \ln(1+z) \tag{3.5}$$

or $H(z) \geq H_0(1+z)$. Thus, we have found a lower limit on the Hubble rate.

Now, we only need to translate this limit into an inequality that can directly be tested by SN data. Therefore, we consider the luminosity distance

$$d_L(z) = \frac{1+z}{H_0\sqrt{|\Omega_k|}}\, \mathcal{S}\left(\sqrt{|\Omega_k|}\int_0^z \frac{H_0}{H(\tilde{z})}\, d\tilde{z}\right)\,, \tag{3.6}$$

where $\mathcal{S}(x) = x$ for a flat, $\mathcal{S}(x) = \sin(x)$ for a closed and $\mathcal{S}(x) = \sinh(x)$ for an open universe. Inserting $H(z) \geq H_0(1+z)$ leads to

$$d_L(z) \leq \frac{1+z}{H_0\sqrt{\Omega_k}}\, \mathcal{S}\left(\sqrt{|\Omega_k|}\int_0^z \frac{d\tilde{z}}{1+\tilde{z}}\right) = \frac{1+z}{H_0\sqrt{|\Omega_k|}}\, \mathcal{S}\left(\sqrt{|\Omega_k|}\ln(1+z)\right)\,. \tag{3.7}$$

Note that the right hand side of this inequality corresponds to the luminosity distance of a universe that neither accelerates, nor decelerates, i.e. a universe with constant deceleration parameter $q(z) \equiv 0$. In terms of the distance modulus $\mu(z) = 5\log d_L(z) + 25$, this inequality reads

$$\Delta\mu(z) = \mu(z) - \mu_{q=0}(z) = \mu(z) - 5\log\left[\frac{1+z}{H_0\sqrt{|\Omega_k|}}\, \mathcal{S}\left(\sqrt{|\Omega_k|}\ln(1+z)\right)\right] - 25 \leq 0\,, \tag{3.8}$$

where $\mu_{q=0}(z)$ denotes the distance modulus of a universe with $q = 0$. By introducing the new quantity $\Delta\mu(z)$, we have reduced the null hypothesis of a never accelerating universe to the simple inequality $\Delta\mu(z) \leq 0$.

Note that $\Delta\mu(z)$ becomes zero at present time ($z = 0$):

$$\begin{aligned}\Delta\mu(0) &= \lim_{z\to 0}\left(5\log\left[\frac{1+z}{H_0\sqrt{|\Omega_k|}}\,\mathcal{S}\left(\sqrt{|\Omega_k|}\int_0^z \frac{H_0}{H(\tilde{z})}\,d\tilde{z}\right)\right]\right. \\ &\qquad \left. -5\log\left[\frac{1+z}{H_0\sqrt{|\Omega_k|}}\,\mathcal{S}\left(\sqrt{|\Omega_k|}\ln(1+z)\right)\right]\right) \\ &= \lim_{z\to 0}\left(5\log\left[\frac{\mathcal{S}\left(\sqrt{|\Omega_k|}z\right)}{\mathcal{S}\left(\sqrt{|\Omega_k|}\ln(1+z)\right)}\right]\right) \\ &= \lim_{z\to 0}\left(5\log\left[\frac{z}{\ln(1+z)}\right]\right) = \lim_{z\to 0}\left(5\log\left[\frac{1}{\frac{1}{1+z}}\right]\right) = 0\,.\end{aligned} \tag{3.9}$$

We use SN data to test the null hypothesis. If the inequality (3.8) is significantly violated, i.e. if the observed distance modulus is significantly larger than that of a universe with $q = 0$, then the null hypothesis can be rejected. In that case, we would have found evidence for acceleration. Note that the rejection of the hypothesis does not imply that there has never been a phase of deceleration between the time the light was emitted from the SN until now. It only implies that at some time there has been a phase of acceleration. Consequently, we cannot determine the transition redshift between deceleration and acceleration. This restriction to our analysis comes from the integral over redshift in the calculation of $d_L(z)$. For the same reason, fulfilling inequality (3.8) does not imply the null hypothesis. Thus, the test can possibly proof acceleration, but it cannot proof that there has never been acceleration.

Figure 3.1a shows $\Delta\mu(z)$ for different cosmological models, where a flat universe is assumed. The case of constant deceleration $q = 0.5$ corresponds to an Einstein-de Sitter universe ($\Omega_m = 1$). The other three models are accelerating, with the de Sitter model showing the largest acceleration. Note that the ΛCDM model does not accelerate within the whole plotted redshift range. With the assumed parameter values ($\Omega_m = 0.28$, $\Omega_\Lambda = 0.72$), the transition between deceleration and acceleration takes place at redshift 0.73. Nevertheless, $\Delta\mu(z)$ stays positive beyond that redshift and even slightly increases until it reaches its maximum at $z \simeq 1.3$. This points out the fact that an increase in $\Delta\mu(z)$ at a certain redshift does not imply a phase of acceleration at that specific redshift. It only proves that there has been acceleration at some point between that redshift and $z = 0$. In figure 3.1b, we give up the assumption of spatial flatness. We fixed the matter density to 0.3 and varied Ω_k. Ω_Λ is calculated by $\Omega_\Lambda = 1 - \Omega_m - \Omega_k$. Remember that not only the cosmological model, but also $\mu_{q=0}(z)$ depends on the assumed curvature.

The plotted curves only depend on the assumed density parameters or on the value of q, but not on the Hubble rate H_0. As H_0 is included in the cosmological model as well as in $\mu_{q=0}(z)$, it cancels in $\Delta\mu$. The only purpose of presenting these two plots is to make the reader more familiar with the quantity $\Delta\mu$. They are not related to the actual test since we do not assume a specific cosmological model.

2.4. Data sets. For the test, we need the observed distance modulus μ_i and the z_i for a set of SNe, where the subscript i stands for the i-th SNe of the set. μ_i is given by

$$\mu_i = m_i - M\,. \tag{3.10}$$

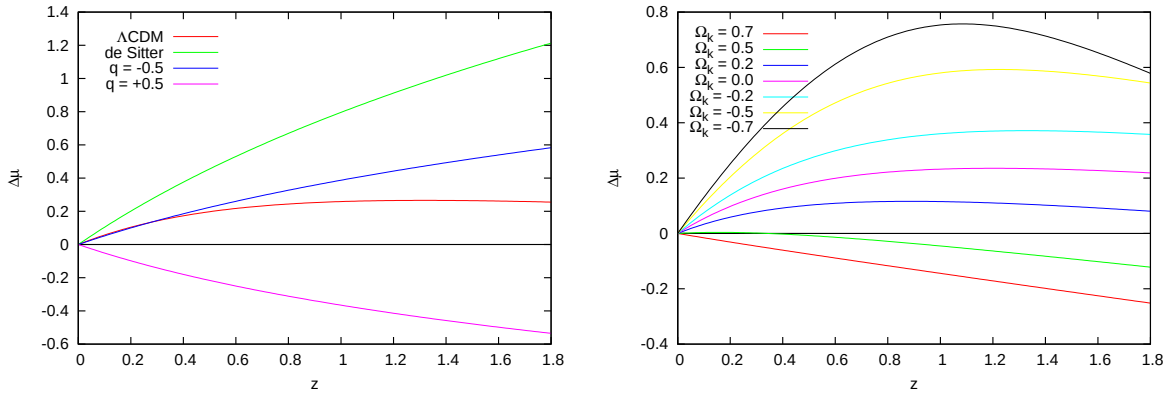

(a) (b)

Figure 3.1: $\Delta\mu$ for different cosmological models. (a) shows the following models assuming a flat universe: ΛCDM ($\Omega_m = 0.28$), de Sitter (i.e. $\Omega_\Lambda = 1$) and models with constant deceleration parameter $q = 0.5$ and $q = -0.5$. (b) shows a universe with $\Omega_m = 0.3$ and different values of Ω_k. Ω_Λ is determined by $\Omega_\Lambda = 1 - \Omega_m - \Omega_k$.

The apparent magnitude m_i of the SNe is obtained by fitting their light-curves. The result depends on the specific fitter that is used. Currently, the two most common fitters are MLCS2k2 [**JRK07**] and SALT [**GAN$^+$05**]. (There also exist modifications of both fitters, which we will consider later.) In all recently published data sets at least one of these fitters is used to obtain the distance modulus of the SNe. Some data sets provide two or more lists of data in order to compare different fitting methods.

We will use the following data sets for our analysis[1]:

- Gold (MLCS2k2): the Gold sample by Riess et al. (2007) [**R$^+$07**], which was obtained by using the MLCS2k2 fitting method
- ESSENCE (MLCS2k2): the set given by Wood-Vasey et al. (2007) [**WV$^+$07**], which includes data from ESSENCE, SNLS [**A$^+$06**] and nearby SNe [**JRK07**], fitted with MLCS2k2
- ESSENCE (SALT): the same set fitted with SALT

As suggested by Riess et al. [**R$^+$07**], we discarded all SNe with a redshift of $z < 0.0233$ from the Gold sample, thus leaving 182 SNe in the redshift range $0.0233 < z < 1.755$. In ESSENCE (MLCS2k2) and ESSENCE (SALT), the SNe with bad light curve fits were rejected for each fitting method separately. This leaves 162 SNe for ESSENCE (MLCS2k2) and 178 for ESSENCE (SALT) with $0.015 < z < 1.01$. 153 of the SNe are contained in both sets.

Comparing the apparent magnitudes of the SNe contained in both ESSENCE sets, one finds that there are large differences in the results obtained by the two light-curve fitters. (Note that the difference in apparent magnitudes is equivalent to the difference in distance moduli.) As shown in figure 3.2, these differences can be as large as 1 mag for single SNe. It is also noticeable that for the majority of SNe the SALT fitter leads to larger apparent magnitudes than the MLCS2k2 fitter. On average, the apparent magnitude is 0.12 mag

[1] We will also consider newer data sets later on, when we apply a modified version of this test.

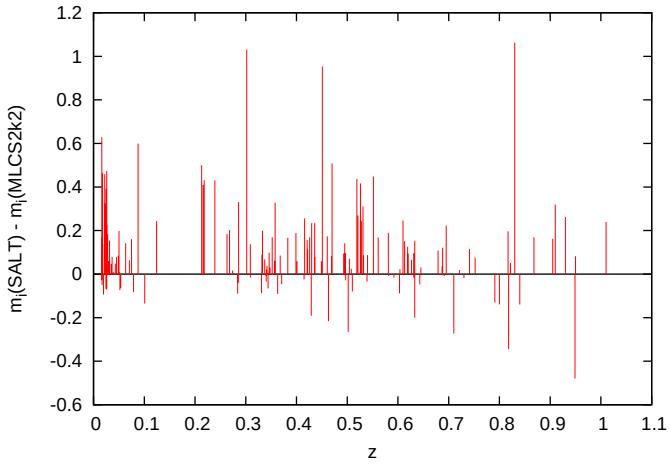

Figure 3.2: Differences in the apparent magnitudes in the ESSENCE set obtained by the SALT and the MLCS2k2 light-curve fitters, $m_i(\text{SALT}) - m_i(\text{MLCS2k2})$.

larger when SALT is used as compared to MLCS2k2k. Thus, we can expect that the choice of light-curve fitter will affect the outcome of the test of cosmic acceleration.

The distance modulus does not only depend on the apparent magnitude m, but also on the absolute magnitude M, which cannot be precisely determined. Thus, μ is always given in relatively arbitrary units in the published data sets depending on the assumed value of M. Different choices of M lead to different luminosity distances of the SNe and subsequently affect the determination of the Hubble rate H_0. For our test, the size of both quantities is important: the value of M is needed for determining the distance modulus of the observed SNe and H_0 affects the theoretical curve for $\mu_{q=0}(z)$. Here, we consider two very discrepant calibrations of M and H_0, namely that of Riess et al. [$\mathbf{R}^{+}\mathbf{05}$] and that of Sandage et al. [$\mathbf{S}^{+}\mathbf{06}$]. In the following we will refer to those results as Riess calibration and Sandage calibration, respectively.

In contrast to model-dependent tests, we cannot get rid of the calibration by means of marginalization. While our approach is to test a null hypothesis, model-dependent tests fit special cosmological models or parameterizations to observational data. An essential difference between these two approaches is that we test an inequality, whereas model-dependent tests use an equality, which requires different analyses. Model-dependent tests are typically based on the minimization of $\chi^2(p_i)$, where $\mathcal{M} = M - 5\log(H_0) + 25$ is one of the model parameters p_i. Then one can estimate the likelihood as a function of the parameters, which allows marginalization over $\mathcal{M}$. As in our test an inequality is tested, this kind of analysis is not suitable. We cannot use $\mathcal{M}$ as a free parameter, since the null hypothesis (3.8) is always fulfilled for large enough $\mathcal{M}$, which can be easily seen when we rewrite (3.8) as

$$m(z) - 5\log\left[\frac{1+z}{\sqrt{|\Omega_k|}}\,\mathcal{S}\left(\sqrt{|\Omega_k|}\ln(1+z)\right)\right] \leq \mathcal{M}\,. \tag{3.11}$$

Thus, for our test $\mathcal{M}$ needs to be calibrated.

The Riess calibration yields a value for the V-band magnitude of $M_{\mathrm{V}}(t_0) = -19.17 \pm 0.07$mag, where t_0 is the time of the B-band maximum. For the Gold sample, $M_{\mathrm{V}}(t_0)$ was considered to be -19.44mag. Therefore, in order to get the appropriate distance modulus $\mu = m - M$, we need to subtract 0.27mag from the value given in the Gold sample. From the distance modulus values in the ESSENCE sets 0.22mag have to be subtracted because in these sets a B-band magnitude of $M_{\mathrm{B}} = -19.5$mag is assumed and Riess et al. [$\mathbf{R}^{+}\mathbf{05}$] give the relation $M_{\mathrm{B}} - M_{\mathrm{V}} = -0.11$. For this calibration one gets a Hubble constant of $H_0 = 73 \pm 4(\text{statistical}) \pm 5(\text{systematic})$.

The results of Sandage et al. [$\mathbf{S}^{+}\mathbf{06}$] for the SNe absolute magnitudes are $M_{\mathrm{V}} = -19.46$mag and $M_{\mathrm{B}} = -19.49$mag and for the Hubble constant $H_0 = 62.3 \pm 1.3(\text{statistical}) \pm 5.0(\text{systematic})$. So considering the Sandage calibration, we have to add 0.02mag to distance moduli of the Gold sample and subtract 0.01mag from the values given in the ESSENCE sets.

Once one has chosen a certain data set, fitting method and calibration of M, one can calculate the magnitude $\Delta\mu$ for each SN of the set:

$$\Delta\mu_i = \mu_i - \mu_{q=0}(z_i) = \mu_i - 5\log\left[\frac{1+z_i}{H_0\sqrt{|\Omega_k|}}\,\mathcal{S}\left(\sqrt{|\Omega_k|}\ln(1+z_i)\right)\right] - 25\,. \tag{3.12}$$

If the error in redshift σ_{z_i} and the error due to peculiar velocities σ_v of the SNe are already included in the error σ_{μ_i} given in the data set, then the error σ_i of $\Delta\mu_i$ equals σ_{μ_i}. Otherwise, the resulting error of $\Delta\mu_i$ is calculated by:

$$\sigma_i = \left[\sigma_{\mu_i}^2 + \left(5\frac{\sqrt{|\Omega_k|}\,\mathcal{S}'\left(\sqrt{|\Omega_k|}\ln(1+z_i)\right)+1}{(1+z_i)\ln 10}\right)^2\left(\sigma_{z_i}^2+\sigma_v^2\right)\right]^{\frac{1}{2}} \tag{3.13}$$

where $\mathcal{S}'(x) = 1/x$ for a flat, $\mathcal{S}'(x) = \cot(x)$ for a closed and $\mathcal{S}'(x) = \coth(x)$ for an open universe.

2.5. Results for a flat universe. In the following, we will assume that the universe is spatially flat. We start by directly using $\Delta\mu_i(z_i)$ for the single SNe. Later, in 2.5.2, we will consider averaged values for $\Delta\mu$.

2.5.1. *Single supernovae.* According to our null hypothesis, we expect $\Delta\mu_i(z_i) \leq 0$. There are, however, some fluctuations in the value of $\Delta\mu_i(z_i)$ due to measurement errors and peculiar velocities. Thus, even if the hypothesis was true, it could very well happen that $\Delta\mu_i(z_i)$ is slightly positive for some SNe. Therefore, we only reject the null hypothesis, if the measured value is significantly positive, i.e. if it lies above a certain action limit A_a, where the subscript a stands for acceleration. We want to keep the risk low that we conclude a late time acceleration of the universe, when there is indeed no acceleration at all. Therefore, the action limit must be relatively high. If we want the confidence level (CL) for concluding an accelerated expansion to be 99%, the action limit must be $A_a(99\%) = 2.326\sigma_i$. For a confidence level of 95%, the limit is $A_a(95\%) = 1.645\sigma_i$. Here, we assume that the measured values $\Delta\mu_i(z_i)$ at a given redshift follow a normal distribution.

Analogously, we can test the hypothesis that the universe expanded accelerated all the time from light emission of a SN until today. This hypothesis can be rejected at a 99% CL if $\Delta\mu_i$ is below the action limit $A_d(99\%) = -2.326\sigma_i$. That would mean that there has been a phase of deceleration in the late time universe, but it would not exclude a phase of acceleration.

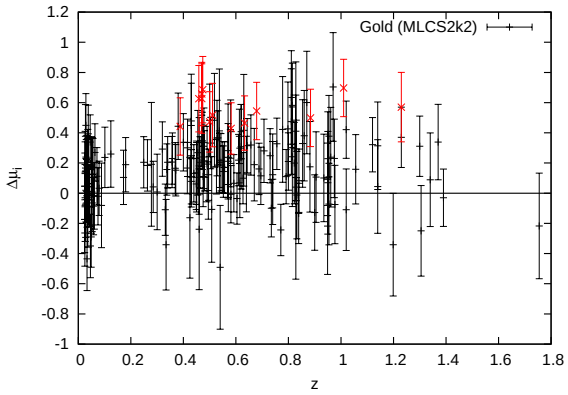

(a) Gold (MLCS2k2), Riess calibration

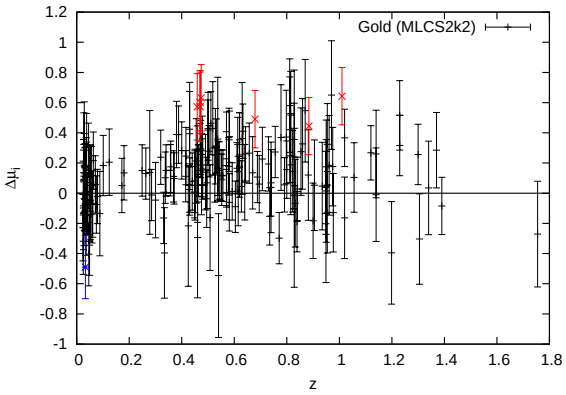

(b) Gold (MLCS2k2), Sandage calibration

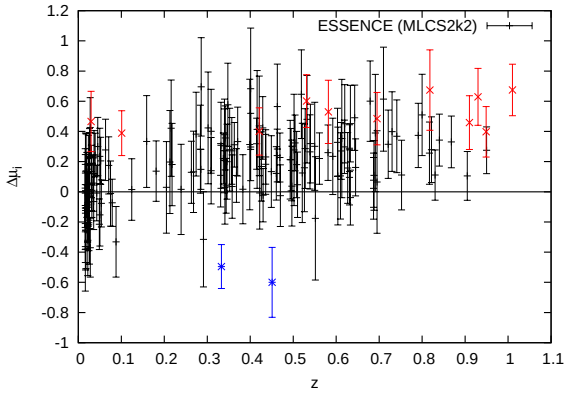

(c) ESSENCE (MLCS2k2), Riess calibration

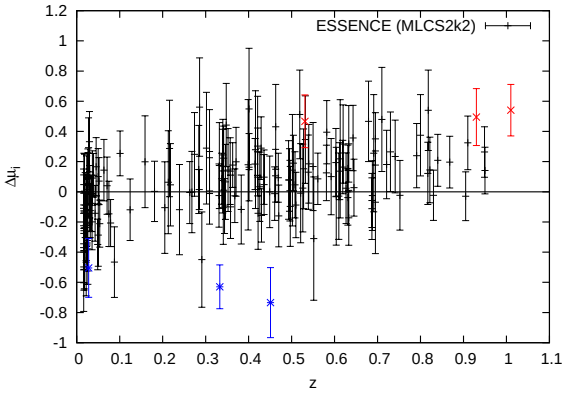

(d) ESSENCE (MLCS2k2), Sandage calibration

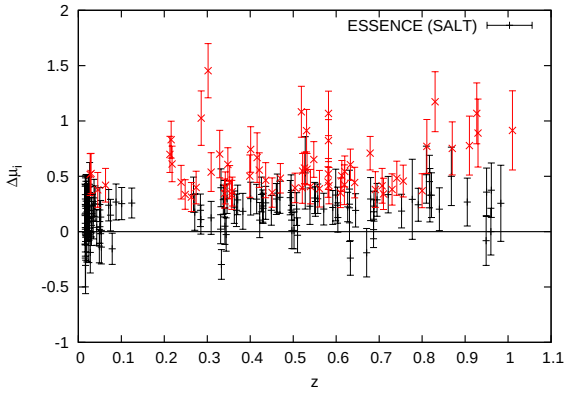

(e) ESSENCE (SALT), Riess calibration

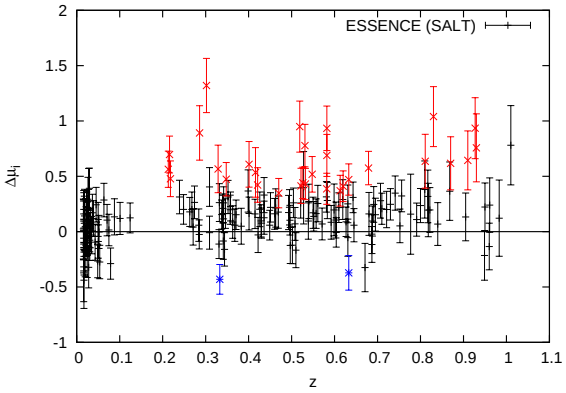

(f) ESSENCE (SALT), Sandage calibration

Figure 3.3: Magnitude $\Delta\mu_i$, as defined in equation (3.12), for the three data sets and two calibrations. SNe indicating acceleration at 99% CL are plotted in red ($\times$), those indicating deceleration in blue ($\ast$). Note that the SALT method leads to a larger spread in $\Delta\mu_i$, whereas the Gold set extends to higher redshifts.

	Gold 2007 (MLCS2k2)		ESSENCE (MLCS2k2)		ESSENCE (SALT)	
	Riess	Sandage	Riess	Sandage	Riess	Sandage
acceleration (95%)	37	27	37	14	96	53
acceleration (99%)	13	7	11	**3**	**64**	30
deceleration (95%)	2	4	3	7	1	7
deceleration (99%)	0	1	2	**3**	**0**	2
number of SNe	182	182	162	162	178	178

Table 3.1: Number of SNe indicating acceleration or deceleration at 95% and 99% CL for the different data sets and calibrations. Also given is the total number of SNe in each set. The most different results are highlighted.

The values of $\Delta\mu_i$ for the SNe in the different data sets obtained by the different light-curve fitters are shown in figure 3.3 for the two considered calibrations. SNe that indicate acceleration at 99% confidence level are highlighted in red, those that indicate deceleration in blue. The majority of SNe has a positive $\Delta\mu_i$, which is a sign for cosmic acceleration. Nevertheless, most of these values stay below $A_a(99\%)$. Considering the size of the data sets, it would not be very surprising to find a few SNe that lie above this action limit, even if the null hypothesis were true. The actual number of such SNe (that are highlighted in red in the figure) depends strongly on the data set, fitting method and calibration. In table 3.1, we have listed the number of SNe lying above the action limits $A_a(95\%)$ and $A_a(99\%)$ and those below $A_d(95\%)$ and $A_d(99\%)$, respectively. Let us take a look at the most different results: In the ESSENCE (MLCS2k2) data set using the Sandage calibration, there are only three SNe indicating acceleration at 99% CL and an equal number indicating deceleration. As there is a total of 162 SNe in the set, this number is certainly not enough to state an accelerated expansion. The situation is quite different for ESSENCE (SALT) in the Riess calibration. Here, 64 SNe are above $A_a(99\%)$, while none indicates deceleration at the same confidence level — a clear sign for acceleration.

As we have suspected earlier, when we analyzed figure 3.2, the light-curve fitter influences the result. Comparing the ESSENCE set fitted with MLCS2k2 directly to that fitted with SALT, we find that for both calibrations the number of SNe indicating acceleration is much larger in the SALT case. Similarly, the Riess calibration always leads to more SNe indicating acceleration than the Sandage calibration. Only the results of Gold (MLCS2k2) and ESSENCE (MLCS2k2) in the Riess calibration are compatible with each other, while this is not the case in the Sandage calibration.

2.5.2. *Averaging the supernova data.* When only counting the SNe above or below a certain action limit, we neglect the information that is given in the distribution of the other SNe. The majority of these SNe between $A_d(95\%)$ and $A_a(95\%)$ have a positive value. Although, none of them can individually provide evidence for acceleration, a combination of their values might be able to do so. As $\Delta\mu(z)$ is a function of redshift, averaging $\Delta\mu_i$ using nearby SNe will result in a different value than averaging over distant SNe. Thus, only combining SNe within small redshift bins will lead to averages that characterize the curve $\Delta\mu(z)$. The situation changes if we use SNe from different redshifts for averaging. Here, the observational average $\Delta\mu$ does not necessarily need to correspond to the value of the curve $\Delta\mu(z)$ at the

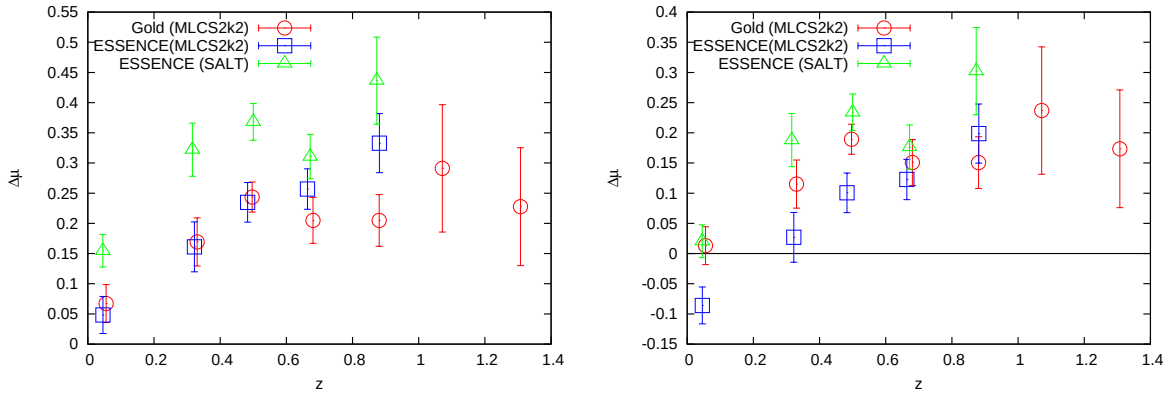

(a) Riess calibration (b) Sandage calibration

Figure 3.4: Magnitude $\Delta\mu$ averaged over redshift bins of width 0.2 for different data sets and calibrations.

average redshift of the SNe. Nevertheless, a significantly positive observational value will only be measured if also the curve $\Delta\mu(z)$ is positive at least within some redshift range between 0 and the redshift of the considered SNe. In that way, the average $\Delta\mu$ can provide evidence for accelerated expansion, if it is significantly positive.

We calculate $\Delta\mu$ as a weighted average:

$$\Delta\mu = \frac{\sum_{i=1}^{N} g_i \Delta\mu_i}{\sum_{i=1}^{N} g_i} \,, \tag{3.14}$$

where $g_i = 1/\sigma_i^2$. Thus, data with small errors have a larger weight than those with large errors. The standard deviation of this mean value is calculated by

$$\sigma = \left[\frac{\sum_{i=1}^{N} g_i \left(\Delta\mu_i - \Delta\mu\right)^2}{(N-1)\sum_{i=1}^{N} g_i} \right]^{\frac{1}{2}} \,. \tag{3.15}$$

We can now apply these formulae to arbitrary subsets of SNe. We choose to start with a redshift binning of 0.2. Then there is a reasonable amount of SNe in each bin up to redshift 1.0. (Of course it is possible to use smaller bin widths, but then one should be careful not to over-interpret the bins that contain only very few SNe. That would be the case, for example, in the redshift range between 0.1 and 0.2. There is a gap in the considered data sets, which can be clearly seen in figure 3.3.) Using binned data has the advantage that the results reflect the actual characteristics of $\Delta\mu(z)$.

Figure 3.4 shows the average $\Delta\mu$ for each redshift bin using the different data sets, light-curve fitters and calibrations. As $\Delta\mu(z = 0) = 0$ per definition, we expect the result of the first bin to be relatively close to zero. The average redshift of the SNe in this bin is approximately 0.05. In a de Sitter universe, i.e. in a universe with exponentially growing scale factor, $\Delta\mu(z = 0.05) = 0.053$ mag. In a universe containing only matter (Einstein-de Sitter), this value would be -0.026 mag. Using the ESSENCE (SALT) data set in the Riess calibration, the value of $\Delta\mu$ in the first bin is about three times as large as in a de Sitter

	Gold (MLCS2k2)		ESSENCE (MLCS2k2)		ESSENCE (SALT)	
z	Riess	Sandage	Riess	Sandage	Riess	Sandage
0.0 – 0.2	2.1	0.4	1.6	-2.8	5.7	0.8
0.2 – 0.4	4.2	2.9	3.9	0.7	7.3	4.3
0.4 – 0.6	9.8	7.6	7.1	3.1	12.1	7.7
0.6 – 0.8	5.4	4.0	7.7	3.7	8.5	4.8
0.8 – 1.0	4.8	3.5	6.8	4.1	6.0	4.2
1.0 – 1.2	2.8	2.2				
1.2 – 1.4	2.3	1.8				

Table 3.2: Statistical evidence $\Delta\mu/\sigma$ within the given redshift ranges. Here, the same binning as in figure 3.4 is used.

model. If that value was true, that would correspond to an extreme acceleration at the present epoch. A similar problem occurs for ESSENCE (MLCS2k2) in the Sandage calibration, where the first bin value implies an extreme deceleration. In the four other cases, the values of $\Delta\mu$ in the first bin seem to be more reasonable.

For all data sets, fitting methods and calibrations, there is an increase of $\Delta\mu$ with increasing redshift. All data points beyond $z = 0.2$ have a positive value, indicating cosmic acceleration. Yet, there are large differences in the actual size of $\Delta\mu$. This can be also seen in table 3.2, which lists the statistical evidences $\Delta\mu/\sigma$ for accelerated expansion obtained from the SNe in the given redshift bins, using different data sets, fitting methods and calibrations. The strongest evidence is given in the redshift range between 0.4 and 0.8. Consistent with our result for the analysis of single SNe in 2.5.1, the SALT fitter again leads to stronger evidences than MLCS2k2. The same is true for the Riess calibration compared to the Sandage calibration.

Our main interest is not to characterize the curve $\Delta\mu(z)$, but to determine the evidence for accelerated expansion. Therefore, we proceed by averaging over all SNe with $z \geq 0.2$. Doing so improves the statistics of the test as compared to using the binned data because the number of SNe that are used to calculate the average is strongly increased. The SNe above redshift 0.2 have comparable values in $\Delta\mu$, whereas those below that redshift have smaller values. Thus, including SNe with $z < 0.2$ in the test would lead to a larger spread in $\Delta\mu_i$, resulting in an increased standard deviation σ and subsequently in a decreased evidence $\Delta\mu/\sigma$. This is the main reason to discard these low redshift SNe. One might also argue that nearby SNe should not be used because local effects due to structures in the universe could modify the result or because these nearby SNe are observed with many different telescopes, which is likely to increase systematic effects. But one should always keep in mind that even when discarded, the nearby SNe indirectly influence the test as they are used to determine the calibration of M and H_0.

The statistical evidences obtained by averaging over all SNe with $z \geq 0.2$ are given in table 3.3. Also listed are the average redshifts z and the mean values and standard deviations of the magnitude $\Delta\mu$. For all data sets, fitters and calibrations, we find significant evidence for cosmic acceleration. The weakest evidence is obtained by using ESSENCE (MLCS2k2) in the Sandage calibration, namely 5.2σ. In the other cases the evidences are stronger and go

	Gold (MLCS2k2)		ESSENCE (MLCS2k2)		ESSENCE (SALT)	
	Riess	Sandage	Riess	Sandage	Riess	Sandage
$\overline{z}$	0.63	0.63	0.54	0.54	0.51	0.51
$\Delta\mu$	0.2196	0.1655	0.2398	0.1056	0.3457	0.2115
σ	0.0167	0.0167	0.0201	0.0201	0.0203	0.0203
$\Delta\mu/\sigma$	13.1	9.9	11.9	5.2	17.0	10.4

Table 3.3: Mean values and standard deviations of $\Delta\mu$ and the average redshift $\overline{z}$ obtained by using only SNe with $z \geq 0.2$ for a flat universe.

up to 17.0σ for ESSENCE (SALT) in the Riess calibration. Although we have found clear evidence for accelerated expansion in the case of a flat universe, it is obvious that changing the light-curve fitter or the calibration leads to vastly different results. This is a clear sign that there are large systematics in the SN data analysis.

2.6. Results for open and closed universes. Observations point towards a universe that is very close to spatially flat ($\Omega_k \simeq 0$). This conclusion is, however, based on model assumptions. Until now there exist no actual model-independent limits on Ω_k. Therefore, we cannot be sure whether the assumption of spatial flatness is really justified. Thus, we allow for arbitrary spatial curvature in the following section. The procedure is analogous to the case of a spatially flat universe. One only needs to choose the appropriate form of equation 3.12 for calculating $\Delta\mu_i$ in an open and closed universe, respectively. This quantity now depends on the value of Ω_k.

Considering an open universe, $\Delta\mu$ (and thus the evidence for accelerated expansion) decreases with increasing Ω_k. As we are interested in the lower limit of the evidence for acceleration, we take the largest possible value of the spatial curvature for the test, namely $\Omega_k = 1$, which corresponds to an empty universe. (Note that $\Omega_k = 1$ is the largest possible curvature only if the rule $\sum_i \Omega_i = 1$ holds, where $i = m, \Lambda, k, \ldots$. This rule is, however, only valid for the usual four-dimensional general relativity and can be different in a modified gravity scenario such as the braneworld model considered in chapter 2.) The result for the binned data (again with bin width 0.2) is shown in figure 3.5. Note that in particular the data points at high redshifts are significantly shifted to lower values as compared to the case of spatial flatness. They even become negative in the highest redshift bin ($1.2 \leq z < 1.4$). Consequently, the evidence for acceleration is reduced and basically vanishes for the ESSENCE (MLCS2k2) set in the Sandage calibration. The quantitative result for each bin is given in table 3.4 for the different data sets and calibrations.

In a closed universe, again the evidence for cosmic acceleration decreases with increasing Ω_k. But now Ω_k is a negative quantity, which means that we get the weakest evidence for $\Omega_k \to 0$. Thus, the results for a closed universe are the same as for a spatially flat universe. Table 3.5 lists the results for a closed/flat universe obtained by averaging over all SNe with $z \geq 0$ compared to an open universe. In the case of an open universe, we have also discarded all SNe with redshifts larger than 1.2 for the following reason: Using SN data at a certain redshift can only lead to evidence for acceleration if the phase(s) of acceleration dominate over the phase(s) of deceleration between the time the light was emitted from the SNe until now. This does not seem to be realized for the high redshift data, which have negative values

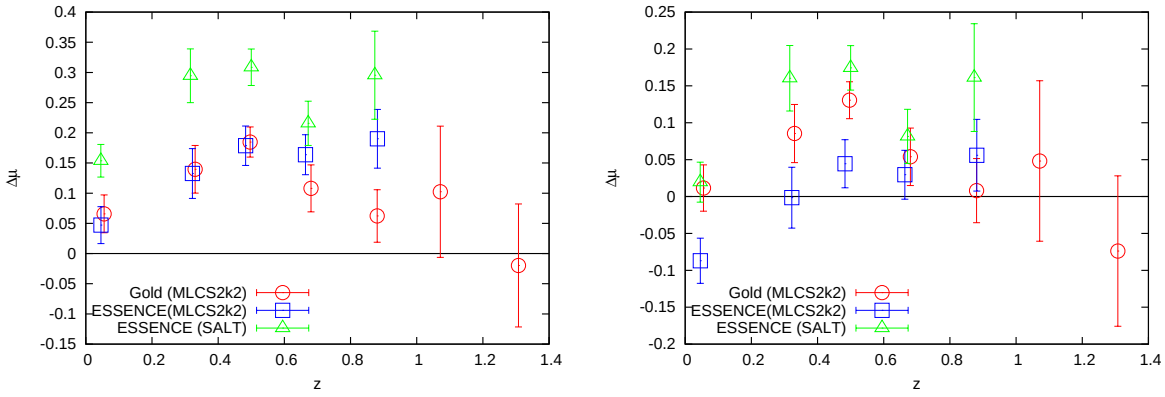

(a) Riess calibration (b) Sandage calibration

Figure 3.5: Magnitude $\Delta\mu$ averaged over redshift bins of width 0.2 for different data sets and calibrations, assuming an empty universe ($\Omega_k = 1$).

	Gold (MLCS2k2)		ESSENCE (MLCS2k2)		ESSENCE (SALT)	
z	Riess	Sandage	Riess	Sandage	Riess	Sandage
0.0 – 0.2	2.1	0.4	1.5	-2.8	5.7	0.7
0.2 – 0.4	3.5	2.2	3.2	-0.0	6.6	3.6
0.4 – 0.6	7.4	5.2	5.5	1.4	10.2	5.8
0.6 – 0.8	2.8	1.4	4.9	0.9	5.9	2.2
0.8 – 1.0	1.4	0.2	3.9	1.2	4.0	2.2
1.0 – 1.2	0.9	0.4				
1.2 – 1.4	-0.2	-0.7				

Table 3.4: Statistical evidences $\Delta\mu/\sigma$ within the given redshift range for an open universe.

	Gold (MLCS2k2)		ESSENCE (MLCS2k2)		ESSENCE (SALT)	
	Riess	Sandage	Riess	Sandage	Riess	Sandage
open universe	8.0	4.9	8.8	1.8	13.8	7.2
flat/closed universe	13.1	9.9	11.9	5.2	17.0	10.4

Table 3.5: Statistical evidence $\Delta\mu/\sigma$ for an open universe (obtained by using SNe within the redshift range $0.2 \leq z < 1.2$), a flat and a closed universe ($0.2 \leq z$).

of $\Delta\mu$ and therefore need to be dismissed. Note that this is not a shortcoming of the test. It just means that in order to test a late time acceleration, we should only use late time data.

The results in table 3.5 show that the evidence for acceleration is much weaker in an open universe compared to a closed or flat universe. For ESSENCE (MLCS2k2) in the Sandage

calibration, it even drops below 2σ, thus leaving merely a hint of acceleration. Yet, for the other sets and calibration, we still find some evidence. Not surprisingly, also for the open universe the systematic effects play an important role and have the same effects as in the case of a flat universe.

2.7. Systematics. In the following, we will take a closer look on the systematics that obviously affect the SN data used for the test. In the published ESSENCE set [**WV$^+$07**], the distance moduli μ_i of the SNe have once been obtained by using the MLCS2k2 fitter and once by SALT. In the same paper, Wood-Vasey et al. argue that the differences due to different fitting methods are not important as they disappear when marginalization is applied. This argument, however, only works if the data are used to determine the parameter values of a specific cosmological model, but not for a model-independent test, where marginalization cannot be applied. Moreover, the argument is not very convincing. The systematics are not important if one throws away some information, namely the information about calibration. As soon as M and H_0 are fixed to certain values, the choice of the light-curve fitter strongly affects the result. This indicates some problems with at least of the two fitting methods. Systematics due to different fitters have also been described in [**C$^+$07, K$^+$09a**].

In our test, we have also found systematics between the ESSENCE (MLCS2k2) and the Gold (MLCS2k2) data sets. While the results for these two sets are consistent in the Riess calibration, they are quite different in the Sandage calibration. Such systematics can occur when different telescopes are used for the observations and if the differences in the observation techniques are not accounted for correctly. These systematics can also be important within one data set if it contains SNe that were observed by different telescopes, which is the case for the Gold sample. Such systematic effects have been analyzed for the 2004 Gold sample [**R$^+$04**] in [**JBP05**] and for the extended 2007 Gold sample in [**NP07**].

As mentioned earlier, our test does not depend on the calibration of M and H_0 individually, but on the quantity $\mathcal{M} = M - 5\log(H_0) + 25$, which can be seen when the null hypothesis is given in the version of inequality (3.11). The fact that we observe huge systematic errors depending on the considered calibration seems somewhat strange: Assume we have found two different values M_1 and M_2 for the absolute magnitude of SNe Ia by comparing their brightness to that of cepheids in the same host galaxy. Such differences can occur if different analysis pipelines are used. Using these results, two values H_{01} and H_{02} for the Hubble constant can be obtained by observations of nearby SNe. Although $M_1 \neq M_2$ and $H_{01} \neq H_{02}$, the resulting values $\mathcal{M}_1$ and $\mathcal{M}_2$ are equal by definition, if the same set of low redshift SNe and the same analysis is used for the determination of the Hubble constant.

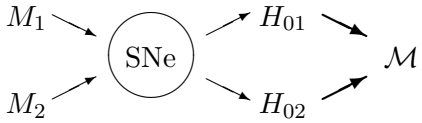

For our test, we adopted the values of M and H_0 given by Riess et al. [**R$^+$05**] and Sandage et al. [**S$^+$06**]. As the two groups analyzed different sets of nearby SNe and used different analysis pipelines, they obtained values of H_{01} and H_{02} which (combined with M_1 and M_2) did not lead to the same $\mathcal{M}$, but different values $\mathcal{M}_1$ and $\mathcal{M}_2$.

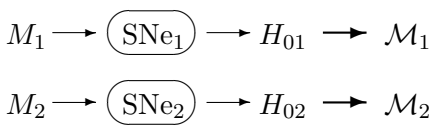

Thus, strictly speaking the observed systematics are not due to a different determination of the absolute magnitude M, but are caused by the systematic errors and the different SN data sets used in the measurement of $\mathcal{M}$.

3. Model- and calibration-independent test

3.1. Modifying the method. It is, however, easy to modify our test in such a way that we can avoid using a certain calibration of $\mathcal{M}$ when testing the accelerated expansion. We just need to consider relative values of $\Delta\mu$ instead of absolute values, i.e. we use $\Delta\mu - \Delta\mu_{\text{nearby}}$ rather than $\Delta\mu$, where $\Delta\mu_{\text{nearby}}$ is the average of $\Delta\mu_i$ using only nearby SNe of a data set [**SS09a**]. In that way, we calibrate the data with respect to a set of nearby SNe. The modified null hypothesis reads

$$\Delta\mu - \Delta\mu_{\text{nearby}} \leq 0 \; . \tag{3.16}$$

The standard deviation σ is obtained by adding the standard deviations of $\Delta\mu$ and $\Delta\mu_{\text{nearby}}$ in quadrature:

$$\sigma^2 = \sigma^2_{\Delta\mu} + \sigma^2_{\Delta\mu_{\text{nearby}}} \; . \tag{3.17}$$

Note that the null hypothesis does *not* correspond to the hypothesis of a never accelerating universe tested by an observer at $\overline{z}_{\text{nearby}}$. E.g. in a ΛCDM universe, $\Delta\mu(z)$ still slightly increases beyond the transition redshift z_t, i.e. it increases despite a phase of deceleration. (Remember the discussion of the ΛCDM curve in figure 3.1a.) Thus, if $\overline{z}_{\text{nearby}}$ is larger than z_t, but smaller than the redshift, where $\Delta\mu(z)$ reaches its maximum, we would observe a positive $\Delta\mu(z) - \Delta\mu_{\text{nearby}}$. Nevertheless, the observer at $\overline{z}_{\text{nearby}}$ would measure a negative $\Delta\mu(z)$ as the universe is in a phase of deceleration at that point.

The set of nearby SNe can be chosen relatively arbitrary. One should only take care that there is a reasonable number of SNe in the set. For example when using the Gold or ESSENCE data sets, it would be problematic to use the SNe between redshift 0.1 and 0.2 as nearby SNe. In this redshift range, there are only four SNe in Gold (MLCS2k2) and ESSENCE (MLCS2k2) and two SNe in ESSENCE (SALT). Thus, the result would not be very reliable due to the bad statistics.

The modified method shifts all data points by a fixed value. If there is accelerated expansion at the present epoch, the measured $\Delta\mu_{\text{nearby}}$ is likely to have a positive value. Subsequently the data points are shifted to lower values when we subtract $\Delta\mu_{\text{nearby}}$, thus weakening the evidence for acceleration as compared to the original method. In the same way, a negative $\Delta\mu_{\text{nearby}}$ would lead to stronger evidence. An additional effect is that the standard deviation is increased because $\sigma_{\Delta\mu_{\text{nearby}}}$ is added to the original standard deviation in quadrature. Since the statistical evidence is obtained by dividing $\Delta\mu$ by σ, an increased σ leads to weaker evidence. Thus, by avoiding systematic errors due to calibrations we expect to obtain a weaker evidence. Nevertheless, this evidence will be more reliable as it is not spoiled by systematics.

3.2. Results for the Gold, ESSENCE and Union data sets.

3.2.1. *Flat universe.* For the analysis we used the same data sets as for the original version of the test. Thus, the results can easily be compared. Additionally, we used the Union set [**K$^+$08**], which is a compilation of several old data sets and newly observed SNe. The Union set contains 307 SNe that were fitted with SALT and is thus much larger than the previously

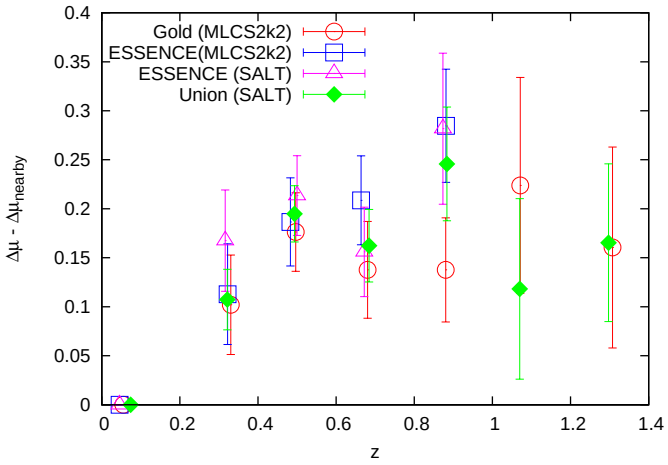

Figure 3.6: $\Delta\mu - \Delta\mu_{\text{nearby}}$ for different data sets and fitting methods, where the nearby SNe are defined as those SNe with redshifts $z_{\text{nearby}} < 0.2$.

considered sets, which contain between 162 and 182 SNe. Again, we start by assuming a flat universe. Open and closed universes will be considered below.

It seems kind of a natural choice to define the nearby SNe as all SNe having a redshift smaller than 0.2 since at this point there is a gap in the considered data sets. Since there are only very few SNe (namely up to six in the Union set) between redshifts 0.1 and 0.2, the choice of nearby SNe is almost equivalent to choosing all SNe with redshifts up to 0.1 as nearby ones. The results of the modified test are shown in figure 3.6, where we have again used a redshift binning of 0.2. Since we use the first bin as calibration bin, its value of $\Delta\mu - \Delta\mu_{\text{nearby}}$ equals zero per definition. The values in all the other bins are significantly above zero which indicates accelerated expansion.

It is noticeable that the values obtained from different data sets and fitting methods are consistent with each other. This is in contrast to the previous version of the test, where even within a certain calibration the results of the different sets and fitters differed quite strongly (see figure 3.4). Thus, all systematics are reduced, although the test was only modified in order to avoid systematics due to calibration. The quantitative results for the considered binning are given in table 3.6. As expected the evidences for acceleration are weakened in almost all cases as compared to those obtained by using the original test (see table 3.2 for the results of the previous test). Only the evidences for ESSENCE (MLCS2k2) in the Sandage calibration were weaker than those of the calibration-independent test for the same data set. This does not come as a surprise as ESSENCE (MLCS2k2) in the Sandage calibration is the only set which has a negative value of $\Delta\mu$ in the first bin. Since the first bin is used as calibration bin, the data points are shifted to higher values, thus increasing the evidence for cosmic acceleration.

Table 3.7 lists the evidences for acceleration when averaging $\Delta\mu$ over all SNe with redshift larger than 0.2. For the data sets that were also considered in the previous version of the test, these evidences lie between 4.3σ and 5.6σ. Before they were between 11.9σ and 17.0σ in the Riess calibration and between 5.2σ and 10.4σ in the Sandage calibration. This points out

Bin	Gold (MLCS2k2)	ESSENCE (MLCS2k2)	ESSENCE (SALT)	Union (SALT)
$0.2 \leq z < 0.4$	2.0	2.2	3.2	3.5
$0.4 \leq z < 0.6$	4.4	4.2	5.2	6.8
$0.6 \leq z < 0.8$	2.8	4.6	3.4	4.4
$0.8 \leq z < 1.0$	2.6	4.9	3.7	4.2
$1.0 \leq z < 1.2$	2.0			1.3
$1.2 \leq z < 1.4$	1.6			2.1

Table 3.6: Evidence for acceleration $(\Delta\mu - \Delta\mu_{\text{nearby}})/\sigma$ for different data sets and fitting methods using SNe in different redshift bins. Nearby SNe are those with redshifts $z_{\text{nearby}} < 0.2$.

	Gold (MLCS2k2)	ESSENCE (MLCS2k2)	ESSENCE (SALT)	Union (SALT)
$(\Delta\mu - \Delta\mu_{\text{nearby}})/\sigma$	4.3	5.2	5.6	7.2
# nearby SNe	40	47	46	57
# SNe in total	182	162	178	307

Table 3.7: Evidence for acceleration $(\Delta\mu - \Delta\mu_{\text{nearby}})/\sigma$ for different data sets and fitting methods, where nearby SNe are those SNe with redshifts $z_{\text{nearby}} < 0.2$. Also given are the numbers of nearby SNe and the total number of SNe.

again that at the cost of a weakened evidence the systematics are reduced in the calibration-independent version of the test. For the Union set with its large number of SNe, we still obtain a strong evidence for acceleration, namely 7.2σ.

The presented test crucially depends on the SNe in the calibration bin. Those are basically the SNe with $z < 0.1$ as there is only a very small number of SNe in the redshift range $0.1 \leq z < 0.2$. As already mentioned in 2.1, where the assumptions of the model-independent test are described, we are confronted with the problem that the assumption of an homogeneous and isotropic universe might not be justified for redshifts smaller than 0.1, i.e. for the SNe in the calibration bin. This could be a serious problem for the test. (Note that this issue basically occurs in all cosmological test using SN data because in some way or another it is necessary to compare data at different redshift.)

In order to analyze how large these effects could be, we split the SNe with $z < 0.1$ of each set into two subsets containing an equal number of SNe. Subset 1 contains the SNe with the lowest redshifts, subset 2 those with the largest redshifts. $\Delta\mu_{\text{nearby}}$ is then calculated using subset 1 and 2, respectively. For the determination of $\Delta\mu$ we use all SNe with $z \geq 0.2$. If there are effects due to local inhomogeneities and anisotropies, they should increase when the considered scale decreases. Thus, they should be larger for subset 1. Differences in the results obtained by using subset 1 and 2, respectively, could therefore be a sign of non-negligible effects.

		Gold (MLCS2k2)	ESSENCE (MLCS2k2)	ESSENCE (SALT)	Union (SALT)
subset 1	$(\Delta\mu - \Delta\mu_{\rm nearby})/\sigma$	3.1	6.6	5.6	6.3
	$\overline{z}_{\rm nearby}$	0.030	0.021	0.021	0.021
subset 2	$(\Delta\mu - \Delta\mu_{\rm nearby})/\sigma$	3.4	3.2	3.9	4.8
	$\overline{z}_{\rm nearby}$	0.056	0.046	0.050	0.051
# SNe		18	21	22	25

Table 3.8: Evidence for acceleration $(\Delta\mu - \Delta\mu_{\rm nearby})/\sigma$, where the SNe used to calculate $\Delta\mu$ fulfill $z \geq 0.2$ and those to calculate $\Delta\mu_{\rm nearby}$ fulfill $z < 0.1$. The nearby SNe are split into two subsets for each data set, each containing an equal number of SNe. Subset 1 contains the SNe with the smallest redshift, subset 2 those with the largest redshifts. Also given is the weighted average redshift $\overline{z}_{\rm nearby}$ and the number of SNe in each subset.

The results of this analysis are listed in table 3.8. With exception of the Gold sample, all sets provide a decreased evidence when the lowest redshift SNe are dismissed. This is not surprising as subset 2 has a larger average redshift than subset 1. Thus if $\Delta\mu(z)$ increases with redshift (which is the case in an accelerated universe), $\Delta\mu_{\rm nearby}$ is smaller for subset 1 than for subset 2, resulting in the observed effect on the evidence. However, this only explains the sign of the effect. In order to find out if also the size of the effect could be expected, let us take a closer look at the Union set.

The data points calibrated with respect to subset 1 and 2 are plotted in figure 3.7, clearly showing larger values for subset 1. Unfortunately, the size of the effect cannot be predicted in a model-independent way. Therefore, we chose to compare the actual effect to that predicted by a ΛCDM model with $\Omega_m = 0.28$ and $\Omega_\Lambda = 0.72$. $\Delta\mu(z) - \Delta\mu_{\rm nearby}(\overline{z}_{\rm nearby})$ for this model is also shown in the figure, where $\overline{z}_{\rm nearby}$ once corresponds to the average redshift of subset 1 and once to that of subset 2. The values for the ΛCDM model using subset 2 drop by only 0.018 mag as compared to the case when subset 1 is used, whereas the actual data points drop by 0.066 mag. Thus, we can state that the effect is larger than expected from standard cosmology. This could be a sign that local inhomogeneities and isotropies might influence the result of the test.

3.2.2. *Open and closed universes.* In the following we consider a universe with arbitrary spatial curvature. Analogous to the analysis in the original version of the test, we find that the lower limit to the evidence of acceleration for a closed universe is equivalent to that of a flat universe. In an open universe, the weakest evidence is again obtained by assuming $\Omega_k = 1$, which corresponds to an empty universe. The results for this scenario are plotted in figure 3.8. The values of $\Delta\mu - \Delta\mu_{\rm nearby}$ become negative beyond $z \simeq 1$. The results of the different data sets are of course again consistent with each other because the only difference compared to the case of a flat universe is that a different curve $\mu_{q=0}$ is subtracted from the observational data μ_i.

In table 3.9, the evidences for acceleration assuming different values of the spatial curvature Ω_k are listed. As in figure 3.8, the nearby SNe are those with redshifts $z < 0.2$. We use all SNe with $z \geq 0.2$ to calculate $\Delta\mu$ and subsequently the evidences $(\Delta\mu - \Delta\mu_{\rm nearby})/\sigma$. In the Gold and Union data sets, there are several SNe with a redshift larger than one. These SNe

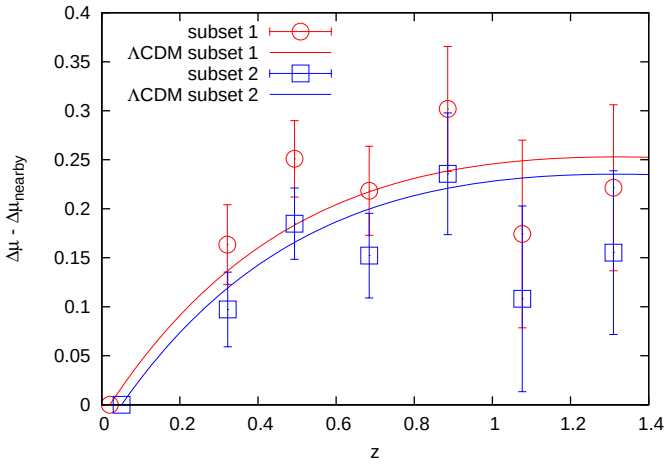

Figure 3.7: $\Delta\mu - \Delta\mu_{\rm nearby}$ for the Union set. The nearby SNe are those of subset 1 and 2, respectively, as given in table 3.8.

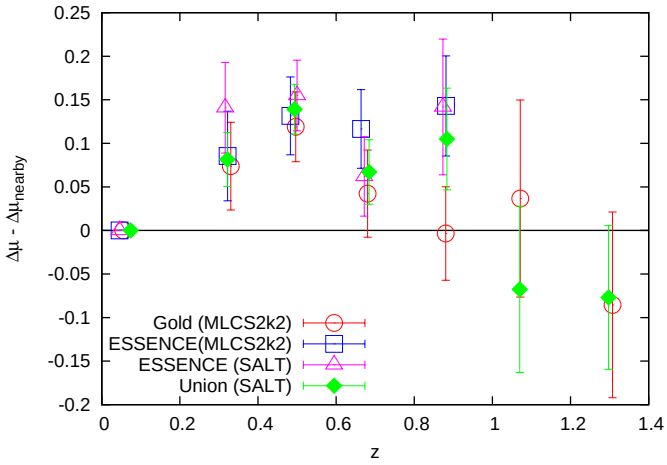

Figure 3.8: $\Delta\mu - \Delta\mu_{\rm nearby}$ for different data sets and fitting methods assuming an empty universe. The nearby SNe are defined as those SNe with redshifts $z_{\rm nearby} < 0.2$.

lead to decreased evidences when considering an open universe as the majority of these SNe has negative values of $\Delta\mu_i - \Delta\mu_{\rm nearby}$. Therefore, we also calculated the evidences obtained by using only SNe with $0.2 \leq z < 1.0$ to determine $\Delta\mu$ for Gold and Union. These evidences are given in parentheses in the table.

For small spatial curvature, we find evidence for acceleration with all data sets, although the evidence obtained from the Gold sample is quite weak. In the extreme case of an empty universe, there is merely a hint of acceleration left in the Gold sample, while the Union set can still provide some evidence, namely 4.5σ.

	Ω_k	Gold (MLCS2k2)		ESSENCE (MLCS2k2)	ESSENCE (SALT)	Union (SALT)	
closed universe	-1.0	6.7	(6.2)	7.0	7.5	10.2	(9.8)
	-0.8	6.3	(5.9)	6.6	7.1	9.6	(9.3)
	-0.6	5.8	(5.4)	6.3	6.8	9.0	(8.8)
	-0.4	5.3	(5.0)	5.9	6.4	8.4	(8.3)
	-0.2	4.8	(4.6)	5.6	6.0	7.8	(7.7)
flat universe	0.0	**4.3**	(**4.2**)	**5.2**	**5.6**	**7.2**	(**7.2**)
open universe	0.2	3.8	(3.8)	4.9	5.3	6.6	(6.7)
	0.4	3.3	(3.4)	4.5	4.9	6.0	(6.1)
	0.6	2.8	(2.9)	4.1	4.5	5.4	(5.6)
	0.8	2.3	(2.5)	3.7	4.1	4.8	(5.1)
	1.0	**1.8**	(**2.1**)	**3.4**	**3.8**	**4.2**	(**4.5**)

Table 3.9: Evidence for acceleration $(\Delta\mu - \Delta\mu_{\rm nearby})/\sigma$ assuming different values of the spatial curvature Ω_k. The lower limits to the evidence for a flat/closed and an open universe are highlighted. Nearby SNe are defined as those with redshift $z < 0.2$. For the calculation of $\Delta\mu$ all SNe with $z \geq 0.2$ are used. The results given in parentheses are obtained by using only SNe with $0.2 \leq z < 1.0$ to calculate $\Delta\mu$.

3.3. Results for the Constitution and SDSS data sets. We now return to the assumption of a spatially flat universe and consider two additional data sets: Constitution and SDSS. These two belong to the newest available data sets.

3.3.1. *Constitution.* We start with the Constitution set [**H$^+$09b**], which is one of the largest data set presently available. It consists of the SNe of the Union set and the recently published CfA3 sample [**H$^+$09a**]. The CfA3 sample contains only nearby SNe with redshift $z \lesssim 0.08$. The Union set, which we have already analyzed, has 57 nearby SNe ($z < 0.2$), which certainly leads to a good statistic in the determination of $\Delta\mu_{\rm nearby}$. Thus, we do not expect a significant improvement in the results of our test by increasing the number of nearby SNe (at least if we keep the definition of nearby SNe as those with redshift $z < 0.2$).

The main reason for applying the test of cosmic acceleration to the Constitution set is that this data set has been published for four different light-curve fitters, or more precisely for two versions of MLCS2k2 and two versions of SALT. In the original version of MLCS2k2, it is assumed that the reddening parameter R_V (which describes the absorption properties of the dust) has the same value as that measured in the Milky Way, namely $R_V = 3.1$. Besides using this value for the analysis, the authors of [**H$^+$09b**] also consider $R_V = 1.7$ as this value minimizes the scatter in the Hubble diagram for the CfA3 sample. In the following, we will refer to the MLCS2k2 fitter assuming $R_V = 3.1$ as MLCS31 and to that assuming $R_V = 1.7$ as MLCS17. Additionally, the SALT fitter and its improved version SALT II [**G$^+$07**] have been used to analyze the data.

We use the Constitution set to find out whether there are significant differences in the results of our test obtained by using different fitters. Figure 3.9 shows these results. Below $z = 0.8$ the data points are very close to each other. At higher redshifts, there is a larger spread in the data. The results are, however, still consistent with each other as there is also

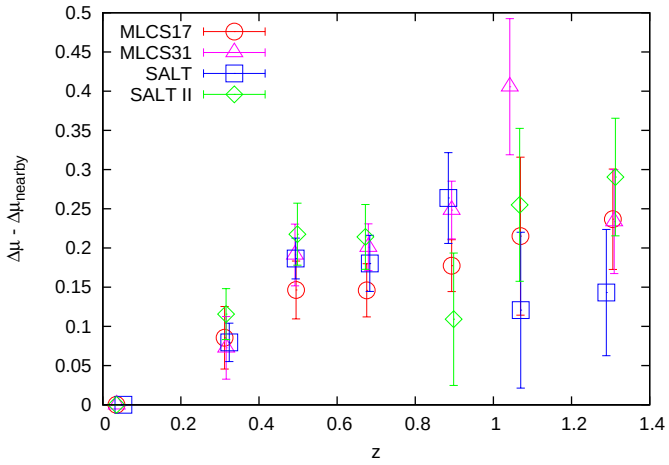

Figure 3.9: Magnitude $\Delta\mu - \Delta\mu_{\text{nearby}}$ averaged over redshift bins of width 0.2 for the Constitution data set.

	MLCS17	MLCS31	SALT	SALT II
$(\Delta\mu - \Delta\mu_{\text{nearby}})/\sigma$	6.5	7.9	8.2	7.6
# nearby SNe	206	204	147	183
# SNe in total	372	366	397	351

Table 3.10: Evidence for acceleration $(\Delta\mu - \Delta\mu_{\text{nearby}})/\sigma$ for the Constitution set and different fitting methods, where nearby SNe are those SNe with redshifts $z_{\text{nearby}} < 0.2$. Also given are the numbers of nearby SNe and the total number of SNe.

an increase in the error bars. The evidences for accelerated expansion are listed in table 3.10. Again, the differences in the results are quite small. Thus, the choice of the light-curve fitter does not seem to affect our result significantly.

3.3.2. *SDSS.* We now present the results obtained by using the SDSS data set [**K$^+$09a**], which contains 288 SNe. This data set fills the gap between low and high redshift SN data that is present in all previously published sets. That allows us to shift the redshift range that defines the nearby SNe into the region of the previously present gap. During the first season of the Sloan Digital Sky Survey II (SDSS) 103 SNe were observed with redshifts $0.04 < z < 0.42$. The published set additionally contains SNe from ESSENCE, SNLS, HST and nearby SNe. The SNe of the set have been fitted with SALT II and a modified version of MLCS2k2, respectively. The modifications of MLCS2k2 include changing the prior on the light extinction in the V-Band A_V, fitting the flux instead of the magnitude, improving the treatment of K-corrections and assuming $R_V = 2.18$ as reddening parameter. This value of R_V has been obtained by simulating SN data assuming different values of R_V and comparing the result to observed data. $R_V = 2.18$ is the value that minimizes the χ^2 between the simulated and the observed data.

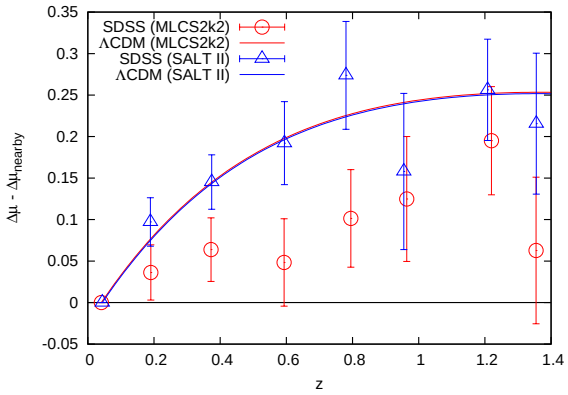

(a) Nearby supernovae: $0.0 \leq z < 0.1$

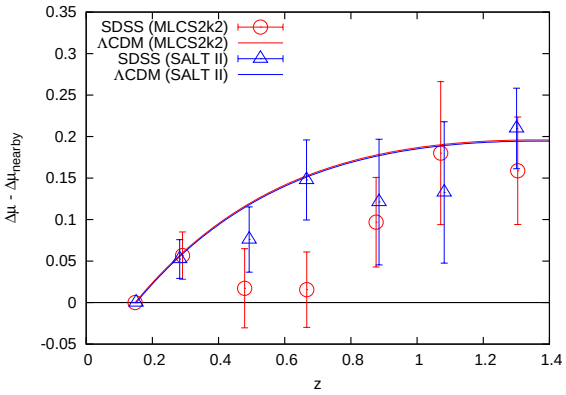

(b) Nearby supernovae: $0.1 \leq z < 0.2$

Figure 3.10: Magnitude $\Delta\mu - \Delta\mu_{\text{nearby}}$ averaged over redshift bins of width 0.2 for the SDSS data set fitted with SALT II and MLCS2k2, respectively. Also shown is the WMAP7 best fit ΛCDM model.

nearby SNe	z	$0.0 \leq z < 0.2$	$0.0 \leq z < 0.1$	$0.1 \leq z < 0.2$	$0.2 \leq z < 0.3$
	#	79	41	38	51
MLCS2k2	$(\Delta\mu - \Delta\mu_{\text{nearby}})/\sigma$	2.7σ	1.7σ	2.0σ	0.3σ
	$\chi^2_{dof}(\Lambda\text{CDM})$	2.01	2.13	1.88	2.10
SALT II	$(\Delta\mu - \Delta\mu_{\text{nearby}})/\sigma$	5.5σ	4.5σ	3.5σ	2.0σ
	$\chi^2_{dof}(\Lambda\text{CDM})$	1.66	1.66	1.67	1.82

Table 3.11: Evidence for acceleration $(\Delta\mu - \Delta\mu_{\text{nearby}})/\sigma$ for the SDSS data set fitted with MLCS2k2 and SALT II, respectively, and for different sets of nearby SNe, which are determined by the given redshift ranges. Also listed are the number of nearby SNe and the χ^2 per degree of freedom of the data with respect to the WMAP7 best fit ΛCDM model.

We have performed our analysis for different sets of nearby SNe. Figure 3.10 shows the result for nearby SNe defined by $0.0 \leq z < 0.1$ and $0.1 \leq z < 0.2$, respectively. In both cases, we use a redshift binning of 0.2 for the higher redshift data. Also plotted is the WMAP7 best fit ΛCDM model ($\Omega_m = 0.272$), where $\Delta\mu_{\Lambda\text{CDM}}(\overline{z}_{\text{nearby}}) - \Delta\mu_{\text{nearby}} = 0$ per definition. Note that $\overline{z}_{\text{nearby}}$ is slightly different for the two fitting methods. It is noticeable that $\Delta\mu - \Delta\mu_{\text{nearby}}$ obtained by SALT II is larger than for MLCS2k2 in almost all bins. Table 3.11 lists the quantitative results for the above choices and two additional choices ($0.0 \leq z < 0.2$ and $0.2 \leq z < 0.3$) of nearby SNe. The obtained evidences are astonishingly small. Using MLCS2k2, we hardly get any evidence for acceleration at all. The largest obtained value, namely 2.7σ provides merely a hint of accelerated expansion.

This result is especially surprising when we compare it to the results obtained by the ESSENCE (MLCS2k2) set. Remember that this set includes data from the ESSENCE and SNLS surveys as well as nearby SNe. These SNe are also included in the SDSS data set.

Thus, the evidence for acceleration has decreased from 5.2σ (ESSENCE (MLCS2k2)) to 2.7σ (SDSS (MLCS2k2)), although the number of SNe has increased, which should lead to better statistics. In [**K$^+$09a**], the differences between ESSENCE (MLCS2k2) and SDSS (MLCS2k2) have been analyzed. According to this paper, these differences are not caused by adding SNe to the set, but by modifying the light-curve fitter. The main sources thereof seem to be different assumptions about the value of the reddening parameter R_V and different priors on the extinction A_V.

The results of our test obtained by using SDSS (SALT II) fitter are, however, very similar to that obtained by ESSENCE (SALT), namely 5.5σ and 5.6σ, respectively. Thus, we find a clear evidence for acceleration when SALT II is used. This evidence is still present when we reject all SNe with $z < 0.1$ (i.e. when we define the set of nearby SNe as those with redshift $0.1 \leq z < 0.2$) and thus avoid problems due to local inhomogeneities and isotropies.

Nevertheless, we are confronted with the problem that we do not know, what fitter is the most reliable one. The results from the SALT II fitter are certainly more consistent with a ΛCDM model. This can be clearly seen in figure 3.10, where $\Delta\mu(z) - \Delta\mu_{\text{nearby}}$ for ΛCDM with the best fit WMAP7 parameter values is plotted and compared to the data. While the data obtained by SALT II fluctuate around this curve, the values obtained by MLCS2k2 are significantly smaller. The χ^2 per degree of freedom for the data with respect to the ΛCDM model is listed in table 3.11. In all cases, the χ^2 for SALT II is smaller than that for MLCS2k2. The fact that SALT II provides results that are more consistent with standard cosmology is, however, not a proof that it is a better fitter than MLCS2k2 as it is not certain, whether ΛCDM is the correct model. As a consequence, we must state that the SDSS data set does not provide evidence for accelerated expansion.

3.4. Conclusion. We have presented a model-independent test of cosmic acceleration. In the first version of the test, which has still been calibration-dependent, the results for different data sets, fitting methods and calibrations were largely affected by systematics. Nevertheless, we could find evidence for acceleration. We then modified the test by analyzing the SNe with respect to a set of nearby SNe, making it independent of a specific calibration. For almost all data set this led to a significant reduction of all systematics. Although the evidence for acceleration was decreased as compared to the original version of the test, it was still large enough to proof acceleration.

The only exception is the SDSS data set. There are large differences between the results obtained by the two light-curve fitters. These differences are caused by modifications of MLCS2k2 that are considered to be an improvement of this fitter. The modified MLCS2k2, however, does not lead to results that proof cosmic acceleration. This is in contrast to the Constitution set, where the modification of MLCS2k2 did not affect the outcome of the test significantly. You should, however, note that the modifications of MLCS2k2 were different in these two cases. It is certainly problematic that changes in the light-curve fitter can significantly influence our test result, but this problem cannot be solved at the moment. A careful analysis of large data sets will be necessary to identify sources of systematics and find a reliable approach to fitting SN light-curves.

CHAPTER 4

Probing backreaction effects with supernova data

1. Backreaction

1.1. Local structure. In the previous chapter, we have mentioned several times that local inhomogeneities and anisotropies could spoil our test. Especially on small scales, i.e. when we use SNe with very small redshift, it is quite possible that the effects due to local structure are not negligible. These problems do not only occur in our test, but are a general issue, which is present in basically all cosmological tests. As soon as one wants to determine cosmological density parameters of a specific model or tries to reconstruct the expansion history of the universe, it is necessary to combine observational data from different redshifts, including very small redshifts. Therefore, it is necessary to analyze the effects of local inhomogeneities and anisotropies on these measurements.

We start by considering the scales, on which local structures might become important. In a homogeneous universe, the number $N(R)$ of galaxies within a sphere of comoving radius R should be proportional to R^3 and independent of the location of the sphere. As there are local structures, this will not be true for arbitrarily small radii, but only for $R \gtrsim R_{\mathrm{hom}}$, where R_{hom} is the homogeneity scale. Using SDSS[1] data [**Y$^+$00**], different groups have consistently found a homogeneity scale of approximately 100 Mpc [**H$^+$05, JSLG$^+$05**]. See figure 4.1 for the measured dependence of the number density of luminous red galaxies on the radius R. The conclusion of [**LVPB09**] (where a newer SDSS data set [**AM$^+$08**] is used) is, however, that the 100 Mpc are only a lower limit to R_{hom}. The authors state that the actual homogeneity scale — if it exists at all — cannot be determined as the current survey volume is too small. We should also remember that the largest known structure in the universe, the Sloan Great Wall [**G$^+$05**], has a size of about 400 Mpc, which corresponds roughly to a redshift of 0.1. Besides structures of clustered matter, there are also large voids in the universe, such as the Boötes void [**KOSS81**] with a diameter of 100 Mpc. The structures in the universe as observed by SDSS are shown in figure 4.2.

Due to the observed local inhomogeneities, we also expect local anisotropies. This has been tested using SNe in [**H$^+$07, SW07**]. A statistically significant violation of isotropy has been found in [**SW07**] for redshifts $z < 0.2$: The fluctuation of the Hubble rate $\Delta H/H$ on opposite hemispheres on the sky is about 5%, which corresponds to a difference in the distance modulus of about 0.1 mag. A similar analysis has been done in [**AP10**] using the recently published Union2 data set [**A$^+$10**]. The authors found some hint of anisotropy in this data set. Yet, it is still consistent with statistical isotropy. However, the axis of maximal asymmetry in Union2 coincides approximately with the anisotropy axes found from other observations, such as the alignment of low multipoles in the CMB [**BGB04, FE09, L$^+$96**], large scale velocity flows [**WFH08, FWH10**] and the alignment of the quasar polarization

[1]Note that SDSS is a survey of various kinds of objects. In the previous chapter, we have only analyzed the SDSS SN data. However for determining the homogeneity scale, galaxy data are used.

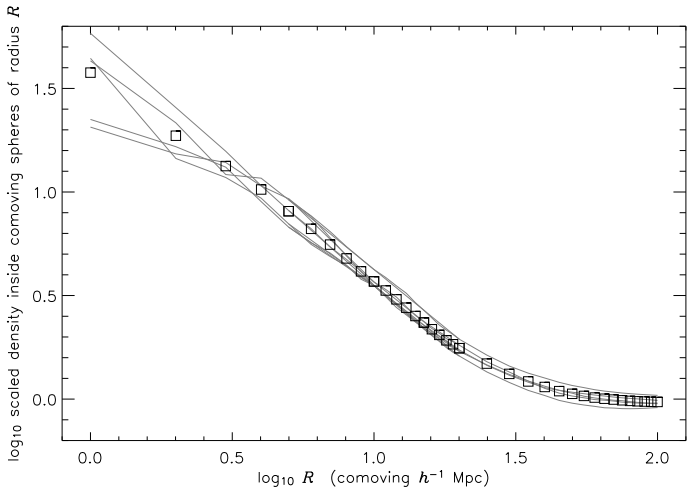

Figure 4.1: Average comoving number density of luminous red galaxies (LRG) inside a sphere of radius R centered on a LRG. As LRGs are clustered, the number density decreases with R at small scales. At large scales (beyond the homogeneity scale), the sample becomes homogeneous and thus the number density approaches a constant. Figure taken from [**H$^+$05**].

vectors [**HL00, HCLS05, H$^+$08**]. This coincidence is very unlikely within the framework of an isotropic universe and thus provides evidence for an anisotropy.

Local structure affects the expansion of the universe via the backreaction mechanism, which will be described below. The theory of these effects on the measurement of the local Hubble rate has been provided by [**LS08**]. In this work, we will test this theory by analyzing nearby SN data.

1.2. Averaging problem. One might naively assume that one can calculate the evolution of the background universe — i.e. a universe with averaged energy density, pressure and metric — without considering the actual deviations from this background. According to this standard approach, the mean expansion rate depends only on the averaged energy density and pressure, but on the fluctuations of these quantities. Then, local inhomogeneities and anisotropies would only lead to peculiar velocities on top of the general expansion, but could not affect the evolution of the background universe.

That these assumptions are not correct has first been realized by Shirokov and Fisher [**SF63**] and analyzed in greater detail by Ellis [**Ell84**]. The problem lies in the non-linearity of the averaging formula (see (4.6)) and of the Einstein equation. The averaged version of this equation (without cosmological constant) would read: $\langle G_{\mu\nu}(g_{\mu\nu})\rangle = 8\pi G\langle T_{\mu\nu}\rangle$. In the standard approach, one inserts, however, quantities of the background universe — i.e. an averaged metric $\langle g_{\mu\nu}\rangle$ and an averaged stress energy tensor $\langle T_{\mu\nu}\rangle$ — directly into the Einstein equation: $G_{\mu\nu}(\langle g_{\mu\nu}\rangle) = 8\pi G\langle T_{\mu\nu}\rangle$. As the Einstein equation is non-linear in the metric,

$$G_{\mu\nu}(\langle g_{\mu\nu}\rangle) \neq \langle G_{\mu\nu}(g_{\mu\nu})\rangle \ . \tag{4.1}$$

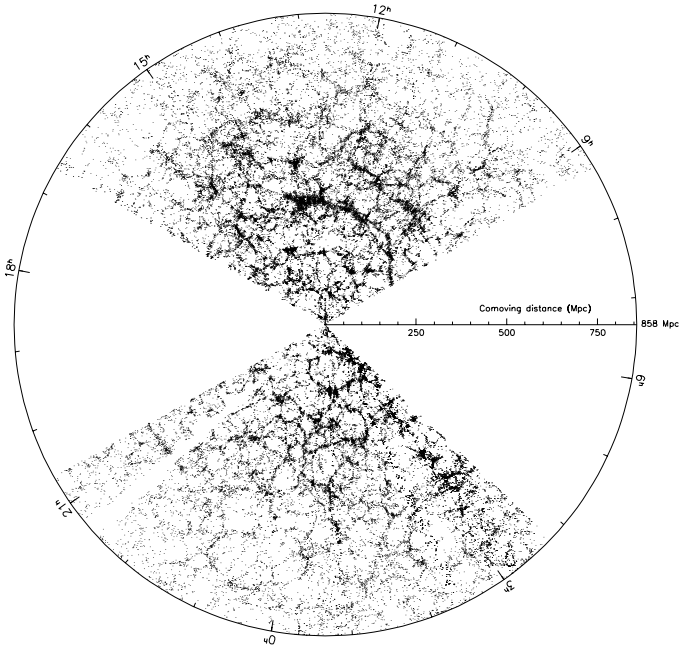

Figure 4.2: Galaxies and quasars in the equatorial slice observed by SDSS in comoving coordinates. The Sloan Great Wall can be seen at a median distance of 310 Mpc and stretches from 8.7h to 14h in right ascension. Figure taken from [**G**$^+$**05**].

Thus, it is obvious that the standard averaging procedure is not the correct one. Consequently, the Friedmann equations are also affected as they are calculated from the Einstein equation. In that way, the evolution of the background universe is influenced by local inhomogeneities.

This is illustrated in figure 4.3. We start with the bottom picture that shows a perturbed metric within a domain D. The standard approach is depicted on the left hand side: one first averages the metric, which leads to a homogeneous model. Then, as the universe expands, also the size of the domain increases. The shape of the domain (here depicted as a circle) stays the same. The situation is different on the right hand side. Here, the evolution of the universe is considered before averaging. The expansion rate is affected by the inhomogeneities, leading to a differently shaped and sized domain. Thus averaging and time evolution do not commute, i.e. $[\partial_t, \langle . \rangle_D] \neq 0$. This is the main idea of the backreaction mechanism.

While it is obvious that backreaction influences the expansion of the universe, the size of these effects is discussed very controversially. Some claim that the effects are negligible, while others believe that cosmic acceleration can be completely explained by backreaction. This controversy emphasizes the necessity to actually calculate to what extent the expansion of the universe is affected by backreaction — a task that turns out to be very complicated. Many

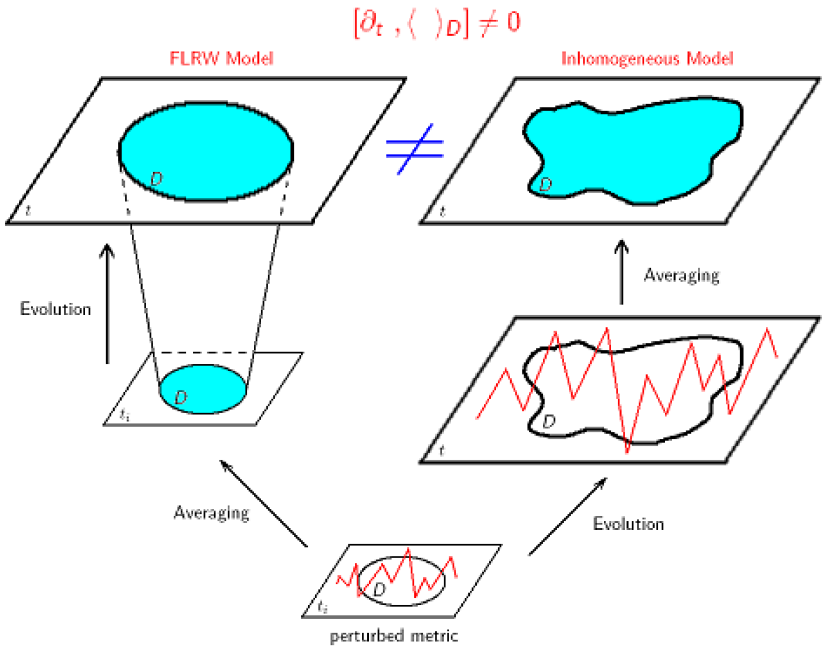

Figure 4.3: Temporal evolution and spatial averaging do not commute. (Figure taken from a talk by J. Larena given on the second Kosmologietag in Bielefeld (2007).)

articles have been published about this topic, see e.g. [**Ell84, Zal92, RMKB96, RSKB97, Buc00, Buc01, Buc08, ZSBP01, Wet03, GB02, Sch02, Ras04, KMNR05, KMR06, CGH08, PS07, LS07, VFW07, LSS08, BBR08, LAB$^+$09, CAL09**].

2. Averaging formalism

2.1. Basic considerations. As all observables lie on our past light-cone, in principle we would have to average the observed quantities over that very light-cone. Unfortunately, a formalism to perform these kind of averages does not exist, yet, which is why we have to use spatial averages. Doing so, we introduce an error to our analysis. We keep this error small by restricting our analysis to low redshifts, i.e. to a time period during which the universe has not greatly evolved. Consequently, we cannot analyze how the expansion rate changes with redshift. The aim of this work is rather to examine, whether significant backreaction effects are present in the measurement of today's Hubble rate.

In the following, we assume that we live in a spatially flat dust universe, i.e. we neglect the possibility of a dark energy term and of a global curvature term. Nevertheless, there will be some local spatial curvature due to inhomogeneities.

The theory should match the situation of a real observer as closely as possible. Therefore, it is useful to use comoving coordinates, which is possible if we assume the universe to be irrotational. Then, the observer sits at a fixed coordinate and can use her own clock. Furthermore, we foliate the spacetime into hypersurfaces of constant time and use the comoving synchronous gauge. The metric of the inhomogeneous universe can then be written as

$$ds^2 = -dt^2 + g_{ij}(t, \mathbf{x}) dx^i dx^j \ . \tag{4.2}$$

2.2. General averaging equations. In this section, we describe how spatial averages within a certain domain D are performed. Imagine we want to determine the average value of an observable O. By observing different objects in the universe, we have obtained N values O_i. Then (assuming equally sized measurement errors) the average value is simply given by:

$$O = \frac{1}{N}\sum_{i=1}^{N} O_i \ . \tag{4.3}$$

For a very large number of observed objects N and assuming that these objects are distributed homogeneously within a volume V, we can transform the sum into an integral:

$$\langle O\rangle = \frac{1}{V}\int_V O(t,\mathbf{x})dV \ . \tag{4.4}$$

The observable $O(t,\mathbf{x})$ will in general depend on space and time. For the averaging procedure, we consider, however, only fixed times t. The brackets $\langle . \rangle$ denote volume averages.

We have assumed that the number density $n(\mathbf{x})$ of observed objects is constant throughout the volume. In practice, this is not always the case. Therefore, we want to generalize the procedure by introducing a window function $W_D(\mathbf{x})$, which is proportional to the number density $n(\mathbf{x})$. The above case can then be reproduced by a window function that is constant within the considered volume and equal to zero outside the volume. Thus, the window function also specifies the domain, in which the averages are performed. In general, the volume of such a domain D is given by the integral over $W_D(\mathbf{x})$:

$$V_D(t) = \int_D W_D(\mathbf{x})\sqrt{\det g_{ij}}\, d\mathbf{x} \ . \tag{4.5}$$

Naturally, also the average value of the observable depends on the window function:

$$\langle O\rangle_D = \frac{1}{V_D(t)}\int_D W_D(\mathbf{x})O(t,\mathbf{x})\sqrt{\det g_{ij}}\, d\mathbf{x} \ . \tag{4.6}$$

As we are interested in the expansion of the universe, it is necessary to define a scale factor. In a perfectly homogeneous and isotropic universe, the expansion rate (i.e. the change in the scale factor) will be the same at each location and in each direction. Given a comoving sphere with radius a_0 at present time, the size of the sphere will increase at the same rate as the universe — its radius at time t corresponding to the scale factor $a(t)$. The situation changes if there are local inhomogeneities and anisotropies in the universe. Then the sphere will not expand uniformly, but change its shape. Consequently, a radius (and thus the scale factor) is no longer defined. This problem can be easily solved by defining an effective scale factor via the volume of the domain:

$$\frac{a_D(t)}{a_{D_0}} = \left(\frac{V_D(t)}{V_{D_0}}\right)^{1/3} \ . \tag{4.7}$$

The subscript 0 denotes the values at the present time. Note that the effective scale factor a_D is no longer a quantity that has the same value throughout the whole universe. It rather depends on the location and on the size and shape of the domain.

The above equation leads to a relation between the averaged volume expansion rate $\langle\theta\rangle_D$ and the linear expansion rate, given by the effective scale factor:

$$\langle\theta\rangle_D = \frac{\dot{V}_D}{V_D} = 3\frac{\dot{a}_D}{a_D} \ . \tag{4.8}$$

We can thus define the effective Hubble rate as

$$H_D = \frac{\dot{a}_D}{a_D} = \frac{1}{3}\langle\theta\rangle_D \,. \tag{4.9}$$

This Hubble rate is an averaged quantity measured in the domain D and will thus depend on the window function $W_D(\mathbf{x})$ that specifies the domain.

2.3. Effective Friedmann equations. Following Buchert's averaging formalism [**Buc00, Buc01, Buc08**], the Einstein equation for a dust universe can be averaged to yield the Friedmann equations of an effective fluid:

$$\left(\frac{\dot{a}_D}{a_D}\right)^2 = \frac{8\pi G}{3}\rho_{\text{eff}} \,, \tag{4.10}$$

$$-\frac{\ddot{a}_D}{a_D} = \frac{4\pi G}{3}(\rho_{\text{eff}} + 3p_{\text{eff}}) \,. \tag{4.11}$$

These equations look just like the Friedmann equations in a homogeneous universe. The only difference is that they do not contain the actual energy density ρ and pressure p (which equals zero for dust) of the matter in the universe, but an effective energy density ρ_{eff} and pressure p_{eff}, which are given by:

$$\rho_{\text{eff}} = \langle\rho\rangle_D - \frac{1}{16\pi G}\left(\langle Q\rangle_D + \langle\mathcal{R}\rangle_D\right) \,, \tag{4.12}$$

$$p_{\text{eff}} = -\frac{1}{16\pi G}\left(\langle Q\rangle_D - \frac{1}{3}\langle\mathcal{R}\rangle_D\right) \,. \tag{4.13}$$

$\langle\rho\rangle_D$ is the average energy density in the domain. As we consider only dust, a corresponding term for the pressure does not occur. $\langle\mathcal{R}\rangle_D$ is the averaged spatial curvature within D and $\langle Q\rangle_D$ denotes the kinematical backreaction term, which is defined as:

$$\langle Q\rangle_D = \frac{2}{3}\left(\langle\theta^2\rangle_D - \langle\theta\rangle_D^2\right) - 2\langle\sigma^2\rangle_D \,. \tag{4.14}$$

Here, θ is the volume expansion rate and $\sigma^2 = \frac{1}{2}\sigma_{\mu\nu}\sigma^{\mu\nu}$ the shear scalar.

Let us take a closer look at the second Friedmann equation (4.11). $\ddot{a}_D/a_D$ is positive if the right hand side of this equation is negative, i.e. if $\rho_{\text{eff}} + 3p_{\text{eff}} < 0$. In that case, we would measure an accelerated expansion within the domain D. Inserting the definitions of ρ_{eff} and p_{eff} into this condition leads to $\langle Q\rangle_D > 4\pi G\langle\rho\rangle_D$. Thus, a kinematical backreaction term that is large compared to the energy density, gives rise to an averaged expansion of the universe that is accelerated. Remember, however, that we have assumed a dust universe, whose local expansion is decelerated everywhere. Consequently, this form of accelerated expansion is purely an averaging effect, which does not violate the strong energy condition.

To approach the problem of determining the size of the unknown quantities in the Friedmann equations, one needs to put in more information. The first step is to assume mass conservation in form of the continuity equation:

$$\dot{\rho} = -\theta\rho \,. \tag{4.15}$$

Averaging this equation and applying the Friedmann equations (4.10) and (4.11), leads to the integrability condition [**Buc00**]:

$$\partial_t\left(a_D^6\langle Q\rangle_D\right) + a_D^4\,\partial_t\left(a_D^2\langle\mathcal{R}\rangle_D\right) = 0 \,, \tag{4.16}$$

showing that the two quantities $\langle\mathcal{R}\rangle_D$ and $\langle Q\rangle_D$ are not independent.

2.4. Cosmological perturbation theory. The Friedmann equations and the integrability condition are, however, not closed: There are four unknown variables, namely $\langle Q\rangle_D$, $\langle\mathcal{R}\rangle_D$, $\langle\rho\rangle_D$ and a_D, constraint by only three equations, namely (4.10), (4.11) and (4.16). They can be closed by using perturbation theory, which we use to second order here. In the comoving synchronous gauge, the linearly perturbed metric of a spatially flat dust universe with scale factor $a(t)$ can be written as [**KMNR05, LS07**]:

$$ds^2 = -dt^2 + a^2(t)\left[(1-2\Psi)\delta_{ij} + \left(\partial_i\partial_j - \frac{1}{3}\delta_{ij}\Delta\right)\chi\right]dx^i dx^j \,. \tag{4.17}$$

Ψ and χ are scalar metric perturbations and Δ is the Laplace operator. Note that the scale factor a is not equivalent to the effective scale factor a_D.

This metric is then be inserted into the Einstein equation, with the stress-energy tensor given by $T^0{}_0 = -\rho = -\rho^{(0)} - \rho^{(1)}$. $\rho^{(0)}$ and $\rho^{(1)}$ are the energy density of the background and at first order, respectively. $\rho^{(1)}$ can be used to define the time-independent peculiar gravitational potential as $\Delta\varphi(\mathbf{x}) = 4\pi G\rho^{(1)}a^2$. Using the integrability condition (4.16), the quantities $\langle Q\rangle_D$, $\langle\mathcal{R}\rangle_D$, $\langle\rho\rangle_D$ and H_D can then be calculated up to second order [**LS07, LS08**]:

$$\langle Q\rangle_D = \frac{a_{D_0}}{a_D}B(\varphi)t_0^2 \,, \tag{4.18}$$

$$\langle\mathcal{R}\rangle_D = \frac{20}{3}\frac{a_{D_0}^2}{a_D^2}\langle\Delta\varphi\rangle_D - 5\frac{a_{D_0}}{a_D}B(\varphi)t_0^2 \,, \tag{4.19}$$

$$\langle\rho\rangle_D = \frac{1}{6\pi G t_0^2}\frac{a_{D_0}^3}{a_D^3} \,, \tag{4.20}$$

$$H_D = \frac{2}{3t_0}\frac{a_{D_0}^{3/2}}{a_D^{3/2}}\left[1 - \frac{5}{4}\frac{a_D}{a_{D_0}}t_0^2\langle\Delta\varphi\rangle + \frac{3}{4}\frac{a_D^2}{a_{D_0}^2}t_0^4\left(B(\varphi) - \frac{25}{24}\langle\Delta\varphi\rangle^2\right)\right] \,, \tag{4.21}$$

where

$$B(\varphi) = \langle\partial^i(\partial_i\varphi\Delta\varphi) - \partial^i(\partial_j\varphi\partial^j\partial_i\varphi)\rangle - \frac{2}{3}\langle\Delta\varphi\rangle^2 \tag{4.22}$$

and

$$\langle O\rangle = \frac{\int_D O d\mathbf{x}}{\int_D d\mathbf{x}} \,. \tag{4.23}$$

Note that in the average denoted by $\langle.\rangle$ the metric is not contained in the integrals, which is in contrast to the average denoted by $\langle.\rangle_D$. The peculiar gravitational potential $\varphi(\mathbf{x})$ is related to Ψ and χ by:

$$\Psi = \frac{1}{2}\Delta\varphi t_0^{4/3}t^{2/3} + \frac{5}{3}\varphi \,, \tag{4.24}$$

$$\chi = -3\varphi t_0^{4/3}t^{2/3} \,. \tag{4.25}$$

2.5. Fluctuation of the Hubble rate. In this work, we are specifically interested in the measurement of the present Hubble rate. Depending on the domain in which it is measured, it will more or less differ from the global value of the Hubble rate H_0. This fluctuation of the effective Hubble rate can be defined as

$$\delta_H = \frac{H_D - H_0}{H_0} \,. \tag{4.26}$$

In a homogeneous and isotropic universe, the expectation value of δ_H is equal to zero. Nevertheless, there will be some fluctuations due to measurement errors and peculiar velocities.

The situation changes, when backreaction effects are taken into account. For a given domain size and shape (specified by the window function $W_D(\mathbf{x})$), one can determine the expectation value by inserting equation (4.21) into the definition of δ_H and calculating the ensemble average $\overline{\delta_H}$. Using

$$\begin{aligned} \overline{\langle\Delta\varphi\rangle^2} &= \int \frac{d\mathbf{x}_1 d\mathbf{x}_2}{V^2} \frac{d\mathbf{k}_1 d\mathbf{k}_2}{(2\pi)^6}\, k_1^2 k_2^2\, \overline{\varphi_{\mathbf{k}_1}\varphi_{\mathbf{k}_2}}\, e^{i(\mathbf{k}_1\cdot\mathbf{x}_1+\mathbf{k}_2\cdot\mathbf{x}_2)} \\ &= \int \frac{d\mathbf{x}_1 d\mathbf{x}_2}{V^2} \frac{d\mathbf{k}}{32\pi^4}\, k\mathcal{P}_\varphi(k)\, e^{i\mathbf{k}\cdot(\mathbf{x}_1+\mathbf{x}_2)}\,, \end{aligned} \tag{4.27}$$

one then finds the ensemble mean [**LS08**]

$$\overline{\delta_H} = -\frac{41}{162}\frac{1}{(1+z)^2}\frac{R_H^4}{V_D^2}\int d\mathbf{x}_1 d\mathbf{x}_2 \frac{d\mathbf{k}}{32\pi^4} k\mathcal{P}_\varphi(k) W_D(\mathbf{x}_1) W_D(\mathbf{x}_2) e^{i\mathbf{k}\cdot(\mathbf{x}_1+\mathbf{x}_2)}\,, \tag{4.28}$$

where R_H is the Hubble radius. As the highest order is also the leading order in the above equation, we could savely use the background redshift z to express the effective scale factor $a_{D_0}/a_D = 1+z$. The dimensionless power spectrum $\mathcal{P}_\varphi(k)$ is defined by $\overline{\varphi_{\mathbf{k}_1}\varphi_{\mathbf{k}_2}} = 2\pi^2\delta(\mathbf{k}_1+\mathbf{k}_2)\mathcal{P}_\varphi(k_1)/k_1^3$, where $k = |\mathbf{k}|$.

Backreaction effects thus lead to a changed expectation value $\overline{\delta_H}$, namely one that is negative instead of zero. Also the variance is affected. In addition to the measurement errors, one finds a theoretical variance caused by backreaction:

$$\mathrm{Var}(\delta_H) = \frac{25}{81}\frac{1}{(1+z)^2}\frac{R_H^4}{V_D^2}\int d\mathbf{x}_1 d\mathbf{x}_2 \frac{d\mathbf{k}}{32\pi^4} k\mathcal{P}_\varphi(k) W_D(\mathbf{x}_1) W_D(\mathbf{x}_2) e^{i\mathbf{k}\cdot(\mathbf{x}_1+\mathbf{x}_2)}\,. \tag{4.29}$$

In order to calculate $\overline{\delta_H}$ and $\mathrm{Var}(\delta_H)$, one needs to make assumptions about the statistical fluctuations in the gravitational potential, i.e. about the power spectrum $\mathcal{P}_\varphi(k)$. Consistent with WMAP7 [$\mathbf{K^+10}$], we take it to be $\mathcal{P}_\varphi(k) = \mathcal{P}_\varphi(k/k_0)^{n_s-1}$, where $n_s = 0.96$ is the spectral index and $k_0 = 0.002\mathrm{Mpc}^{-1}$. The quantity $\Delta^2_{\mathcal{R}}(k_0) = 2.45\cdot 10^{-9}$ given in [$\mathbf{K^+10}$] must be multiplied by 9/25 to obtain $\mathcal{P}_\varphi$ [**LS08**].

Both quantities, $\overline{\delta_H}$ as well as $\mathrm{Var}(\delta_H)$, depend on the window function $W_D(\mathbf{x})$. It is not obvious, for which kind of window function backreaction effects are most likely to be detected in the observed data. A good choice of $W_D(\mathbf{x})$ needs to reflect the actual distribution SN data in the sense that it is proportional to their number density. On the other hand, we would like to use a window function that gives rise to large effects. In this work, we consider the following two spherically symmetric window functions:

- Tophat:
  The domain is a spherical shell with inner radius R_D and outer radius αR_D.

$$W_D(\tilde{r}) = \Theta(\tilde{r}-R_D)\,\Theta\left(\alpha R_D - \tilde{r}\right) \tag{4.30}$$

- Gaussian:
  The domain follows a Gaussian function.

$$W_D(\tilde{r}) = \frac{1}{\sqrt{2\pi}R_D}\exp\left(-\frac{\tilde{r}^2}{2R_D^2}\right) \tag{4.31}$$

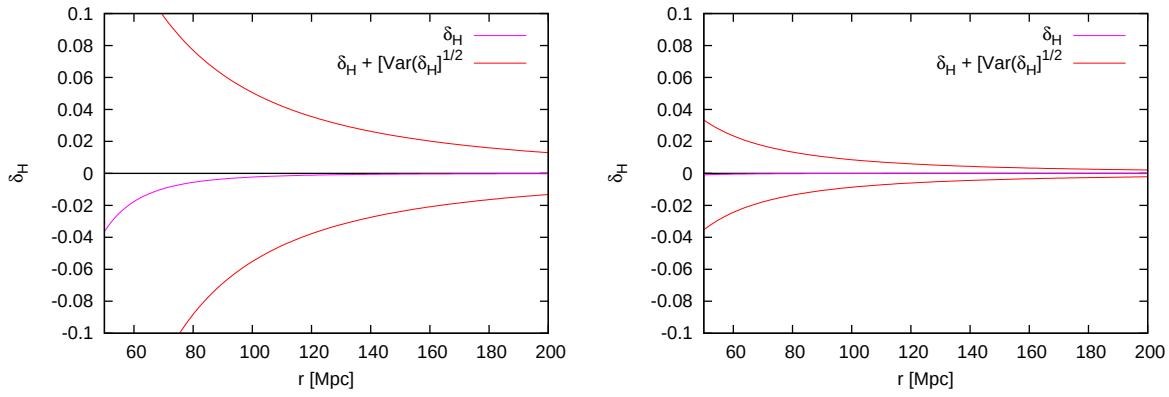

(a) Tophat (b) Gauss

Figure 4.4: Ensemble mean and variance of δ_H for tophat ($\alpha = 5/3$) and Gaussian window functions. H_0 is taken to be 70 km/(s Mpc).

In both cases the size of the domain can be modified by varying R_D and in the case of the tophat window function also by varying α, which defines the thickness of the shell. We translate R_D to an average distance r for each window function:

$$r = \frac{1}{V_D(t)} \int_0^\infty \tilde{r}\, W_D(\tilde{r})\, 4\pi \tilde{r}^2 d\tilde{r}\ , \tag{4.32}$$

i.e. $r = [3(\alpha^4 - 1)]/[4(\alpha^3 - 1)]\, R_D$ for the tophat window function and $r = \sqrt{8/\pi}\, R_D$ for the Gaussian window function. Then, for a certain domain, $\overline{\delta_H}$ and $\mathrm{Var}(\delta_H)$ are functions of r. Observed values of δ_H obtained from SNe with mean distance r can thus be compared to the theoretical curves. Note that for the considered window functions, small average distances r correspond to small domain sizes.

Figure 4.4 shows the ensemble mean $\overline{\delta_H}$ enveloped by the 1-σ limits $[\mathrm{Var}(\delta_H)]^{1/2}$ for the tophat and Gaussian window functions. For the plot, we have assumed $H_0 = 70$ km/(s Mpc). $\overline{\delta_H}$ and $\mathrm{Var}(\delta_H)$ are proportional to $r^{-(3+n_s)}$ for both window functions. Thus, backreaction effects are larger for small domain sizes. It turns out that there are large differences in the size of the backreaction effects between the two window functions. $\overline{\delta_H}$ is about 50 times larger for tophat than for Gauss, $[\mathrm{Var}(\delta_H)]^{1/2}$ is approximately 7 times larger. The reason why the effects are so small for the Gaussian window function is probably that it extends to infinity. Although the Gauss function drops rapidly at large distances — meaning that only very few distant data points are used for the analysis, while the vast majority of data points is nearby — the far away data points have a large lever arm on the effects.

3. Probing backreaction effects

3.1. Supernova data. As we can only use spatial averages, we need to restrict our analysis to low redshift data. The Constitution set [**H$^+$09b**] has the largest amount of SNe with $z < 0.1$. We mainly use the 178 SNe of this set that were fitted with SALT II, but also compare the results to that obtained by MLCS17. We use the redshift z_i and distance modulus μ_i to calculate the Hubble rate H_i and distance r_i for each SN of the set. After that

we average over the SNe that are assigned to a certain domain and compare the result to the theory.

We start by calculating the luminosity distance

$$d_{L,i} = 10^{(\mu_i - 25)/5}\,\mathrm{Mpc}\ . \tag{4.33}$$

The general relation between the luminosity distance and the Hubble rate is given by:

$$d_L = (1+z_i)\int_0^{z_i} \frac{d\tilde{z}}{H(z)}\ . \tag{4.34}$$

Thus, it depends on the assumed cosmological model, which determines the redshift dependence of $H(z)$. One might argue that we could just take a linear Hubble law as we only use low redshift data (which we have done in [**SS09b**]). However, it turned out that this approximation would significantly change the outcome of the test. Therefore, it is necessary to make some model assumptions.

The aim of this work is to test, whether nearby SNe are compatible with standard cosmology or if we need to take backreaction effects into account. Remember that for the calculation of the backreaction effects, a dust universe has been assumed. Thus, we need to calculate the Hubble rate differently for these two cases — once assuming a ΛCDM universe and no backreaction effects and once CDM with backreaction:

- ΛCDM (no backreaction):

$$H_i = \frac{1+z_i}{d_{L,i}}\int_0^{z_i} \frac{d\tilde{z}}{\sqrt{\Omega_m(1+\tilde{z})^3+\Omega_\Lambda}} \tag{4.35}$$

- CDM (backreaction):

$$H_i = \frac{1+z_i}{d_{L,i}}\int_0^{z_i} \frac{d\tilde{z}}{\sqrt{(1+\tilde{z})^3}} \tag{4.36}$$

In both cases, the comoving distance is simply given by

$$r_i = \frac{d_{L,i}}{1+z_i}\ . \tag{4.37}$$

The error of H_i is calculated using the error σ_i of the distance modulus:

$$\sigma_{H_i} = \frac{z_i}{5} 10^{(-\mu_i+25)/5}\ln 10\ \sigma_i \tag{4.38}$$

For calculating the mean values H_D and r, weighted averages are used:

$$H_D = \frac{\sum_{i=1}^{N_D} g_i H_i}{\sum_{i=1}^{N_D} g_i}\ , \qquad r = \frac{\sum_{i=1}^{N_D} g_i r_i}{\sum_{i=1}^{N_D} g_i}\ , \tag{4.39}$$

where $g_i = 1/\sigma_{H_i}$ and N_D is the number of SNe in the domain. The empirical variance of H_D is determined by

$$\sigma^2_{H_D} = \frac{\sum_{i=1}^{N_D} g_i (H_i - H_D)^2}{(N_D-1)\sum_{i=1}^{N_D} g_i}\ . \tag{4.40}$$

3.2. Calibration. The calibration of the SN data is an issue for our test. It is necessary to assume a certain value of the absolute magnitude M in order to determine H_i and r_i and thus the averages H_D and r. Without knowing the correct calibration, we cannot compare H_D to a global Hubble rate H_0 that has been obtained from other observations, e.g. from WMAP measurements. Instead we need to determine H_0 from the same data set, we use for the calculation of H_D.

This is done in the following way: First, the SNe of the set (with $z < 0.1$) are assigned to different subsets corresponding to the different domains. E.g. in the case of the tophat window function, we use four domains, i.e. four spherical shells, with the outer radius of one shell being the inner radius of the next shell. All SNe within a given shell are assigned to that subset. Then, we choose a specific calibration and calculate H_D and r for each domain. Again (as in the first version of the model-independent test of cosmic acceleration), we use the Riess calibration [**R**$^+$**05**] and the Sandage calibration [**S**$^+$**06**], respectively.

The next step is to determine H_0. This has to be done separately for the two cases — the model with backreaction effect and that without these effects. We use a Markov chain Monte Carlo to determine the maximum likelihood H_0 for each model, i.e. we maximize the likelihood

$$\prod_{i=1}^{n} \left[\frac{1}{\sqrt{2\pi}\sigma_i} \exp\left(-\frac{\left(\delta_{H,i} - \overline{\delta_H}(r_i)\right)^2}{2\sigma_i^2} \right) \right] . \tag{4.41}$$

Here, n is the number of considered domains. $\delta_{H,i} = (H_{D,i} - H_0)/H_0$ is the measured value of δ_H and r_i the average distance in the i-th domain. Assuming no backreaction effects, the ensemble mean $\overline{\delta_H}$ equals zero and σ_i is only the empirical error $\sigma_{\delta_{H,i}} = \sigma_{H_{D_i}}/H_0$. With backreaction effects, $\overline{\delta_H}(r_i)$ is given by equation (4.28) and $\sigma_i^2 = \sigma_{\delta_{H,i}}^2 + \mathrm{Var}(\delta_H)$.

The observational values $\delta_{H,i}$ and $\sigma_{\delta_{H,i}}$ as well as the theoretical curves $\overline{\delta_H}$ and $\mathrm{Var}(\delta_H)$ (which both include H_0) depend on the calibration of the SNe. Note that this dependence does not cancel during the analysis. Thus, our test result is affected by the calibration.

3.3. Results for the tophat window function. Using the tophat window function as given in equation (4.30), we can still choose the parameters R_D and α. As a first choice, we set $\alpha = 5/3$, but we will also consider different values later on. For the first domain, we use $R_{D,1} = 46$ Mpc, which is the inner radius of the domain. The outer radius $5/3\ R_{D,1}$ of this domain is the inner radius $R_{D,2}$ of the next domain. We proceed this way until we have reached four domains. Assigning all SNe between $R_{D,i}$ and $5/3\ R_{D,i}$ to the i-th subset, which corresponds to the i-th domain, there is a reasonable number of SNe in each domain. As can be seen in figure 4.5, this number depends on the calibration because the distance of each SN is calculated via the distance modulus. Thus, a different calibration leads to a shift in distance, which is why some SNe can be assigned to a different subset.

Following the above mentioned procedure, we determine the global Hubble rate H_0 for the model with and that without backreaction effects using the two different calibrations. The results are listed in table 4.1. Using the obtained Hubble rates H_0, the fluctuation δ_H is plotted in figure 4.6. The error bars of the data points include only the empirical errors. The blue data points indicate the results for the ΛCDM model without backreaction and thus should be compatible with zero. For CDM with backreaction, all data points (plotted in red) lie within the 1-σ limits (red curve) that envelop the expectation value $\overline{\delta_H}$ of the backreaction model and thus are consistent with this theory.

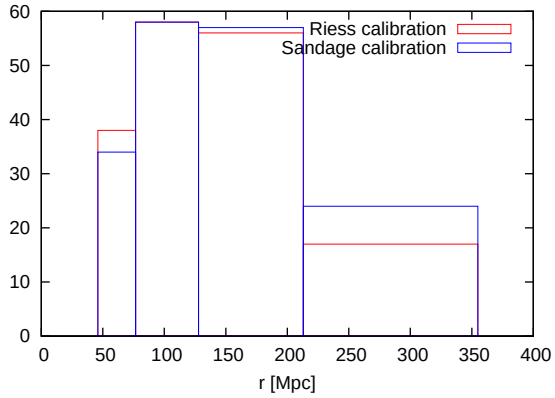

Figure 4.5: Number of SNe in the four domains of the tophat window function with $\alpha = 5/3$.

	Riess	Sandage
backreaction (CDM)	68.7	62.7
no backreaction (ΛCDM)	70.1	64.0

Table 4.1: Global Hubble rate H_0 for the models with and without backreaction for the tophat window function with $\alpha = 5/3$ using the two calibrations.

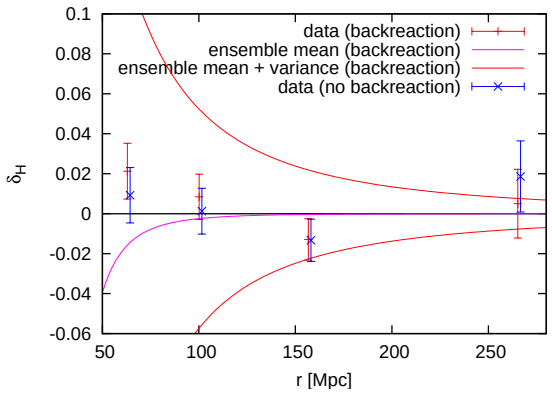

(a) Riess calibration

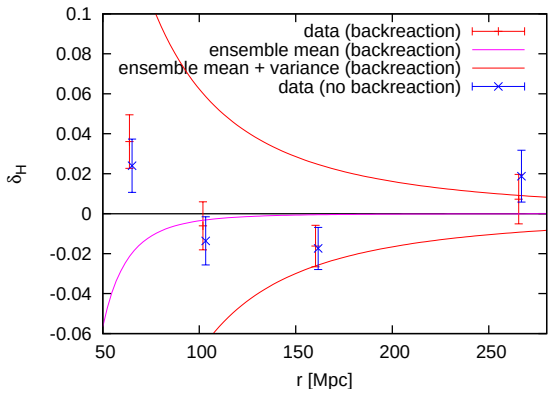

(b) Sandage calibration

Figure 4.6: δ_H for a CDM model with backreaction effects and ΛCDM without backreaction for the tophat window function with $\alpha = 5/3$ in the Riess and Sandage calibration, respectively.

α	n	model	Riess	Sandage
$\frac{5}{3}$	4	backreaction (CDM)	13.2%	61.1%
		no backreaction (ΛCDM)	86.8%	38.9%
$\frac{3}{2}$	5	backreaction (CDM)	34.0%	54.0%
		no backreaction (ΛCDM)	66.0%	46.0%
2	3	backreaction (CDM)	17.4%	9.9%
		no backreaction (ΛCDM)	82.6%	90.1%

Table 4.2: Likelihoods for the models with and without backreaction effects for the tophat window function with different values of α in the Riess and Sandage calibration, respectively. Also given is the number of domains n.

		Riess	Sandage
SALT II	backreaction (CDM)	13.2%	61.1%
	no backreaction (ΛCDM)	86.8%	38.9%
MLCS17	backreaction (CDM)	3.6%	4.7%
	no backreaction (ΛCDM)	96.4%	95.3%

Table 4.3: Likelihoods for the models with and without backreaction effects for the tophat window function with $\alpha = 5/3$ using SN data fitted with SALT II and MLCS2k2, respectively.

Using equation (4.41), we can compare the likelihoods of the two models given the data. In the Riess calibration the model without backreaction (likelihood 86.8%) is slightly preferred to that with backreaction effects (13.2%), whereas in the Sandage calibration backreaction is preferred with 61.1%. We have also done this test for other values of α. By thus changing the thickness of the considered shells, also the possible number of domains n changes as we are limited to small distances. For $\alpha = 5/3$, we had four domains. We can get five domains for $\alpha = 3/2$ and three for $\alpha = 2$. The likelihoods of the models for these values of α are listed in table 4.2. There are slight shifts in the likelihoods, but in none of the cases we get a significant result.

Table 4.3 compares the results that were obtained by using the SNe that were fitted with SALT II to those from the SNe fitted with MLCS17 (MLCS2k2 assuming $R_V = 1.7$). The model without backreaction effects is preferred in both calibrations when MLCS2k2 is used. But again, the result is not significant.

3.4. Results for the Gaussian window function. The analysis for the Gaussian window function (4.31) is slightly different. Using the tophat window function, there was a unique assignment of SNe to the different subsets representing the domain. But now the domains overlap, which is why a SN at a certain distance could in principle be assigned to different subsets.

Remember that the window function $W_D(r)$ should be proportional to the number density of SNe. Thus, the number of SNe in the distance interval $[r, r + dr]$ should be proportional to

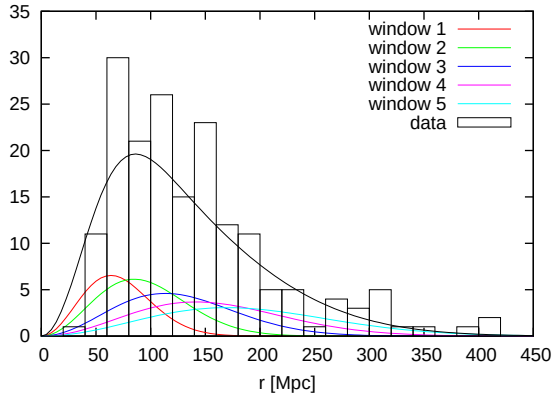

Figure 4.7: Distribution of the SNe and the Gaussian window function $r^2 W_D(r)$ for five different values of $R_D = 45, 60, 80, 100, 120$. The black curve is the sum of all five window functions $r^2 W_D(r)$.

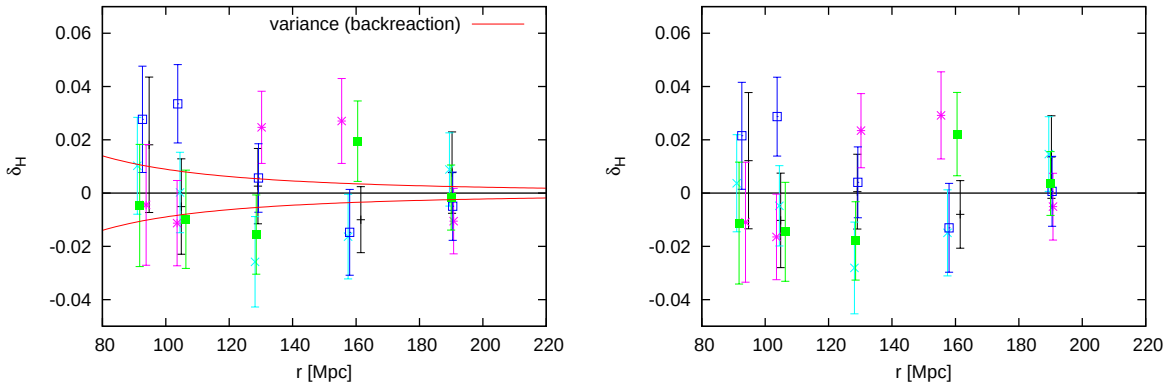

(a) CDM with backreaction

(b) ΛCDM without backreaction

Figure 4.8: δ_H obtained from five different realizations of subsets for the Gaussian window function using the Riess calibration.

$r^2 W_D(r)$. Figure 4.7 shows $r^2 W_D(r)$ for five different values of the parameter R_D. We have chosen the values of R_D such that the sum of these five functions (indicated by the black curve) follows approximately the distribution of SNe. The window function determines how many SNe at a certain distance are assigned to the subset representing the domain, but not which individual SNe. The actual assignment of SNe to a subset within one realization is done randomly, but in a way that all subsets are disjoint and thus statistically independent. As soon as one uses many realizations, i.e. different assignments of SNe to the subsets, the statistical independence is lost.

The results for five randomly chosen realizations using the Riess calibration are shown in figure 4.8. Each color indicates another realization. For each realization, the global Hubble

rate H_0 has been determined individually for the model with and that without backreaction effects. In figure 4.8a, the results for CDM with backreaction are plotted. While all data points were within the 1-σ limits when we considered the tophat window function, now the spread in the data is larger than these limits. (In the figure, the ensemble mean is not explicitly plotted as it is very close to zero.) Due to the large empirical errors, the data are, however, consistent with both models.

For the quantitative analysis, we have tested 100 realizations. Using the Riess calibration, the model with backreaction effects is slightly favored in 24 realizations, whereas it is favored in 17 realizations for the Sandage calibration. In the other cases, the standard ΛCDM model is favored. Yet, again none of the results is significant.

The analysis for the Gaussian window function should, however, be considered with caution. As the window function should be proportional to the number density of SNe, we would theoretically need to take SN at very large distances into account. Although the number of large distance SNe would be very small compared to the nearby ones that we have used for the analysis, these SNe might have a large influence on the test result.

3.5. Conclusion. Backreaction should theoretically affect the measurement of the averaged present day Hubble rate. The expectation value for the fluctuation of the Hubble rate δ_H becomes slightly negative, but the main effect is an increased variance. The size of these effects depends on the size and shape of the domain, in which the averages are performed. For our test, we used two different window functions specifying the domain, namely the tophat and the Gaussian window function. We compared the values of the Hubble rate that were observed in different domains to the theoretical values in a CDM model with backreaction effects and in a ΛCDM universe without backreaction, respectively, in order to find out which of the two models describes the data better.

For neither window function, we could find a significant result. This is due to restrictions in the test: If it was possible to measure the Hubble rate at different locations in the universe, we should theoretically see the large spread in H_D for small domain sizes, which is caused by backreaction. As we can only perform measurements from our very location in the universe, it is quite possible that this measurement is by chance consistent with vanishing backreaction effects. In that way, our test only has the potential to prove backreaction effects, but cannot exclude their possible existence. Such an exclusion would only be possible, if we had measurements of H_D from different locations in the universe without the expected spread in its size.

Yet, there is a possibility to improve the test. In the present work, we have only used spherically symmetric domains. Thus, we could only obtain one averaged data point at a given distance. But in order to see the expected spread in δ_H, we would need several data points at the same distance. This can in principle be achieved by using non-spherically symmetric domains. Given a fixed size and shape of the domain, we can put this domain in different locations, but at a fixed distance to the observer. Thus, we would obtain several data points at this distance.

Nevertheless, there are problems with this approach: The first problem is that the SN data sets are still too small for this test. Remember that for the tophat window function, there were less than 40 SNe in the closest domain, for which backreaction should have the largest effect on the measurement of the Hubble rate. Splitting this domain into two hemispheres, each containing almost 20 SNe, would still be reasonable. A further splitting up would, however, lead to bad statistics. While we can expect this problem to be solved in the near future,

when larger data sets are published, the second problem remains: We are still restricted to our local universe. Even if we observe SNe in different directions, they might be affected by the same local structure. Thus, the results from domains that lie in different direction might not be completely statistically independent. This is likely to cause a spread in the data that is smaller than that expected from theory. Due to these problems the test might not be able to prove the existence of backreaction effects. Nevertheless, it has the potential to do so.

CHAPTER 5

Concluding remarks

In this work, we have considered different aspects of the expanding universe and used SN Ia data for various cosmological tests. We started with analyzing a braneworld model with timelike extra-dimension, which is only one theory among an uncounted number of cosmological models. Although this braneworld model appears to be very exotic with its two time dimensions, we could not exclude it with the currently available observational data. This is, however, not too surprising, considering that the model has five free parameters. The same argument applies to most models. As they are usually more complicated than ΛCDM and thus have more free parameters, it seems to be very hard to rule them out by observations. Consequently, the number of viable cosmological models is constantly increasing.

Instead of following the trend to investigate specific models, it might thus be useful to first ask more fundamental questions. In this thesis, we have addressed the question of accelerated expansion: How certain are we of its existence? What are the assumptions we need to make in order to infer cosmic acceleration?

The question concerning the assumptions can be easily answered: The universe needs to be homogeneous and isotropic and the SNe need to be a fair representation of the universe. The question about the evidence for cosmic acceleration is, however, more complicated. Although we could significantly reduce the systematics in the calibration-independent version of the test and find evidence for acceleration for most SN data sets, the results obtained from SDSS is somewhat confusing. The systematics, that we thought were under control, reappeared in this set and while we found evidence for acceleration for all other data sets and light-curve fitters, in both versions of the test, when assuming a flat universe, this evidence was no longer present for SDSS (MLCS2k2).

This came very much as a surprise — especially when considering that observation and data analysis techniques should have improved compared to earlier SN surveys. Furthermore, SDSS is the first data set that closes the gap at intermediate redshifts that was present in previously published sets. Thus, we would have expected the results to be at least as good as those from other data sets. Consequently, we would have expected to find evidence for acceleration — if cosmic acceleration is actually taking place. Therefore, a future task must be to investigate, whether there are some problems in the observation or analysis pipelines in the SDSS data set. As systematics are certainly an issue, it is important to find out, which of the fitters is more reliable. Only after this is done, we can actually decide, whether there is a significant evidence for acceleration under the made assumptions.

We have also addressed the problem that the assumptions of the test might not be justified. The universe is only statistically homogeneous on large scales. Local structures might, however, affect the measurement of the present Hubble rate via the backreaction mechanism. These effects become important when the average Hubble rate is measured in small domain sizes. Yet, we could not detect any backreaction effects using the SNe of the Constitution set. One reason for this might be that a single local measurement can by chance be compatible

with a cosmological model that does not include backreaction because the main effect is an increase of the variance of the measured Hubble rate. Other problems are the dependence of the test on the cosmological model and on the calibration of the SNe. All of these issues could be avoided if it was possible to perform various measurements at different locations in the universe. This is, however, an impossible task.

While we have presented some promising cosmological tests in this work, there are still some issues in applying these tests. The biggest problem are systematics in the observational SN data. Thus, it is on the one hand important to reduce these systematic errors and on the other hand to modify the tests such that the impact of the systematics on the test result is less significant. Maybe then we will be able to draw some reliable conclusions from the presented tests.

There are still lots of open questions in cosmology. But that is what makes it so interesting.

APPENDIX A

Notation

In this work, we use a metric with signature $(-,+,+,+)$. Latin indeces run from 1 to 3 with exception of chapter 2, where also five-dimensional quantities have latin indeces. Greek indeces always run from 0 to 3.

A dot over a physical quantity denotes a time derivative, while a prime stands for a derivative with respect to redshift.

We use the Einstein summation convention, i.e. we sum over all indeces that appear twice in a term.

Brackets $\langle . \rangle_D$ denote spatial averages that include $\sqrt{\det g_{ij}}$ in the integral, while $\langle . \rangle$ denotes spatial averages without this term. A bar over a quantity denotes its ensemble average.

We set the speed of light $c = 1$.

In the following table, we list the symbols and definitions of frequently used quantities. Some of the symbols can have different meanings. The particular meaning should, however, become clear in the context.

Symbol	Definition
α	parameter determining the thickness of the shell in the tophat window function
δ_H	fluctuation of the Hubble rate
θ	volume expansion rate
Λ	cosmological constant
Λ_5	bulk cosmological constant
μ	distance modulus
$\Delta\mu$	distance modulus minus distance modulus of a universe with $q = 0$
ρ	energy density
ρ_c	critical density
ρ_{eff}	energy density of the effective fluid
σ	brane tension
σ	standard deviation
σ^2	shear scalar
φ	peculiar gravitational potential
χ	scalar metric perturbations in the synchronous gauge
Ψ	scalar metric perturbations in the synchronous gauge

Symbol	Definition
Ω_Λ	dimensionless energy density of the cosmological constant
Ω_{Λ_5}	dimensionless energy density of the five-dimensional cosmological constant
Ω_σ	dimensionless energy density of the brane tension
Ω_C	dimensionless energy density of dark radiation
Ω_k	dimensionless energy density of curvature
Ω_ℓ	dimensionless energy density of the length scale ℓ
Ω_m	dimensionless energy density of matter
Ω_r	dimensionless energy density of radiation
a	scale factor
a_D	effective scale factor in domain D
A_V	extinction in the V-band
D	domain
d_L	luminosity distance
E_{B-V}	color excess
F	flux
G	gravitational constant
$g_{\mu\nu}$	metric
$G_{\mu\nu}$	Einstein tensor
$\mathcal{G}_{ab}$	five-dimensional Einstein tensor
H	Hubble rate
H_D	effective Hubble rate in domain D
h_{ab}	induced brane metric
K_{ab}	extrinsic curvature
ℓ	length scale of the braneworld model
m	apparent magnitude
m	four-dimensional Planck mass
M	absolute magnitude
M	five-dimensional Planck mass
$M_\odot$	sun mass
n_a	inner normal vector to the brane
n_s	spectral index
p	pressure
p_{eff}	pressure of the effective fluid
q	deceleration parameter
$\langle Q \rangle_D$	kinematical backreaction
R	scalar curvature

Symbol	Definition
$\mathcal{R}$	scalar curvature of the bulk
$\langle\mathcal{R}\rangle_D$	averaged spatial curvature in domain D
R_H	Hubble radius
R_V	reddening parameter
S	action
t	cosmic time
t_0	age of the universe
$T_{\mu\nu}$	stress-energy tensor
$\mathcal{T}_{ab}$	five-dimensional stress-energy tensor
u_μ	4-velocity
V	volume
w	equation of state
W_D	window function specifying domain D
z	redshift
z_t	transition redshift between deceleration and acceleration

APPENDIX B

Physical quantities

The following table lists the values of some quantities used in this work. In the first part of the table, some basic cosmological quantities are given. The second and third part of the table contain the primary and derived maximum likelihood (ML) and mean values from WMAP7 measurements [**K**$^+$**10**]. In this work, we use the maximum likelihood values.

Parameter	Value	
Mpc	$3.0857 \cdot 10^{22}\,\mathrm{m}$	
R_H	$2.998\,h^{-1} \cdot 10^3\,\mathrm{Mpc}$	
ρ_c	$1.878\,h^2 \cdot 10^{-26}\,\mathrm{kg/m^3}$	
	ML	mean
$\Omega_b h^2$	0.02246	0.0260 ± 0.00053
$\Omega_{\mathrm{CDM}} h^2$	0.1120	0.1123 ± 0.0035
Ω_Λ	0.728	$0.728^{+0.015}_{-0.016}$
n_s	0.961	0.963 ± 0.012
$\Delta^2_{\mathcal{R}}(k_0)$	$2.45 \cdot 10^{-9}$	$\left(2.441^{+0.088}_{-0.092}\right) \cdot 10^{-9}$
H_0	$70.2\,\mathrm{km/(s\,Mpc)}$	$70.4^{+1.3}_{-1.4}\,\mathrm{km/(s\,Mpc)}$
Ω_b	0.0455	0.0456 ± 0.0016
Ω_{CDM}	0.227	0.227 ± 0.014
$\Omega_m h^2$	0.1344	0.1349 ± 0.0036
t_0	13.78 Gyr	13.75 ± 0.11 Gyr

APPENDIX C

Abbreviations

ΛCDM	Λ cold dark matter
BAO	baryon acoustic oscillations
B-band	frequency band of blue light
BBN	Big Bang nucleosynthesis
CDM	cold dark matter
CfA	Harvard-Smithonian Center for Astrophysics
CL	confidence level
CMB	cosmic microwave background
DGP	Dvali-Gabadadze-Porrati
ESSENCE	Equation of State: SupErNovae trace Cosmic Expansion
HST	Hubble Space Telescope
LRG	luminous red galaxy
MLCS2k2	Multicolor Light Curve Shape
MLCS17	MLCS2k2 assuming $R_V = 1.7$
MLCS31	MLCS2k2 assuming $R_V = 3.1$
RS	Randall-Sundrum
SALT	Spectral Adaptive Light-curve Template
SDSS	Sloan Digital Sky Survey
SEC	strong energy condition
SN	supernova
SNLS	SuperNova Legacy Survey
U-band	frequency band of ultra-violet light
V-band	frequency band of visible light
WMAP	Wilkinson Microwave Anisotropy Probe

APPENDIX D

Supernova data sets

In the following, we provide a list of the SN data sets that are used within this work. Each set contains SNe from different surveys, which are listed in the table below. Note that in some cases the data sets are named after one specific survey (e.g. ESSENCE), whose SNe are included in the set. Small surveys are summarized under "other surveys". Also the nearby SNe have been observed during different surveys.

data set	survey
Gold	SNLS + HST + other surveys + nearby
ESSENCE	ESSENCE + SNLS + nearby
Union	ESSENCE + SNLS + HST + other surveys + nearby
Constitution	ESSENCE + SNLS + HST + other surveys + CfA3 + nearby
SDSS	ESSENCE + SNLS + HST + SDSS + nearby

The following table lists the references of the first publication of the survey data.

survey	references
nearby SNe	Hamuy et al. [**HPS$^+$96**], Riess et al. [**R$^+$99**], Jha et al. [**J$^+$06**], Krisciunas et al. [**K$^+$01, K$^+$04a, K$^+$04b**]
ESSENCE	Wood-Vasey et al. [**WV$^+$07**]
SNLS	Astier et al. [**A$^+$06**]
HST	Knop et al. [**K$^+$03**], Riess et al. [**R$^+$04, R$^+$07**]
CfA3	Hicken et al. [**H$^+$09a**]
SDSS	Kessler et al. [**K$^+$09a**]
other surveys	Riess et al. [**R$^+$98**], Garnavich et al. [**G$^+$98**], Schmidt et al. [**S$^+$98**], Perlmutter et al. [**P$^+$99**], Barris et al. [**B$^+$04**], Tonry et al. [**T$^+$03**]

APPENDIX E

Theoretical constraints of the braneworld model

The parameters of the braneworldmodel with timelike extra-dimension need to fulfill certain constraints such that the Friedmann equation has a physical solution within the whole observable universe. As usual, we assume the matter density Ω_m to be positive. $\Omega_\ell = 1/\ell^2 H_0^2$ is positive per definition. For simplicity, we assume $\Omega_k = 0$ and $\Omega_C = 0$. The BRANE1 and BRANE2 models as well as the cases of negative and positive brane tension are discussed seperately.

1. BRANE1

1.1. Negative brane tension. The Friedmann equation is given by

$$\frac{H^2(z)}{H_0^2} = \Omega_m(1+z)^3 + \Omega_\sigma - 2\Omega_\ell + 2\sqrt{\Omega_\ell}\sqrt{\Omega_\ell - \Omega_m(1+z)^3 - \Omega_\sigma - \Omega_{\Lambda_5}}\,, \tag{E.1}$$

where

$$\Omega_\sigma = 1 - \Omega_m - 2\sqrt{\Omega_\ell}\sqrt{-1 - \Omega_{\Lambda_5}}\,. \tag{E.2}$$

The right handside of the Friedmann equation as well as all terms under square roots must not be negative, which leads to the following conditions:

$$\Omega_\ell \geq 0 \tag{E.3}$$

$$\Omega_{\Lambda_5} \leq -1 \tag{E.4}$$

$$\Omega_m(1+z)^3 + \Omega_\sigma - 2\Omega_\ell + 2\sqrt{\Omega_\ell}\sqrt{\Omega_\ell - \Omega_m(1+z)^3 - \Omega_\sigma - \Omega_{\Lambda_5}} \geq 0 \tag{E.5}$$

$$\Omega_\ell - \Omega_m(1+z)^3 - \Omega_\sigma - \Omega_{\Lambda_5} \geq 0 \tag{E.6}$$

Inequalities (E.5) and (E.6) must be fulfilled for all redshifts $0 \leq z \leq z_{\text{rec}} = 1090$, i.e between now and the time of recombination. We want to rewrite conditions (E.5) and (E.6) such that we get constraint equations for Ω_ℓ. In order to do that, we need to consider the two following cases:

- Case 1: $\Omega_m(1+z)^3 \leq 2\Omega_\ell - \Omega_\sigma$ for $0 \leq z \leq z_{\text{rec}}$
  Inequality (E.5) is equivalent to:

$$\begin{aligned} 2\sqrt{\Omega_\ell}\sqrt{\Omega_\ell - \Omega_m(1+z)^3 - \Omega_\sigma - \Omega_{\Lambda_5}} &\geq 2\Omega_\ell - \Omega_m(1+z)^3 - \Omega_\sigma \\ -4\Omega_\ell\Omega_{\Lambda_5} &\geq \left(\Omega_m(1+z)^3 + \Omega_\sigma\right)^2 \\ \Omega_m(1+z)^3 &\leq 2\sqrt{-\Omega_\ell\Omega_{\Lambda_5}} - \Omega_\sigma \end{aligned} \tag{E.7}$$

  Writing inequality (E.6) as

$$\Omega_m(1+z)^3 \leq \Omega_\ell - \Omega_\sigma - \Omega_{\Lambda_5}\,, \tag{E.8}$$

we see that with increasing z the equality in (E.7) is always reached sooner than in (E.8) since

$$\begin{aligned} 2\sqrt{-\Omega_\ell\Omega_{\Lambda_5}} - \Omega_\sigma &\leq \Omega_\ell - \Omega_\sigma - \Omega_{\Lambda_5} \\ 0 &\leq \left(\sqrt{\Omega_\ell} - \sqrt{-\Omega_{\Lambda_5}}\right)^2 \end{aligned}$$

is always fulfilled.

Thus, inequalities (E.5) and (E.6) can be reduced to (E.7), which gives a constraint for Ω_ℓ:

$$\Omega_\ell \geq \left(\frac{\Omega_m(1+z)^3 + 1 - \Omega_m}{2\left(\sqrt{-\Omega_{\Lambda_5}} + \sqrt{-\Omega_{\Lambda_5} - 1}\right)}\right)^2 . \tag{E.9}$$

If it is fulfilled for $z_{\rm rec} = 1090$, it is fulfilled for all redshifts in the considered range.

- Case 2: $\Omega_m(1+z)^3 \geq 2\Omega_\ell - \Omega_\sigma$ for $z^* \leq z \leq z_{\rm rec}$

In this case we assume that $\Omega_m(1+z)^3$ is larger than $2\Omega_\ell - \Omega_\sigma$ beyond a certain redshift z^* which is defined by

$$\Omega_m(1+z^*)^3 = 2\Omega_\ell - \Omega_\sigma . \tag{E.10}$$

Note that we still need to consider the whole redshift range from 0 to $z_{\rm rec}$.

We start by analysing the interval $z^* \leq z \leq z_{\rm rec}$. Again, inequality (E.5) is equivalent to:

$$2\sqrt{\Omega_\ell}\sqrt{\Omega_\ell - \Omega_m(1+z)^3 - \Omega_\sigma - \Omega_{\Lambda_5}} \geq 2\Omega_\ell - \Omega_m(1+z)^3 - \Omega_\sigma . \tag{E.11}$$

For $z > z^*$ this inequality is always fulfilled as the right hand side is negative. Thus, inequalitiy (E.7) constrains the parameter values more than is actually needed in this case. Nevertheless, all parameters that fulfill (E.9) are allowed in both considered cases. But while in case 1 all other parameter values are excluded, in case 2 we have an additional allowed region in parameter space.

As condition (E.5) is always fulfilled, we only need to consider inequality (E.6) and the case 2 condition for $z > z^*$:

$$\Omega_m(1+z)^3 \leq \Omega_\ell - \Omega_\sigma - \Omega_{\Lambda_5} \tag{E.12}$$

$$\Omega_m(1+z)^3 \geq 2\Omega_\ell - \Omega_\sigma \tag{E.13}$$

These two inequalities imply that

$$\begin{aligned} 2\Omega_\ell - \Omega_\sigma &\leq \Omega_\ell - \Omega_\sigma - \Omega_{\Lambda_5} \\ \Omega_\ell &\leq -\Omega_{\Lambda_5} \end{aligned} \tag{E.14}$$

must be fulfilled.

Thus, the conditions for a physical solution within the redshift range $z^* \leq z \leq z_{\rm rec}$ are the inequalities (E.6) and (E.14).

Let us now consider the interval $0 \leq z \leq z^*$. According to the calculations in case 1, now only (E.7) needs to be fulfilled up to z^*. This happens automatically when we apply the conditions for case 2 (actually we only need $\Omega_\ell \leq -\Omega_{\Lambda_5}$):

$$\Omega_m(1+z)^3 \leq \Omega_m(1+z^*)^3 = 2\Omega_\ell - \Omega_\sigma \leq 2\sqrt{-\Omega_\ell\Omega_{\Lambda_5}} - \Omega_\sigma . \tag{E.15}$$

Rewriting (E.6) as

$$\sqrt{\Omega_\ell} \geq \sqrt{\Omega_m(1+z)^3 - \Omega_m} - \sqrt{-1-\Omega_{\Lambda_5}}\,, \tag{E.16}$$

the two cases can easily be combined. In order to get a physical solution of the Friedmann equation, either

$$\Omega_\ell \geq \left(\frac{\Omega_m(1+z_{\rm rec})^3 + 1 - \Omega_m}{2\left(\sqrt{-\Omega_{\Lambda_5}} + \sqrt{-\Omega_{\Lambda_5}-1}\right)} \right)^2 \tag{E.17}$$

or

$$\sqrt{\Omega_\ell} \geq \sqrt{\Omega_m(1+z_{\rm rec})^3 - \Omega_m} - \sqrt{-1-\Omega_{\Lambda_5}} \qquad \text{and} \qquad \Omega_\ell \leq -\Omega_{\Lambda_5} \tag{E.18}$$

need to be fulfilled.

1.2. Positive brane tension. The Friedmann equation is the same as in the case of negative brane tension

$$\frac{H^2(z)}{H_0^2} = \Omega_m(1+z)^3 + \Omega_\sigma - 2\Omega_\ell + 2\sqrt{\Omega_\ell}\sqrt{\Omega_\ell - \Omega_m(1+z)^3 - \Omega_\sigma - \Omega_{\Lambda_5}}\,, \tag{E.19}$$

but now

$$\Omega_\sigma = 1 - \Omega_m + 2\sqrt{\Omega_\ell}\sqrt{-1-\Omega_{\Lambda_5}}\,. \tag{E.20}$$

With analogous calculations it follows that

$$\Omega_\ell \geq \left(\frac{\Omega_m(1+z_{\rm rec})^3 + 1 - \Omega_m}{2\left(\sqrt{-\Omega_{\Lambda_5}} - \sqrt{-\Omega_{\Lambda_5}-1}\right)} \right)^2 \tag{E.21}$$

or

$$\sqrt{\Omega_\ell} \geq \sqrt{\Omega_m(1+z_{\rm rec})^3 - \Omega_m} + \sqrt{-1-\Omega_{\Lambda_5}} \qquad \text{and} \qquad \Omega_\ell \leq -\Omega_{\Lambda_5} \tag{E.22}$$

must be fulfilled. Here, the first constraint (E.21) is much stronger than the second one (E.22).

2. BRANE2

2.1. Positive brane tension. The Friedmann equation is given by

$$\frac{H^2(z)}{H_0^2} = \Omega_m(1+z)^3 + \Omega_\sigma - 2\Omega_\ell - 2\sqrt{\Omega_\ell}\sqrt{\Omega_\ell - \Omega_m(1+z)^3 - \Omega_\sigma - \Omega_{\Lambda_5}}\,, \tag{E.23}$$

where

$$\Omega_\sigma = 1 - \Omega_m + 2\sqrt{\Omega_\ell}\sqrt{-1-\Omega_{\Lambda_5}}\,. \tag{E.24}$$

Here, the conditions are

$$\Omega_\ell \geq 0 \tag{E.25}$$

$$\Omega_{\Lambda_5} \leq -1 \tag{E.26}$$

$$\Omega_m(1+z)^3 + \Omega_\sigma - 2\Omega_\ell - 2\sqrt{\Omega_\ell}\sqrt{\Omega_\ell - \Omega_m(1+z)^3 - \Omega_\sigma - \Omega_{\Lambda_5}} \geq 0 \tag{E.27}$$

$$\Omega_\ell - \Omega_m(1+z)^3 - \Omega_\sigma - \Omega_{\Lambda_5} \geq 0 \tag{E.28}$$

Inequalities (E.27) and (E.28) must be fulfilled for all redshifts $0 \leq z \leq z_{\rm rec}$.

We start with constraint (E.27):

$$\Omega_m(1+z)^3+\Omega_\sigma-2\Omega_\ell \geq 2\sqrt{\Omega_\ell}\sqrt{\Omega_\ell-\Omega_m(1+z)^3-\Omega_\sigma-\Omega_{\Lambda_5}}\,. \tag{E.29}$$

Obviously, the left hand side must be positive, i.e.:

$$\Omega_m(1+z)^3+1-\Omega_m+2\sqrt{\Omega_\ell}\sqrt{-1-\Omega_{\Lambda_5}}-2\Omega_\ell \geq 0\,. \tag{E.30}$$

Setting $z=0$, this leads to:

$$\Omega_\ell \leq -\frac{1}{2}\Omega_{\Lambda_5}+\frac{1}{2}\sqrt{-1+\Omega_{\Lambda_5}^2}\,. \tag{E.31}$$

Now that we have ensured the positiveness of the left hand side, we can savely square inequality (E.29):

$$\left(\Omega_m(1+z)^3+\Omega_\sigma-2\Omega_\ell\right)^2 \geq 4\Omega_\ell\left(\Omega_\ell-\Omega_m(1+z)^3-\Omega_\sigma-\Omega_{\Lambda_5}\right) \tag{E.32}$$

$$\Omega_m^2(1+z)^6+2\Omega_\sigma\Omega_m(1+z)^3+\Omega_\sigma^2 \geq -4\Omega_\ell\Omega_{\Lambda_5} \tag{E.33}$$

$$\Omega_m(1+z)^3+1-\Omega_m+2\sqrt{\Omega_\ell}\sqrt{-1-\Omega_{\Lambda_5}} \geq 2\sqrt{-\Omega_\ell\Omega_{\Lambda_5}} \tag{E.34}$$

With $z=0$ we get:

$$\Omega_\ell \leq \frac{1}{4(\sqrt{-\Omega_{\Lambda_5}}-\sqrt{-1-\Omega_{\Lambda_5}})^2}\,, \tag{E.35}$$

which is a stronger constraint than inequality (E.31).

Constraint (E.28) can be written as

$$\Omega_\ell \geq (\sqrt{\Omega_m(1+z)^3-\Omega_m}+\sqrt{-1-\Omega_{\Lambda_5}})^2\,. \tag{E.36}$$

Inequalities (E.35) and (E.36) have to be fulfilled simultaneously. It follows that

$$(\sqrt{\Omega_m(1+z)^3-\Omega_m}+\sqrt{-1-\Omega_{\Lambda_5}})^2 \leq \frac{1}{4(\sqrt{-\Omega_{\Lambda_5}}-\sqrt{-1-\Omega_{\Lambda_5}})^2}\,. \tag{E.37}$$

Thus,

$$\begin{aligned}
\sqrt{\Omega_m(1+z)^3-\Omega_m} &\leq \frac{1}{2(\sqrt{-\Omega_{\Lambda_5}}-\sqrt{-1-\Omega_{\Lambda_5}})}-\sqrt{-1-\Omega_{\Lambda_5}} \\
&= \frac{-1-2\sqrt{-\Omega_{\Lambda_5}}\sqrt{-1-\Omega_{\Lambda_5}}-2\Omega_{\Lambda_5}}{2(\sqrt{-\Omega_{\Lambda_5}}-\sqrt{-1-\Omega_{\Lambda_5}})} \\
&= \frac{(\sqrt{-\Omega_{\Lambda_5}}-\sqrt{-1-\Omega_{\Lambda_5}})^2}{2(\sqrt{-\Omega_{\Lambda_5}}-\sqrt{-1-\Omega_{\Lambda_5}})} \\
&= \frac{1}{2}(\sqrt{-\Omega_{\Lambda_5}}-\sqrt{-1-\Omega_{\Lambda_5}}) \qquad \text{(E.38)}
\end{aligned}$$

The largest possible value for the right hand side of this inequality is 1/2 (for $\Omega_{\Lambda_5}=-1$). Therefore,

$$\Omega_m(1+z)^3-\Omega_m \leq \frac{1}{4}\,. \tag{E.39}$$

This inequality can only be fulfilled for redshifts $z \lesssim 0.2$. Thus, in the case of a flat universe without dark radiation, the BRANE2 model can be ruled out.

2.2. Negative brane tension. Now we have

$$\frac{H^2(z)}{H_0^2} = \Omega_m(1+z)^3 + \Omega_\sigma - 2\Omega_\ell - 2\sqrt{\Omega_\ell}\sqrt{\Omega_\ell - \Omega_m(1+z)^3 - \Omega_\sigma - \Omega_{\Lambda_5}} \tag{E.40}$$

with

$$\Omega_\sigma = 1 - \Omega_m - 2\sqrt{\Omega_\ell}\sqrt{-1-\Omega_{\Lambda_5}}\ . \tag{E.41}$$

The calculations are analogous to the previous case with the following result:

$$\sqrt{\Omega_m(1+z)^3 - \Omega_m} - \sqrt{-1-\Omega_{\Lambda_5}} \leq \sqrt{\Omega_\ell} \leq \frac{1}{2\left(\sqrt{-\Omega_{\Lambda_5}} + \sqrt{-1-\Omega_{\Lambda_5}}\right)}\ . \tag{E.42}$$

This constraint for Ω_ℓ can only be fulfilled if

$$\sqrt{\Omega_m(1+z)^3 - \Omega_m} \leq \frac{1}{2}\left(\sqrt{-\Omega_{\Lambda_5}} + \sqrt{-1-\Omega_{\Lambda_5}}\right)\ . \tag{E.43}$$

Inserting this result into the right inequality of (E.42) yields

$$\Omega_\ell \leq \frac{1}{4\left(\sqrt{-\Omega_{\Lambda_5}} + \sqrt{-1-\Omega_{\Lambda_5}}\right)^2} \tag{E.44}$$

$$\leq \frac{1}{16\left(\Omega_m(1+z)^3 - \Omega_m\right)} \tag{E.45}$$

Assuming $\Omega_m = 0.3$ and claiming that the above inequalities are at least valid up to $z = 1100$, we find that $\Omega_{\Lambda_5} \gtrsim -2 \cdot 10^8$ and $\Omega_\ell \lesssim 1.6 \cdot 10^{-10}$ must be fulfilled for the BRANE2 model with negative brane tension.

Bibliography

[A$^+$00] Laura Andrianopoli et al., *Isometric embedding of BPS branes in flat spaces with two times*, Class. Quant. Grav. **17** (2000), 1875–1896.

[A$^+$06] Pierre Astier et al., *The Supernova Legacy Survey: Measurement of Ω_M, Ω_Λ and w from the First Year Data Set*, Astron. Astrophys. **447** (2006), 31–48.

[A$^+$10] R. Amanullah et al., *Spectra and Light Curves of Six Type Ia Supernovae at 0.511 ¡ z ¡ 1.12 and the Union2 Compilation*, Astrophys. J. **716** (2010), 712–738.

[AA07] Havard Alnes and Morad Amarzguioui, *The supernova Hubble diagram for off-center observers in a spherically symmetric inhomogeneous universe*, Phys. Rev. **D75** (2007), 023506.

[AHDD98] Nima Arkani-Hamed, Savas Dimopoulos, and G. R. Dvali, *The hierarchy problem and new dimensions at a millimeter*, Phys. Lett. **B429** (1998), 263–272.

[AM$^+$08] Jennifer K. Adelman-McCarthy et al., *The Sixth Data Release of the Sloan Digital Sky Survey*, Astrophys. J. Suppl. **175** (2008), 297–313.

[AP10] I. Antoniou and L. Perivolaropoulos, *Searching for a Cosmological Preferred Axis: Union2 Data Analysis and Comparison with Other Probes*, [arXiv:1007.4347], 2010.

[B$^+$04] Brian J. Barris et al., *23 High Redshift Supernovae from the IfA Deep Survey: Doubling the SN Sample at z¿0.7*, Astrophys. J. **602** (2004), 571–594.

[Bar01] Itzhak Bars, *Survey of two-time physics*, Class. Quant. Grav. **18** (2001), 3113–3130.

[Bar06] ———, *The standard model of particles and forces in the framework of 2T-physics*, Phys. Rev. **D74** (2006), 085019.

[Bar08] ———, *Gravity in 2T-Physics*, Phys. Rev. **D77** (2008), 125027.

[BBR08] Juliane Behrend, Iain A. Brown, and Georg Robbers, *Cosmological Backreaction from Perturbations*, JCAP **0801** (2008), 013.

[BDA98] I. Bars, C. Deliduman, and O. Andreev, *Gauged duality, conformal symmetry and spacetime with two times*, Phys. Rev. **D58** (1998), 066004.

[Bea10] Rachel Bean, *TASI Lectures on Cosmic Acceleration*, [arXiv:1003.4468], 2010.

[BGB04] Pawel Bielewicz, K. M. Gorski, and A. J. Banday, *Low order multipole maps of CMB anisotropy derived from WMAP*, Mon. Not. Roy. Astron. Soc. **355** (2004), 1283.

[BK07] Itzhak Bars and Yueh-Cheng Kuo, *Supersymmetric field theory in 2T-physics*, Phys. Rev. **D76** (2007), 105028.

[BT92] D. Branch and G. A. Tammann, *Type Ia supernovae as standard candles*, Ann. Rev. Astron. Astrophys. **30** (1992), 359–389.

[Buc00] Thomas Buchert, *On average properties of inhomogeneous fluids in general relativity. I: Dust cosmologies*, Gen. Rel. Grav. **32** (2000), 105–125.

[Buc01] ———, *On average properties of inhomogeneous fluids in general relativity: Perfect fluid cosmologies*, Gen. Rel. Grav. **33** (2001), 1381–1405.

[Buc08] ———, *Dark Energy from Structure - A Status Report*, Gen. Rel. Grav. **40** (2008), 467–527.

[C$^+$07] Alexander J. Conley et al., *Is there evidence for a Hubble bubble? The nature of Type Ia Supernova colors and dust in external galaxies*, Astrophys. J. **664** (2007), L13–L16.

[CAL09] Chris Clarkson, Kishore Ananda, and Julien Larena, *The influence of structure formation on the cosmic expansion*, Phys. Rev. **D80** (2009), 083525.

[Cel00] Marie-Noelle Celerier, *Do we really see a cosmological constant in the supernovae data?*, Astron. Astrophys. **353** (2000), 63–71.

[CGH08] Chia-Hsun Chuang, Je-An Gu, and W-Y. P. Hwang, *Inhomogeneity-Induced Cosmic Acceleration in a Dust Universe*, Class. Quant. Grav. **25** (2008), 175001.

[CHSS10] Craig J. Copi, Dragan Huterer, Dominik J. Schwarz, and Glenn D. Starkman, *Large angle anomalies in the CMB*, [arXiv:1004.5602], 2010.

[CST06] Edmund J. Copeland, M. Sami, and Shinji Tsujikawa, *Dynamics of dark energy*, Int. J. Mod. Phys. **D15** (2006), 1753–1936.

[CV07] Celine Cattoen and Matt Visser, *The Hubble series: Convergence properties and redshift variables*, Class. Quant. Grav. **24** (2007), 5985–5998.

[Def01] Cedric Deffayet, *Cosmology on a brane in Minkowski bulk*, Phys. Lett. **B502** (2001), 199–208.

[DG01] G. R. Dvali and Gregory Gabadadze, *Gravity on a brane in infinite-volume extra space*, Phys. Rev. **D63** (2001), 065007.

[DGP00] G. R. Dvali, Gregory Gabadadze, and Massimo Porrati, *4D gravity on a brane in 5D Minkowski space*, Phys. Lett. **B485** (2000), 208–214.

[E+05] Daniel J. Eisenstein et al., *Detection of the Baryon Acoustic Peak in the Large-Scale Correlation Function of SDSS Luminous Red Galaxies*, Astrophys. J. **633** (2005), 560–574.

[Ein17] Albert Einstein, *Cosmological Considerations in the General Theory of Relativity*, Sitzungsber. Preuss. Akad. Wiss. Berlin (Math. Phys.) **1917** (1917), 142–152.

[Ell84] G. F. R. Ellis, *Relativistic cosmology - Its nature, aims and problems*, General Relativity and Gravitation Conference (B. Bertotti, F. de Felice, & A. Pascolini, ed.), 1984, pp. 215–288.

[EM06] Oystein Elgaroy and Tuomas Multamaki, *Bayesian analysis of Friedmannless cosmologies*, JCAP **0609** (2006), 002.

[EM07] Kari Enqvist and Teppo Mattsson, *The effect of inhomogeneous expansion on the supernova observations*, JCAP **0702** (2007), 019.

[F+07] Anna Frebel et al., *Discovery of HE 1523-0901, a Strongly r-Process Enhanced Metal-Poor Star with Detected Uranium*, Astrophys. J. **660** (2007), L117–L120.

[FE09] Mona Frommert and Torsten A. Ensslin, *The axis of evil - a polarization perspective*, [arXiv:0908.0453], 2009.

[FM07] E. L. Fitzpatrick and D. Massa, *An Analysis of the Shapes of Interstellar Extinction Curves. V. The IR-Through-UV Curve Morphology*, Astrophys. J. **663** (2007), 320–341.

[FTH08] Joshua Frieman, Michael Turner, and Dragan Huterer, *Dark Energy and the Accelerating Universe*, Ann. Rev. Astron. Astrophys. **46** (2008), 385–432.

[FWH10] Hume A. Feldman, Richard Watkins, and Michael J. Hudson, *Cosmic Flows on 100 Mpc/h Scales: Standardized Minimum Variance Bulk Flow, Shear and Octupole Moments*, Mon. Not. Roy. Astron. Soc. **392** (2010), 756.

[G+98] Peter M. Garnavich et al., *Supernova Limits on the Cosmic Equation of State*, Astrophys. J. **509** (1998), 74–79.

[G+05] J. Richard Gott, III et al., *A Map of the Universe*, Astrophys. J. **624** (2005), 463.

[G+07] Julien Guy et al., *SALT2: using distant supernovae to improve the use of Type Ia supernovae as distance indicators*, Astron. Astrophys. **466** (2007), 11–21.

[GAN+05] Julien Guy, P. Astier, S. Nobili, N. Regnault, and R. Pain, *SALT: a Spectral Adaptive Light curve Template for Type Ia Supernovae*, Astron. Astrophys. **443** (2005), 781–791.

[GB02] Ghazal Geshnizjani and Robert Brandenberger, *Back reaction and local cosmological expansion rate*, Phys. Rev. **D66** (2002), 123507.

[GBH08] Juan Garcia-Bellido and Troels Haugboelle, *Confronting Lemaitre-Tolman-Bondi models with Observational Cosmology*, JCAP **0804** (2008), 003.

[GSW87a] Michael B. Green, J. H. Schwarz, and Edward Witten, *Superstring Theory. Vol. 1: Introduction*, Cambridge University Press, 1987.

[GSW87b] ———, *Superstring Theory. Vol. 2: Loop Amplitudes, Anomalies and Phenomenology*, Cambridge University Press, 1987.

[Gut81] Alan H. Guth, *The Inflationary Universe: A Possible Solution to the Horizon and Flatness Problems*, Phys. Rev. **D23** (1981), 347–356.

[GWWZ07] Yungui Gong, Anzhong Wang, Qiang Wu, and Yuan-Zhong Zhang, *Direct evidence of acceleration from distance modulus redshift graph*, JCAP **0708** (2007), 018.

[H+05] David W. Hogg et al., *Cosmic homogeneity demonstrated with luminous red galaxies*, Astrophys. J. **624** (2005), 54–58.

[H+07] Troels Haugboelle et al., *The Velocity Field of the Local Universe from Measurements of Type Ia Supernovae*, Astrophys. J. **661** (2007), 650–659.

[H+08] D. Hutsemekers et al., *Large-Scale Alignments of Quasar Polarization Vectors: Evidence at Cosmological Scales for Very Light Pseudoscalar Particles Mixing with Photons?*, [arXiv:0809.3088], 2008.

[H+09a] Malcolm Hicken et al., *CfA3: 185 Type Ia Supernova Light Curves from the CfA*, Astrophys. J. **700** (2009), 331–357.

[H+09b] ———, *Improved Dark Energy Constraints from 100 New CfA Supernova Type Ia Light Curves*, Astrophys. J. **700** (2009), 1097–1140.

[HCLS05] D. Hutsemekers, R. Cabanac, H. Lamy, and Dominique Sluse, *Mapping extreme-scale alignments of quasar polarization vectors*, Astron. Astrophys. **441** (2005), 915–930.

[HL00] D. Hutsemekers and H. Lamy, *Confirmation of the existence of coherent orientations of quasar polarization vectors on cosmological scales*, [arXiv:astro-ph/0012182], 2000.

[HPS+96] Mario Hamuy, M. M. Phillips, Nicholas B. Suntzeff, Robert A. Schommer, and Jose Maza, *BVRI Light Curves for 29 Type Ia Supernovae*, Astron. J. **112** (1996), 2408–2437.

[HS07] Wayne Hu and Ignacy Sawicki, *Models of f(R) Cosmic Acceleration that Evade Solar-System Tests*, Phys. Rev. **D76** (2007), 064004.

[Hub29] Edwin Hubble, *A relation between distance and radial velocity among extra–galactic nebulae*, Proc. Nat. Acad. Sci. **15** (1929), 168–173.

[IRWG08] Mustapha Ishak, James Richardson, Delilah Whittington, and David Garred, *Dark Energy or Apparent Acceleration Due to a Relativistic Cosmological Model More Complex than FLRW?*, Phys. Rev. **D78** (2008), 123531.

[J+06] Saurabh Jha et al., *UBVRI Light Curves of 44 Type Ia Supernovae*, Astron. J. **131** (2006), 527–554.

[JB01] Jennifer A. Johnson and Michael Bolte, *Th Ages for Metal-Poor Stars*, [arXiv:astro-ph/0103299], 2001.

[JBP05] Harvinder Kaur Jassal, J. S. Bagla, and T. Padmanabhan, *Observational constraints on low redshift evolution of dark energy: How consistent are different observations?*, Phys. Rev. **D72** (2005), 103503.

[Joh04] Moncy V. John, *Cosmographic evaluation of deceleration parameter using SNe Ia data*, Astrophys. J. **614** (2004), 1.

[JRK07] Saurabh Jha, Adam G. Riess, and Robert P. Kirshner, *Improved Distances to Type Ia Supernovae with Multicolor Light Curve Shapes: MLCS2k2*, Astrophys. J. **659** (2007), 122–148.

[JSLG+05] Michael Joyce, F. Sylos Labini, A. Gabrielli, M. Montuori, and L. Pietronero, *Basic properties of galaxy clustering in the light of recent results from the Sloan Digital Sky Survey*, Astron. Astrophys. **443** (2005), 11.

[K+01] Kevin Krisciunas et al., *Optical and Infrared Photometry of the Type Ia Supernovae 1999da, 1999dk, 1999gp, 2000bk, and 2000ce*, The Astronomical Journal **122** (2001), no. 3, 1616.

[K+03] Robert A. Knop et al., *New Constraints on Ω_M, Ω_Λ, and w from an Independent Set of Eleven High-Redshift Supernovae Observed with HST*, Astrophys. J. **598** (2003), 102.

[K+04a] Kevin Krisciunas et al., *Optical and Infrared Photometry of the Nearby Type Ia Supernovae 1999ee, 2000bh, 2000ca, and 2001ba*, The Astronomical Journal **127** (2004), no. 3, 1664.

[K+04b] ———, *Optical and Infrared Photometry of the Type Ia Supernovae 1991T, 1991bg, 1999ek, 2001bt, 2001cn, 2001cz, and 2002bo*, The Astronomical Journal **128** (2004), no. 6, 3034.

[K+07] D. J. Kapner et al., *Tests of the gravitational inverse-square law below the dark-energy length scale*, Phys. Rev. Lett. **98** (2007), 021101.

[K+08] M. Kowalski et al., *Improved Cosmological Constraints from New, Old and Combined Supernova Datasets*, Astrophys. J. **686** (2008), 749–778.

[K+09a] Richard Kessler et al., *First-year Sloan Digital Sky Survey-II (SDSS-II) Supernova Results: Hubble Diagram and Cosmological Parameters*, Astrophys. J. Suppl. **185** (2009), 32–84.

[K+09b] E. Komatsu et al., *Five-Year Wilkinson Microwave Anisotropy Probe (WMAP) Observations:Cosmological Interpretation*, Astrophys. J. Suppl. **180** (2009), 330–376.

[K+10] ———, *Seven-Year Wilkinson Microwave Anisotropy Probe (WMAP) Observations: Cosmological Interpretation*, [arXiv:1001.4538], 2010.

[Kal21] Theodor Kaluza, *On the Problem of Unity in Physics*, Sitzungsber. Preuss. Akad. Wiss. Berlin (Math. Phys.) **1921** (1921), 966–972.

[Kle26] O. Klein, *Quantum theory and five-dimensional theory of relativity*, Z. Phys. **37** (1926), 895–906.

[KMNR05] Edward W. Kolb, Sabino Matarrese, Alessio Notari, and Antonio Riotto, *The effect of inhomogeneities on the expansion rate of the universe*, Phys. Rev. **D71** (2005), 023524.

[KMR06] Edward W. Kolb, S. Matarrese, and A. Riotto, *On cosmic acceleration without dark energy*, New J. Phys. **8** (2006), 322.

[KOSS81] R. P. Kirshner, A. Oemler, Jr., P. L. Schechter, and S. A. Shectman, *A million cubic megaparsec void in Bootes*, Astrophys. J. **248** (1981), L57–60.

[Koy08] Kazuya Koyama, *The cosmological constant and dark energy in braneworlds*, Gen. Rel. Grav. **40** (2008), 421–450.

[KPRS07] Kimmo Kainulainen, Johanna Piilonen, Vappu Reijonen, and Daniel Sunhede, *Spherically symmetric spacetimes in f(R) gravity theories*, Phys. Rev. **D76** (2007), 024020.

[KW04] J. Kocinski and M. Wierzbicki, *The Schwarzschild solution in a Kaluza-Klein theory with two times*, Rel. Grav. Cosmol. **1** (2004), 19–36.

[L$^+$96] C. H. Lineweaver et al., *The Dipole Observed in the COBE DMR Four-Year Data*, Astrophys. J. **470** (1996), 38–42.

[LAB$^+$09] Julien Larena, Jean-Michel Alimi, Thomas Buchert, Martin Kunz, and Pier-Stefano Corasaniti, *Testing backreaction effects with observations*, Phys. Rev. **D79** (2009), 083011.

[Lin82] Andrei D. Linde, *A New Inflationary Universe Scenario: A Possible Solution of the Horizon, Flatness, Homogeneity, Isotropy and Primordial Monopole Problems*, Phys. Lett. **B108** (1982), 389–393.

[Lin83] ———, *Chaotic Inflation*, Phys. Lett. **B129** (1983), 177–181.

[LS07] Nan Li and Dominik J. Schwarz, *On the onset of cosmological backreaction*, Phys. Rev. **D76** (2007), 083011.

[LS08] ———, *Scale dependence of cosmological backreaction*, Phys. Rev. **D78** (2008), 083531.

[LSS08] Nan Li, Marina Seikel, and Dominik J. Schwarz, *Is dark energy an effect of averaging?*, Fortsch. Phys. **56** (2008), 465–474.

[LVPB09] Francesco Sylos Labini, Nikolay L. Vasilyev, Luciano Pietronero, and Yurij V. Baryshev, *Absence of self-averaging and of homogeneity in the large scale galaxy distribution*, Europhys. Lett. **86** (2009), 49001.

[Maa04] Roy Maartens, *Brane-world gravity*, Living Rev. Rel. **7** (2004), 7.

[Nor14] Gunnar Nordstrom, *On the possibility of unifying the electromagnetic and the gravitational fields*, Phys. Z. **15** (1914), 504–506.

[NP07] S. Nesseris and Leandros Perivolaropoulos, *Tension and Systematics in the Gold06 SnIa Dataset*, JCAP **0702** (2007), 025.

[P$^+$99] S. Perlmutter et al., *Measurements of Omega and Lambda from 42 High-Redshift Supernovae*, Astrophys. J. **517** (1999), 565–586.

[Per08] L. Perivolaropoulos, *Six Puzzles for LCDM Cosmology*, [arXiv:0811.4684], 2008.

[Phi93] M. M. Phillips, *The absolute magnitudes of Type IA supernovae*, Astrophys. J. **413** (1993), L105–L108.

[Pol98a] J. Polchinski, *String theory. Vol. 1: An introduction to the bosonic string*, Cambridge University Press, 1998.

[Pol98b] ———, *String theory. Vol. 2: Superstring theory and beyond*, Cambridge University Press, 1998.

[PS07] Aseem Paranjape and T. P. Singh, *The Spatial Averaging Limit of Covariant Macroscopic Gravity - Scalar Corrections to the Cosmological Equations*, Phys. Rev. **D76** (2007), 044006.

[R$^+$98] Adam G. Riess et al., *Observational Evidence from Supernovae for an Accelerating Universe and a Cosmological Constant*, Astron. J. **116** (1998), 1009–1038.

[R$^+$99] ———, *BVRI Light Curves for 22 Type Ia Supernovae*, Astron. J. **117** (1999), 707–724.

[R$^+$04] ———, *Type Ia Supernova Discoveries at $z > 1$ From the Hubble Space Telescope: Evidence for Past Deceleration and Constraints on Dark Energy Evolution*, Astrophys. J. **607** (2004), 665–687.

[R$^+$05] ———, *Cepheid Calibrations from the Hubble Space Telescope of the Luminosity of Two Recent Type Ia Supernovae and a Re- determination of the Hubble Constant*, Astrophys. J. **627** (2005), 579–607.

[R$^+$07] ———, *New Hubble Space Telescope Discoveries of Type Ia Supernovae at $z > 1$: Narrowing Constraints on the Early Behavior of Dark Energy*, Astrophys. J. **659** (2007), 98–121.

[RAAB07] David Rapetti, Steven W. Allen, Mustafa A. Amin, and Roger D. Blandford, *A kinematical approach to dark energy studies*, Mon. Not. Roy. Astron. Soc. **375** (2007), 1510–1520.

[Ras04] Syksy Rasanen, *Dark energy from backreaction*, JCAP **0402** (2004), 003.

[RMKB96] Heinz Russ, Masaaki Morita, Masumi Kasai, and Gerhard Borner, *The Zel'dovich-type approximation for an inhomogeneous universe in general relativity: second-order solutions*, Phys. Rev. **D53** (1996), 6881–6888.

[RPK96] Adam G. Riess, William H. Press, and Robert P. Kirshner, *A Precise distance indicator: Type Ia supernova multicolor light curve shapes*, Astrophys. J. **473** (1996), 88.

[RS99a] Lisa Randall and Raman Sundrum, *A large mass hierarchy from a small extra dimension*, Phys. Rev. Lett. **83** (1999), 3370–3373.

[RS99b] ———, *An alternative to compactification*, Phys. Rev. Lett. **83** (1999), 4690–4693.

[RSKB97] Heinz Russ, Michael H. Soffel, Masumi Kasai, and Gerhard Borner, *Age of the universe: Influence of the inhomogeneities on the global expansion-factor*, Phys. Rev. **D56** (1997), 2044–2050.

[S$^+$92] George F. Smoot et al., *Structure in the COBE differential microwave radiometer first year maps*, Astrophys. J. **396** (1992), L1–L5.

[S$^+$98] Brian P. Schmidt et al., *The High-Z Supernova Search: Measuring Cosmic Deceleration and Global Cur vature of the Universe Using Type Ia Supernovae*, Astrophys. J. **507** (1998), 46–63.

[S$^+$05] Uros Seljak et al., *Cosmological parameter analysis including SDSS Ly-alpha forest and galaxy bias: Constraints on the primordial spectrum of fluctuations, neutrino mass, and dark energy*, Phys. Rev. **D71** (2005), 103515.

[S$^+$06] A. Sandage et al., *The Hubble Constant: A Summary of the HST Program for the Luminosity Calibration of Type Ia Supernovae by Means of Cepheids*, Astrophys. J. **653** (2006), 843–860.

[Sah05] Varun Sahni, *Cosmological surprises from braneworld models of dark energy*, JGRG14: Proceedings (W. Hikida, M. Sasaki, T. Tanaka, and T. Nakamura, eds.), 2005, pp. 95–115.

[SAPR07] J. Santos, J. S. Alcaniz, N. Pires, and Marcelo J. Reboucas, *Energy Conditions and Cosmic Acceleration*, Phys. Rev. **D75** (2007), 083523.

[SC09] Marina Seikel and Max Camenzind, *Braneworlds with timelike extra-dimension*, Phys. Rev. **D79** (2009), 083531.

[Sch02] Dominik J. Schwarz, *Accelerated expansion without dark energy*, On the nature of dark energy (J. Martin P. Brax and J.-P. Uzan, eds.), 2002, p. 331.

[SF63] M. F. Shirokov and I. Z. Fisher, *Isotropic Space with Discrete Gravitational-Field Sources. On the Theory of a Nonhomogeneous Isotropic Universe*, Sov. Astron. J. **6** (1963), 699, reprinted in Gen. Rel. Grav. **30** (1998), 1411.

[Sht02] Yuri V. Shtanov, *Closed equations on a brane*, Phys. Lett. **B541** (2002), 177–182.

[SS02] Yuri Shtanov and Varun Sahni, *Unusual cosmological singularities in braneworld models*, Class. Quant. Grav. **19** (2002), L101–L107.

[SS03a] Varun Sahni and Yuri Shtanov, *Braneworld models of dark energy*, JCAP **0311** (2003), 014.

[SS03b] Yuri Shtanov and Varun Sahni, *Bouncing braneworlds*, Phys. Lett. **B557** (2003), 1–6.

[SS08] Marina Seikel and Dominik J. Schwarz, *How strong is the evidence for accelerated expansion?*, JCAP **0802** (2008), 007.

[SS09a] ———, *Model- and calibration-independent test of cosmic acceleration*, JCAP **0902** (2009), 024.

[SS09b] ———, *Probing Backreaction Effects with Supernova Data*, PoS **Cosmology2009** (2009), 024.

[SSV05] Varun Sahni, Yuri Shtanov, and Alexander Viznyuk, *Cosmic Mimicry: Is LCDM a Braneworld in Disguise?*, JCAP **0512** (2005), 005.

[ST06] Charles Shapiro and Michael S. Turner, *What Do We Really Know About Cosmic Acceleration?*, Astrophys. J. **649** (2006), 563–569.

[STR04] A. Sandage, G. A. Tammann, and Bernd Reindl, *New Period-Luminosity and Period-Color Relations of Classical Cepheids: II. Cepheids in LMC*, Astron. Astrophys. **424** (2004), 43–71.

[SW07] Dominik J. Schwarz and Bastian Weinhorst, *(An)isotropy of the Hubble diagram: comparing hemispheres*, Astronomy and Astrophysics **474** (2007), 717–729.

[T$^+$03] John L. Tonry et al., *Cosmological Results from High-z Supernovae*, Astrophys. J. **594** (2003), 1–24.

[T$^+$04] Max Tegmark et al., *Cosmological parameters from SDSS and WMAP*, Phys. Rev. **D69** (2004), 103501.

[T$^+$05] Nial R. Tanvir et al., *Determination of Cepheid parameters by light-curve template-fitting*, Mon. Not. Roy. Astron. Soc. **363** (2005), 749–762.

[TR02] Michael S. Turner and Adam G. Riess, *Do SNe Ia Provide Direct Evidence for Past Deceleration of the Universe?*, Astrophys. J. **569** (2002), 18.

[TSR03] G. A. Tammann, A. Sandage, and Bernd Reindl, *New Period-Luminosity and Period-Color Relations of Classical Cepheids: I. Cepheids in the Galaxy*, Astron. Astrophys. **404** (2003), 423–448.

[UB05] Albrecht Unsöld and Bodo Baschek, *Der neue Kosmos*, Springer Verlag, 2005.

[VFW07] R. Ali Vanderveld, Eanna E. Flanagan, and Ira Wasserman, *Systematic corrections to the measured cosmological constant as a result of local inhomogeneity*, Phys. Rev. **D76** (2007), 083504.

[Vis97] Matt Visser, *General Relativistic Energy Conditions: The Hubble expansion in the epoch of galaxy formation*, Phys. Rev. **D56** (1997), 7578–7587.

[Wet03] Christof Wetterich, *Can structure formation influence the cosmological evolution?*, Phys. Rev. **D67** (2003), 043513.

[WFH08] Richard Watkins, Hume A. Feldman, and Michael J. Hudson, *Consistently Large Cosmic Flows on Scales of 100 Mpc/h: a Challenge for the Standard LCDM Cosmology*, [arXiv:0809.4041], 2008.

[WT05] Yun Wang and Max Tegmark, *Uncorrelated Measurements of the Cosmic Expansion History and Dark Energy from Supernovae*, Phys. Rev. **D71** (2005), 103513.

[WV$^+$07] W. Michael Wood-Vasey et al., *Observational Constraints on the Nature of the Dark Energy: First Cosmological Results from the ESSENCE Supernova Survey*, Astrophys. J. **666** (2007), 694–715.

[Y$^+$00] Donald G. York et al., *The Sloan Digital Sky Survey: technical summary*, Astron. J. **120** (2000), 1579–1587.

[Zal92] Roustam M. Zalaletdinov, *Averaging out the Einstein equations and macroscopic space-time geometry*, Gen. Rel. Grav. **24** (1992), 1015–1031.

[ZSBP01] Winfried Zimdahl, Dominik J. Schwarz, Alexander B. Balakin, and Diego Pavon, *Cosmic antifriction and accelerated expansion*, Phys. Rev. **D64** (2001), 063501.